Development of a methodology linking protein phase behavior and Hydrophobic Interaction Chromatography

zur Erlangung des akademischen Grades eines
DOKTORS DER INGENIEURWISSENSCHAFTEN (Dr.-Ing.)

der Fakultät für Chemieingenieurwesen und Verfahrenstechnik des
Karlsruher Instituts für Technologie (KIT)
vorgelegte

genehmigte
DISSERTATION

von
Dipl.-Ing. Kai Baumgartner
aus Oberndorf am Neckar

Referent: Prof. Dr. Jürgen Hubbuch
Korreferent: Prof. Dr.-Ing. Matthias Franzreb
Korreferent: PD Dr. Egbert Müller
Tag der mündlichen Prüfung: 18.12.2015

Danksagungen

Ohne die Unterstützung einer Vielzahl von Personen hätte ich es nicht geschafft dahin zu kommen, wo ich heute bin. Diesen Personen möchte ich danken:

Ich danke Herrn Prof. Dr. Jürgen Hubbuch für die Möglichkeit, meine Dissertation am Institut für Molekulare Aufarbeitung von Bioprodukten anfertigen zu können.

Des Weiteren danke ich Herrn Prof. Dr.-Ing. Matthias Franzreb sowie Herrn PD Dr. Egbert Müller für die freundlichen Übernahmen des Korreferates.

Großer Dank gilt meinen Kollegen, die mich nicht nur fachlich sondern auch persönlich sehr unterstützt haben und mich gerne an die letzten Jahre zurückdenken lassen.

Besonders möchte ich an dieser Stelle Pascal Baumann nennen, mit dem ich gemeinsam auch schon das Studium bewältigt habe und der mein Trauzeuge sein wird. Ich werde mich auch gerne an die gemeinsamen regelmäßigen Besuche des Fitnessstudios mit ihm und meinem ehemaligen Bürokollegen Frank Hämmerling, der zu einem besten Freund geworden ist, zurückerinnern.

Danke auch an meine Kollegen, mit denen ich Kooperationsprojekte machen durften. Hervorzuheben sind hier Juliane Schütz und Lara Galm; zusammen haben wir monatelang unendliche viele Liquid-Klassen aufgenommen und Phasendiagramme produziert.

Dank gilt auch dem Betreuer meiner Studienarbeit Stefan Oelmeier, der mich in den Anfängen meiner Dissertation auch als PostDoc unterstützt hat. Besonderer Dank gilt Benjamin Maiser, dem Betreuer meiner Diplomarbeit, durch den ich großen Spaß an der Arbeit an diesem Institut entwickelt habe.

Außerdem danke ich Margret Meixner, Susanna Suhm, Josefine Morgenstern und meinen früheren Kolleginnen Franca Diehl und Marie-Luise Schwab sowie Marc Hoffmann unter anderem für die lustigen gemeinsamen Mittagessen und Kaffeerunden.

Meiner Diplomandin Nina Brestrich, meinem Diplomanden Sylvius Willerich und meinem Masteranden Steffen Großhans möchte ich für die sehr guten Arbeiten im Labor danken.

Der größte Dank gilt meiner Familie, die mich all die Jahre unterstützt hat sowie meiner Verlobten Alexandra, die mir auch in stressigen Zeiten persönlichen Rückhalt gegeben hat und immer für mich da war. Danke! Ich liebe dich!

Abstract

During the production of biopharmaceuticals the target protein passes diverse process steps starting from cell cultivation to purification of the final product. At each sub-process the environment changes and the protein properties, like surface charge, surface hydrophobicity or the protein structure, are influenced. Since every protein has distinct characteristics, it responds differently to these changes. The altered properties can have negative effects on the product yield. For example, formation of inclusion bodies in the upstream part can cause severe product loss. Inclusion bodies are misfolded protein agglomerates, often accompanied by a loss of functionality. But also correctly folded proteins can form precipitates or crystals at undesired stages in the process and lead to pipe and filter clogging or blockage of chromatography columns. These problems can also happen during formulation or storage. For the above-mentioned reasons, it is important to characterize each process step in the biopharmaceutical industry and to estimate the impact on the phase behavior of the target molecule. Factors influencing protein properties are for example salt type, salt concentration, additives, pH value, and the protein concentration. Besides the undesired aspects, phase transitions like precipitation or crystallization, which are based on for example electrostatic and hydrophobic interactions, can be specifically used as purification steps. These interactions also play an important role during ion-exchange chromatography (IEC) or hydrophobic interaction chromatography (HIC). To sufficiently characterize the phase behavior of the protein and to meet the 'Time to Market' demands, high-throughput (HT) systems are the method of choice. Here, robot-based pipetting platforms are used to parallelize experiments in microliter scale to enable high-throughput screenings (HTS). Due to the huge number of generated experiments when using HTS methods, a parallel development of HT compatible analytical technologies is necessary. In this way, the experiments can be evaluated fast and precisely, so that correlations can be found and optimal purification strategies can be developed.
As a consequence of the 'Quality by Design'(QbD) guidelines in the industry, various types of statistical 'Design of Experiments' (DoE) have become the method of choice for exploring the design space. Whereas HTS and QbD are implemented as the gold standard in the development of various pharmaceutical sub-processes, the purification using HIC is still based on experience and heuristic approaches. Predominantly, purification takes place at neutral pH values and common salt types in predefined ranges are used independent of the protein's nature. Hence, it may happen that the purification is performed under suboptimal conditions further reducing the comparably low binding capacities of HIC adsorbers.
The first part of this thesis is focused on the phase behavior of proteins in dependence of various precipitants and pH values. Therefore, a robot-based high-throughput methodology for the generation of phase diagrams in microliter scale was developed. By the use of this fast and automated methodology, phase diagrams were generated using small sample volumes. Less than 150 mg of protein are necessary for creating a phase diagram to determine the phase behavior at a constant pH value under varying protein and salt concentrations. No silicone oils were used to avoid heterogenic nucleation. The disadvantage of vapor diffusion, occurring in 'hanging drop' and 'sitting drop' methods, leading to unknown precipitant and protein concentrations at the point of phase transition, was also excluded. The microbatch plates were sealed with a UV compatible sealing tape to create

a saturated atmosphere within the wells and to avoid evaporation. By storing the microbatch plates in a fully automated and temperature controlled device (Rock Imager 54), that takes pictures of the samples regularly, short-term and long-term stability studies were possible. Phase diagrams were evaluated after 40 days, when samples were considered to be in equilibrium. This new methodology for generating phase diagrams in HT was used for four different proteins at four different pH values using four different precipitants. The effect of the protein and precipitant concentration, and the pH value on the protein phase behavior was investigated after two hours (immediate effect) and after 40 days (effect of time).

The second and the third part of this thesis focused on the purification using HIC. Hydrophobic interaction chromatography is generally based on protein phase behavior and on the solubility of proteins in particular.

In the second part of this thesis, mixtures of kosmotropic and chaotropic salts were investigated. Usually, kosmotropic salts, that increase hydrophobic interactions between the adsorber ligand and the protein, are used in HIC, whereas chaotropic salts are known to increase the protein solubility up to a certain extend. By mixing kosmotropic with chaotropic salts, with a higher degree of chaotropic salt, increased binding capacities of different HIC adsorbers were achieved. By using an in-house-developed stalagmometric high-throughput technique, for determining the surface tension of protein solutions, a predictive method for forecasting binding behavior on HIC adsorbers was generated. Additionally, it was shown that the 'Cavity Theory', that states that higher surface tensions lead to higher binding capacities, is not valid for salt mixtures. Furthermore, a correlation between the aggregation temperature of the protein in the salt solution, that indicates the temperature at which the proteins in the solution start to aggregate, and the binding behavior was found. Lower aggregation temperatures were determined at conditions that yielded in the highest dynamic binding capacities.

The third part of this thesis questions the standard environmental conditions for HIC purification strategies. HIC is usually performed at neutral pH independent of the protein's nature. For critical questioning of this standard procedure, a high-throughput method on a robot-based pipetting platform was developed and used for three different proteins (with isoelectric points in the acidic, neutral and alkaline region) at six different pH values and at a constant salt concentration. In this way, the influence of the environmental pH on the binding behavior was investigated. Therefore, miniaturized robot-based chromatography columns (RoboColumns) were loaded with a constant protein concentration and the dynamic binding capacities were determined. It was shown, that binding close to the protein's isoelectric point leads to an increased binding capacity. The major influence on the binding capacity of HIC adsorbers was proven to be the vicinity to the solubility limit. Conditions closer to the solubility limit resulted in higher binding capacities. In addition, an inverse correlation between the binding kinetics and the binding capacity was discovered. Slower binding kinetics entailed higher binding capacities. Thus, it was assumed that at slower binding kinetics a reorientation of the protein during the binding process takes place. As a consequence of this directed binding, more proteins can bind to the adsorber surface. The increased binding capacity is not accompanied by a change of the protein structure. This was proven by a multi-variate data analysis (MVDA) of protein spectra of the applied sample and the elution fractions.

The last part of this thesis connects the aforementioned fields. Reaching the equilibri-

um of protein precipitant solutions is a time-consuming process. Therefore, estimating protein phase behavior in a fast way is desirable. The method for generating phase diagrams, developed in the first part of this thesis, was used to evaluate the phase behavior of glucose isomerase at twelve different pH values with four different salts at a constant protein concentration. By using a multi-component buffer, a constant buffer capacity in the investigated pH range was ensured. The phase behavior of glucose isomerase in a pH range of pH 4.2 to pH 7.0 using sodium sulfate, ammonium sulfate, sodium chloride, and ammonium chloride as precipitants was determined. Besides soluble conditions precipitation, crystallization, and skin formation were observed. Using HIC bind-elute experiments to determine the hydrophobicity of glucose isomerase, a correlation of crystal form and size to the retention behavior in HIC was found. By measuring the melting and aggregation temperatures with an Optim®2 system, conformational and colloidal stability were investigated. Stabilizing and destabilizing effects of the different precipitants were determined by these measurements and directly correlated to the phase behavior. The anions of the investigated salts were identified to have the main influence on protein stability. In summary, the phase behavior of glucose isomerase can be estimated by HIC experiments and thermal stability measurements in relation to variations of parameter settings in a fast way.

Usually, generating phase diagrams and reaching equilibrium in protein-precipitant solutions is a very time-consuming process. Thus, the linking and predicting of protein stability with fast analytical methods is a great advantage for the biopharmaceutical industry. Additionally, increased dynamic binding capacities for HIC adsorbers, founded on knowledge of protein phase behavior, is a great improvement, making HIC a good alternative to ion-exchange chromatography.

Zusammenfassung

In der Entwicklung eines Biopharmazeutikums durchläuft das Zielprotein viele Prozessschritte in der Kulitiverung (Upstream) und Aufarbeitung (Downstream). Bei jedem Teilprozess ändern sich die Umgebungsbedingungen und beeinflussen somit die Proteineigenschaften, wie beispielsweise die Oberflächenladung, -hydrophobizität oder die Proteinstruktur. Da jedes Protein andere Eigenschaften besitzt, reagiert es unterschiedlich auf Umgebungsänderungen. Die veränderten Eigenschaften können diverse negative Auswirkungen auf die Ausbeute des Produktes haben. Beispielsweise kann es bei der Kultivierung und Produktbildung zu Produktverlust durch Bildung von Einschlusskörperchen (inclusion bodies) kommen. Hierbei handelt es sich um falsch gefaltete Proteinagglomerate, die meist mit einem Funktionsverlust des Proteins einhergehen. Doch auch richtig gefaltete Proteine können im späteren Verlauf des Prozesses ungewollt präzipitieren oder kristallisieren und somit Rohre, Filter oder Chromatographiesäulen verblocken. Diese Effekte können auch bei der Formulierung und Lagerung auftreten. Aus diesen Gründen ist es notwendig, Prozessschritte in der biopharmazeutischen Industrie zu charakterisieren, um Auswirkungen auf das Phasenverhalten des Proteins abschätzen zu können. Faktoren, die die Proteineigenschaften beeinflussen, sind beispielsweise Salztyp, Salzkonzentration, Additive, der pH-Wert oder die Proteinkonzentration. Neben den genannten negativen Aspekten solcher Phasenübergänge können Präzipitation und Kristallisation, unter anderem basierend auf elektrostatischen und hydrophoben Wechselwirkungen, auch gezielt als Aufreinigungsschritte eingesetzt werden. Diese Interaktionen spielen auch bei der Ionenaustauschchromatographie (IEC) und der hydrophoben Interaktionschromatographie (HIC) eine entscheidende Rolle.
Um das Phasenverhalten von Proteinen ausreichend zu charakterisieren und den 'Time to Market'-Ansprüchen zu genügen, sind Hochdurchsatzexperimente das Mittel der Wahl. Hierbei wird auf robotergestützte Pipettierplattformen zurückgegriffen, um im Mikrolitermaßstab parallelisiert Experimente (high-througput screenings – HTS) durchführen zu können. Durch die Generierung großer Datenmengen unter Verwendung von HTS-Methoden ist eine parallele Entwicklung schneller Hochdurchsatz-Analytikmethoden unabdingbar. So können alle Experimente schnell und genau ausgewertet und Zusammenhänge erkannt werden.
Als Konsequenz der 'Quality by Design'(QbD)-Richtlinien in der Industrie sind verschiedene Arten der statistischen Versuchsplanung ('Design of Experiments' – DoE) zur Regel geworden. Während für die Entwicklung vieler pharmazeutischer Teilprozesse HTS und QbD bereits als Standard implementiert sind, basieren Aufreinigungsmethoden mittels HIC hauptsächlich noch auf Erfahrungswerten und Daumenregeln (heuristische Ansätze). Überwiegend wird bei neutralem pH und einer Standardsalzkonzentration aufgereinigt, unabhängig von der Natur des Zielproteins. So kann es je nach Protein vorkommen, dass die Aufreinigung unter suboptimalen Bedingungen durchgeführt und die vergleichsweise schon geringe Bindekapazität von HIC-Adsorbern noch weiter herabgesetzt wird.
Der erste Teil dieser Dissertation beschäftigt sich mit dem Phasenverhalten von Proteinen in Abhängigkeit von Präzipitanten und pH-Werten. Dazu wurde eine robotergestützte Hochdurchsatzmethode zur Generierung von Phasendiagrammen im Mikroliter-Maßstab entwickelt. Mithilfe dieser schnellen und automatisierten Methode wurden erfolgreich Phasendiagramme mit geringem Materialaufwand erstellt. Für das Anfertigen eines sol-

chen Phasendiagrammes, zur Untersuchung des Phasenverhaltens eines Proteins bei variierender Proteinkonzentration und variierender Salzkonzentration bei einem konstanten pH-Wert, werden weniger als 150 mg Protein benötigt. Es wurden im Gegensatz zu bisherigen Studien keine Silikonöle verwendet, um heterogene Keimbildung zu vermeiden. Der Nachteil der mit Dampfdiffusion ('Hanging Drop' und 'Sitting Drop') einhergehenden nicht bestimmbaren tatsächlichen Präzipitanten- und Proteinkonzentrationen beim Phasenübergang, konnte ebenso ausgeschlossen werden. Hierfür wurde in den verwendeten Microbatch-Wells durch Abkleben mit einer nicht im UV-Bereich absorbierenden Folie eine gesättigte Atmosphäre geschaffen. Durch die Lagerung der Microbatch-Platten in einer vollautomatisierten, temperierten Einheit (Rock Imager 54), zum regelmäßigen Fotografieren der Proben, konnten unmittelbare sowie Langzeitstabilitätsuntersuchungen durchgeführt werden. So wurden die Phasendiagramme nach 40 Tagen ausgewertet, da zu diesem Zeitpunkt davon ausgegangen werden konnte, dass sich ein Gleichgewicht eingestellt hatte. Diese neue Methodik zur Erstellung von Phasendiagrammen im Hochdruchsatz wurde für vier verschiedene Proteine bei vier verschiedenen pH-Werten mit vier verschiedenen Präzipitanten angewandt. So konnten innerhalb kürzester Zeit (zwei Stunden) die unmittelbaren und die zeitlichen (40 Tage) Einflüsse der verschiedenen Parameter auf das Phasenverhalten des jeweiligen Proteins untersucht werden.
Die hydrophobe Interaktionschromatographie ist ebenfalls eng mit dem Proteinphasenverhalten verknüpft. Insbesondere das Löslichkeitsverhalten der Proteine spielt eine vordergründige Rolle. Auf die Aufreinigung mittels HIC fokussieren sich der zweite und der dritte Teil dieser Dissertation.
Im zweiten Teil dieser Arbeit wurden zunächst Mischungen von kosmotropen und chaotropen Salzen untersucht. Üblicherweise werden bei HIC ausschlielich kosmotrope Salze verwendet, da diese hydrophobe Wechselwirkungen zwischen Adsorber und Protein steigern, während chaotrope Salze bis zu einem gewissen Grad die Löslichkeit von Proteinen steigern. Durch das Mischen von kosmotropen mit chaotropen Salzen mit einem höheren Anteil an chaotropem Salz, konnten erfolgreich Bindekapazitätssteigerungen auf verschiedenen HIC-Adsorbern erzielt werden. Durch das Verwenden eines in der Arbeitsgruppe entwickelten stalagmometrischen Hochdurchsatzverfahrens zur Bestimmung der Oberflächenspannung von Proteinlösungen, konnte eine prädiktive Methodik generiert werden, die Vorhersagen des Bindeverhaltens auf HIC-Adsorbern ermöglicht. Zusätzlich konnte gezeigt werden, dass die 'Kavitätstheorie', die besagt, dass eine höhere Oberflächenspannung zu höheren Bindekapazitäten führt, nicht für Salzmischungen gültig ist. Des Weiteren konnte erfolgreich eine Korrelation zwischen der Aggregationstemperatur des Proteins, die angibt ab welcher Temperatur die Proteine in der Lösung aggregieren und des Bindeverhaltens in verschiedenen Salzlösungen gefunden werden. Geringere Aggregationstemperaturen wurden bei den Bedingungen ermittelt, bei denen die höchsten dynamischen Bindekapazitäten erzielt wurden.
Im dritten Teil dieser Arbeit wurden die Standardumgebungsbedingungen bei der Aufreinigung mit HIC hinterfragt. Da HIC üblicherweise bei neutralem pH durchgeführt wird, ohne die Natur des Proteins zu berücksichtigen, wurde zur kritischen Hinterfragung eine Hochdurchsatzmethode auf einer robotergestützten Pipettierplattform für drei Proteine (mit isoelektrischen Punkten im sauren, neutralen und basischem Bereich) bei sechs verschiedenen pH-Werten und einer konstanten Salzkonzentration entwickelt. So konnte der Einfluss des Umgebungs-pH-Wertes auf das Bindeverhalten untersucht werden. Da-

zu wurden miniaturisierte, roboterbasierte Chromatographiesäulen (RoboColumns) mit einer konstanten Proteinkonzentration beladen und die Bindekapazitäten ermittelt. Es konnte gezeigt werden, dass das Binden in der Nähe des isoelektrischen Punktes des Proteins zu einer erhöhten Bindekapazität führt. Den generell größten Einfluss auf die Bindekapazität von HIC-Adsorbern zeigte die Wahl des Arbeitspunktes in Abhängigkeit der Löslichkeitsgrenze. Je näher die Bedingung an der Löslichkeitsgrenze des Proteins gewählt wurde, desto höher war die erreichte Bindekapazität. Zustätzlich wurde ein reziproker Zusammenhang zwischen der Bindekinetik und der Bindekapazität festgestellt. Eine hohe Bindekapazität hatte somit eine langsame Bindekinetik zur Folge. Es wird vermutet, dass bei langsamerer Kinetik eine Umorientierung des Proteins während der Bindung stattfindet und sich durch diese gerichtete Bindung mehr Proteine an den Adsorber anlagern können. Die gesteigerte Bindekapazität ging nicht mit einem Strukturverlust des Proteins einher, was durch eine multi-variate Datenanalyse von Proteinspektren der Ausgangs- und Elutionsproben gezeigt werden konnte.
Der letzte Teil dieser Dissertation verbindet die zuvor genannten Bereiche. Das Einstellen des Gleichgewichtes von Protein-Präzipitant Lösungen dauert lange. Deshalb ist es wünschenswert, die Stabilität von Proteinen schnell und prädiktiv vorhersagen zu können. Die im ersten Teil dieser Dissertation entwickelte Methode zur Generierung von Phasendiagrammen wurde angewandt, um das Phasenverhalten von Glucose Isomerase bei zwölf verschiedenen pH-Werten und mit vier verschiedenen Salzen bei einer konstanten Proteinkonzentration zu evaluieren. Durch Verwenden eines Mehrkomponenten-Puffers konnte eine konstante Pufferkapazität im gesamten untersuchten pH-Bereich gewährleistet werden. Das Phasenverhalten von Glucose Isomerase in einem pH-Bereich von pH 4.2 bis pH 7.0 wurde für die Präzipitanten Natriumsulfat, Ammoniumsulfat, Natriumchlorid und Ammoniumchlorid bestimmt. Neben löslichen Bedingungen wurden Präzipitation, Kristallisation und Hautbildung beobachtet. HIC Binde- und Elutionsexperimente wurden verwendet, um die Hydrophobizität von Glucose Isomerase zu bestimmen. Dadurch konnte eine Korrelation zwischen Kristallform und -größe und dem Retentionsverhalten in HIC gefunden werden. Die Messung von Schmelz- und Aggregationstemperaturen mit einem Optim®2 System ermöglichte zusätzlich die Untersuchung von konformativer und kolloidaler Stabilität. Stabilisierende und destabilisierende Effekte der unterschiedlichen Präzipitanten konnten durch diese Messungen bestimmt und direkt mit dem Phasenverhalten korreliert werden. Als Haupteinflussfaktoren auf die Proteinstabilität konnten die Anionen der untersuchten Salze bestimmt werden. Es wurde deutlich, dass mittels HIC-Experimenten und thermischen Stabilitätsmessungen das Phasenverhalten von Glucose Isomerase in Bezug auf die Variation von Parametern in einer schnellen Art und Weise abgeschätzt werden kann.
Üblicherweise ist das Erstellen von Phasendiagrammen und das Erreichen des Gleichgewichtes der Protein-Präzipitant-Lösung ein sehr zeitintensiver Prozess. Deshalb ist die Verbindung von Proteinstabilität mit schnellen analytischen Methoden ein großartiger Vorteil für die biopharmazeutische Industrie. Zusätzlich ist die Steigerung der dynamischen Bindekapazität von HIC-Adsorbern, basierend auf dem Proteinphasenverhalten, eine große Verbesserung. HIC ist damit eine gute Alternative zur Ionenaustauschchromatographie.

Contents

1 Introduction

1.1 Biopharmaceutical Process Development

The main challenge in downstream process (DSP) development for a new biomolecule is that little is known about protein stability and solubility behavior of the target molecule and the impurities. Formerly, the one-factor-at-a-time methodology was the state-of-the-art approach to investigate the design space in DSP of biopharmaceuticals. This approach of varying only one parameter while the rest stays constant allows no investigation of correlated variables. Due to material and time restrictions, only a limited number of experiments could be performed with this methodology. The probability of missing the overall optimum was high. In many areas heuristic approaches, like experience of operators and rules of thumb have been the method of choice. In the last years and decades, high-throughput experimentation (HTE) has taken the place of the one-factor-at-a-time method. HTE means miniaturization and parallelization of experiments allowing for a variation of two or more factors at a time. This approach enhances the sample throughput, and results in a reduction of time, materials and costs (Czitrom [1999]). HTE can be realized and automated using robotic pipetting platforms, making it an easy tool for exploring the design space and finding the overall optimum. In contrast to the one-factor-at-a-time approach, HTE includes the consideration of interactions between different parameters. On the basis of HTE and HTS (high-throughput screening) new substantiated rules of thumb can be developed.
A commentary of Rathore et al. (Rathore and Winkle [2009]) stated that 'Quality by Design' (QbD) is now a central point in the 'Food and Drug Administration' (FDA) regulatory system. All biopharmaceutical drugs have to be approved by the FDA before reaching the market. The aim of QbD is to characterize a process and to find critical process steps influencing product quality. In this context HTE methods as well as 'Design of Experiments' (DoE) get into the focus. DoE includes the use of computational power to propose useful experiments. Generating phase diagrams for investigating protein phase behavior is one example of HTE as described in more detail in Chapter 1.3.5. Additionally, fast analytical tools for investigating protein properties, like measuring melting and aggregation temperatures or determining surface tension in high-throughput have to be developed. A fast analytical tool for investigating the different protein properties is multi-variate data analysis (MVDA) of protein spectra as published by Hansen et al. in 2013 (Hansen *et al.* [2013]). For example, by measuring the absorption spectra of a sample only, conclusions on the proteins' integrity can be drawn.

1.2 Protein Stability

During each step of upstream, downstream, and formulation processes it is essential to generate knowledge of the current phase behavior of the molecule of interest. During these steps the protein environment changes constantly: for instance, the pH value is adjusted for virus inactivation or the salt concentration is changed for binding to a chromatography column. These changes in the environment of the protein affect its phase behavior and can lead to undesired protein aggregation. Unwanted and uncontrolled precipitation or crystallization can lead to clogging of pipes or to column blocking during

the purification processes. In addition to these processing issues, injection of aggregates, for instance formed during the formulation processes or during storage, could even have lethal consequences for the patient. Thus, it is important to know under which mobile phase conditions the molecule of interest is stable or changes its phase state.
There are two forms of protein stability, namely, conformational (structural) and colloidal stability. The protein stability depends on long-range and short-range forces. One part of short-range forces are hydrophobic interactions. They are the main factor contributing to the protein conformation in terms of native and non-native form (Pace *et al.* [1996]). Hydrophobic interactions occur between non-polar and uncharged atoms. Amino acids with hydrophobic residues are oriented towards the core of the protein, when solvated in an aqueous solution. Hydrophobic amino acid residues include glycine, alanine, valine, leucine, isoleucine, phenylalanine, and tryptophan (Kyte and Doolittle [1982], Rose *et al.* [1985]). The orientation and accumulation of hydrophobic patches in the protein core is thermodynamically favorable (Carta and Jungbauer [2010]). Additionally, due to this accumulation in the core and the resulting small distances between the amino acids, attractive van-der-Waals forces come into play to stabilize the protein structure.
When salts are present, the overall dominating effect is the electrostatic shielding. When electrostatic long-range forces are shielded, the intermolecular distance of proteins is reduced. When this distance drops below a certain threshold, the short-range van-der-Waals forces become dominating and attractive forces between proteins are enhanced. This phenomenon is described in the DLVO (Deryagin-Landau-Verwey-Overbeek) theory (De Young *et al.* [1993]) which is illustrated in Figure 1 and describes effects during colloidal instability. Here, the free energy is shown as a function of the intermolecular distance in dependence of the salt concentration. The free energy is the energy that

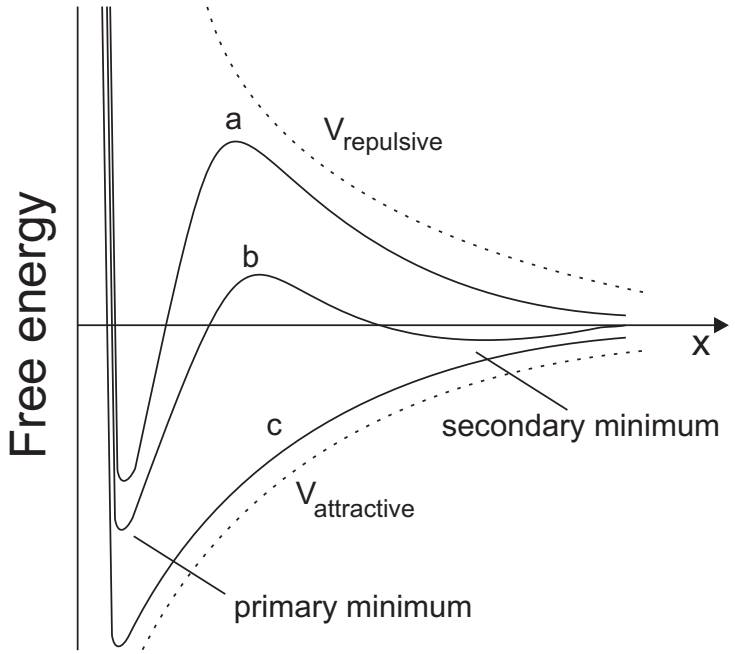

Figure 1: DLVO theory based on De Young *et al.* [1993]: $V_{attractive}$ (attractive van-der-Waals forces) and $V_{repulsive}$ (repulsive electrostatic forces) are plotted in dependence of the intermolecular distance. If the sum of these forces at low (a), medium (b), and high (c) salt concentrations is in the primary or secondary minimum, proteins aggregate. Otherwise the solution is stable.

is necessary to create a system that is in its equilibrium at a certain temperature. At positive free energy values, the protein stays soluble, whereas at negative free energy values the protein thermodynamically tends to aggregate. At low salt concentrations (curve a), the electrostatic repulsion between the protein molecules is dominating and a high free energy barrier (local curve maximum) prevents the protein from aggregating. At medium salt concentrations (curve b) the repulsive and the attractive forces become more balanced. In the primary minimum the proteins aggregate irreversibly, whereas the aggregation in the secondary minimum is usually reversible. Using high salt concentrations (curve c), the electrostatic charges are strongly shielded and the van-der-Waals forces dominate, leading to irreversible aggregation in the primary minimum (De Young *et al.* [1993]). Under high salt conditions the energy barrier is entirely eliminated.

1.3 Influencing Factors on Protein Stability

As indicated above, various factors can influence protein stability. The most common parameters influencing protein stability are salt type and salt concentration. However, parameters like temperature and pH value also play an important role.

1.3.1 Influence of Salts on Protein Stability

Salts have complex effects on the stability of proteins. The ionic strength of salts influences long-range electrostatic forces and short-range forces, like hydrophobic interactions, hydrogen bonding, and van-der-Waals forces (Chi *et al.* [2003], Neal *et al.* [1999]) as partially described in the DLVO theory. Furthermore, these effects are described in the preferential interaction theory, postulated by Arakawa et al. (Arakawa *et al.* [1990], Arakawa and Timasheff [1984a]). The effect of salt ions can be divided into two types: preferential binding of ions to the protein and preferential exclusion from the protein surface. In 1888 Franz Hofmeister arranged salt ions in order of their propensity of precipitating proteins (Hofmeister [1888]). This Hofmeister series (Figure 2) can be divided into kosmotropic ions (left side) and chaotropic ions (right side). Chaotropic ions/salts are nonpolar and weakly hydrated. They preferentially bind to proteins and therefore enhance protein solubility (salting-in) (Arakawa and Timasheff [1984a]) but destabilize the native protein conformation at the same time at high salt concentrations. Preferential exclusion from the protein surface is rather induced by polar kosmotropic ions/salts. Kosmotropic ions increase the protein stability but decrease the protein solubility (salting-out) due to their strongly hydrated character. As a consequence, water molecules around the protein surface are retracted and, thus, hydrophobic patches are exposed leading to an

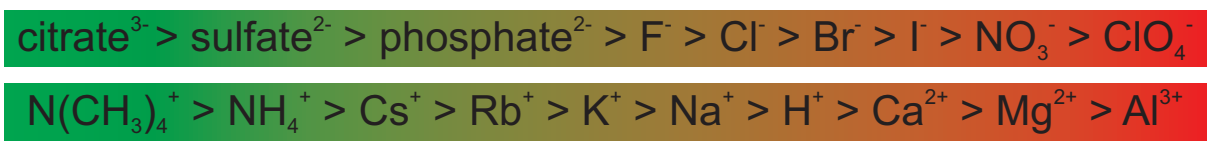

Figure 2: In the Hofmeister series, postulated by Franz Hofmeister in 1888 (Hofmeister [1888]), salt ions are arranged due to their propensity of precipitating proteins. Kosmotropic ions (left side) decrease the solubility of proteins whereas chaotropic salts (right side) increase the solubility.

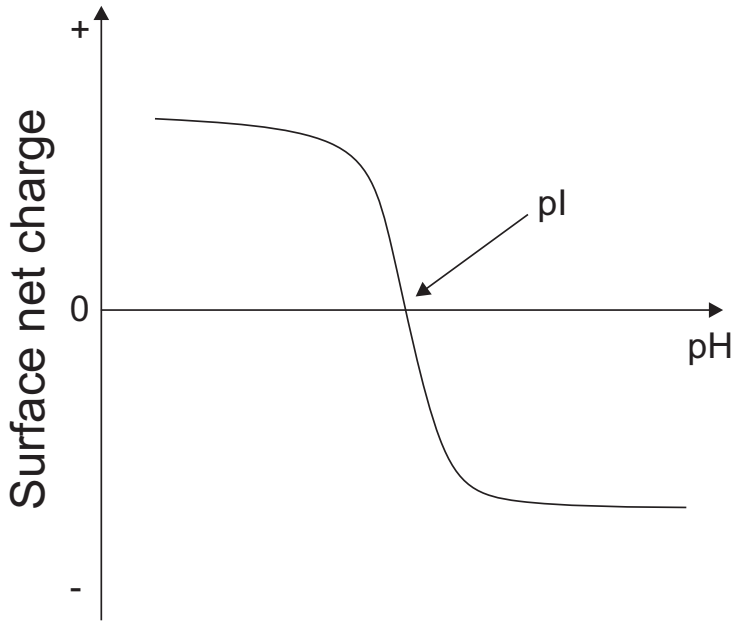

Figure 3: Surface net charge of a protein in dependence of the pH value. At the isoelectric point (pI) the surface net charge is zero.

enhanced aggregation propensity. Due to their propensity of enhancing protein solubility, chaotropic salts can be used for the unfolding step in inclusion body refolding (Berg *et al.* [2012]). Ammonium sulfate as a kosmotropic salt can be used for selective precipitation as a purification step. In 2002, Arakawa et al. (Arakawa [2002]) renewed a postulation of a constant protein hydration independent from the preferential interaction or exclusion of the salt.

1.3.2 Influence of pH Value on Protein Stability

Besides salt influences, also other factors like the pH value have to be considered regarding protein stability. The pH value of a buffer in the environment of a protein has a big influence on the protein and its phase behavior (Furuike *et al.* [1999]). The pH value defines the charge distribution of the acidic and alkaline amino acid residues of proteins (Klempnauer *et al.* [2011]). Depending on the pH value the charge of the amino acids changes. The isoelectric point (pI) describes the pH value at which the protein's net surface charge is zero (Figure 3). At pH values below the pI, the protein carries a positive net charge. With increasing pH value the amino acids get deprotonated and the protein net charge shifts to negative (McMurry [2010]). Equally charged proteins and protein patches repel each other and the aggregation propensity decreases. In the vicinity of the pI, these electrostatic forces are minimized, leading to intermolecular interactions (Chapter 1.2).

1.3.3 Influence of Temperature on Protein Stability

The temperature is another factor influencing protein stability. Temperature describes the degree of kinetic energy in form of vibrational motion of molecules (Wang *et al.* [2010b]). In solution, the Stokes-Einstein equation (1) describes the diffusion coefficient D in dependence of temperature T, dynamic viscosity of the solvent η, Boltzmann constant k_B, and the hydrodynamic radius R_0.

$$D = \frac{k_B T}{6\pi\eta R_0} \tag{1}$$

A temperature increase leads to an increase in the diffusion velocity of proteins in solution and thus in an increased probability of protein molecule collision. These collisions have an increased chance of overcoming the activation energy for protein aggregation. Thus, aggregation can happen without previous protein unfolding (Chi *et al.* [2003]). Additionally, degradative reactions like deamination or oxidation are enhanced (Mahler *et al.* [2009]). The reaction velocity of chemical reactions can be described by the Arrhenius equation (2).

$$k = Ae^{-\frac{E_A}{RT}} \tag{2}$$

With k being the reaction velocity constant, A being a frequency factor, E_A being the activation energy, R being the universal gas constant, and T being the temperature. Nevertheless, there is no linear correlation between this Arrhenius equation and protein aggregation behavior because also other interactions, like hydrophobic interactions, are present. By temperature increase, hydrogen bridges and hydrophobic interactions in the protein core are weakened (Wang *et al.* [2010b]) and proteins can unfold. As mentioned above, this can result in protein aggregation. In 2008, Lin et al. (Lin *et al.* [2008]) showed, that temperature modifies the protein nucleation zone in an unpredictable way. Lysozyme in solution, for example, precipitates when stored at low temperatures which contradicts the temperature effects discussed earlier.
Additionally, temperature has an indirect influence on the phase behavior as the pK_a value of a buffer is temperature dependent (Equation 3) (Debye and Hückel [1923]).

$$pK_a^* = pK_a - \frac{1.82410^6}{(\epsilon T)^{3/2}}|z^+ z^-|\sqrt{I} \tag{3}$$

With pK_a^* being the corrected pK_a value, ϵ being the dielectric constant of the solution, T being the temperature, z being the charge of the ion, and I being the ionic strength. Therefore, a temperature shift changes the pH value of the buffer and thus the protein phase behavior (Chapter 1.3.4).

1.3.4 Protein Phase Behavior

All the effects influencing protein phase behavior can result in different phase states depending on the environmental conditions like present precipitants, the pH value of the buffer and many other parameters. Depending on these conditions, the protein can either stay in solution or form aggregates. Aggregation includes every form of phase transition.

Figure 4: Proteins can undergo phase transitions into different phase states: clear solution (soluble), crystal, precipitate, gel, skin, and liquid-liquid phase separation.

Typical phase transitions are precipitation or protein crystallization. Besides clear solution, crystals, and precipitate, also gel and skin formation as well as liquid-liquid phase separation can occur (Figure 4). Partial or total protein denaturation are assumed to be the cause for the formation of gel and skin (Ahamed *et al.* [2007a], Asherie [2004], Baumgartner *et al.* [2015]). Liquid-liquid phase separation is induced by depletion of polymers like polyethylene glycol (Vlachy *et al.* [1993]) resulting in protein-rich droplets. These droplets are said to be protein-rich subphases that often induce protein crystallization.

1.3.5 Protein Phase Diagrams

With the aforementioned guidelines, protein stability can be estimated. However, a distinct knowledge of real phase behavior is mandatory. The common way of determining and illustrating protein phase behavior in a certain environment is the generation of protein phase diagrams. Typically, a phase diagram visualizes the phase behavior at varying protein and precipitant concentrations (Figure 5). The classical diagram is separated into an undersaturated area, in which the protein remains soluble and an oversaturated area, in which the protein tends to aggregate. The oversaturated area itself is divided into three subareas: the metastable, the labile, and the precipitation area. In the metastable area, the oversaturation of the protein solution is not sufficient for crystal seed formation,

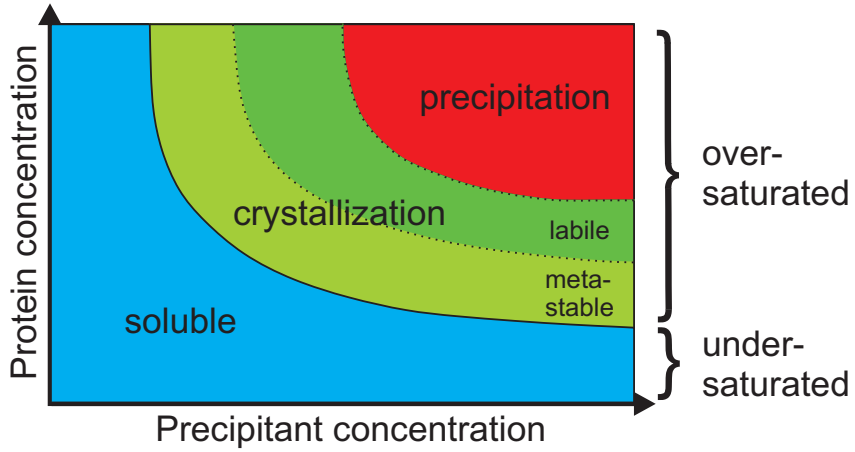

Figure 5: Protein phase behavior is shown at varying protein concentration in dependence of precipitant concentration. The phase diagram can be divided into two parts: an undersaturated and an oversaturated area. In the undersaturated area the protein remains soluble. The oversaturated area itself can be divided into three subareas. In the metastable area the protein oversaturation is not sufficient to cause spontaneous crystallization. Existing nuclei are needed. In the labile region the protein crystallizes and in the precipitation area the protein precipitates.

but existing crystals will already grow. In the labile region, the protein crystallizes and in the precipitation area the protein forms amorphous structures called precipitate.
A fast and elegant way of generating protein phase diagrams is using robotic pipetting platforms. This high-throughput methodology allows for parallel pipetting of small volumes of protein and precipitant solutions. State of the art is using vapor diffusion experiments like hanging or sitting drop (Chayen and Saridakis [2008], Luft and DeTitta [2009]). Here, an undersaturated protein solution equilibrates against a reservoir with a higher precipitant concentration. Thus, the drop volume of the protein solution decreases and the protein and precipitant concentrations increase. Phase transitions occur when the supersaturation is sufficiently high (Asherie [2004]). The disadvantage of these methodologies is the unknown exact composition of the protein-precipitant solution, when the phase transition happens. To eliminate these shortcomings microbatch experiments can be used. Commonly, silicone oils are used to cover the protein-precipitant solution in the microbatch plates to prevent evaporation. The drawback of this technique is that the oils can interfere with the protein and its phase behavior and can for example result in heterogeneous nucleation.

1.4 Column Chromatography for Proteins

The environment of the target molecule is decisive for biopharmaceutical downstream process steps, like chromatography, when purifying biomolecules. Unwanted aggregation during purification steps can have fatal consequences. The environmental conditions that can be applied for the purification, can be screened by using robotic platforms and HTE methods (Chapter 1.1) and by generating protein phase diagrams (Chapter 1.3.5).
Chromatography is the most frequently used methodology for purifying biomolecules (Jungbauer [2005]). It is mainly based on interactions of the target molecule in the mobile phase with the stationary phase. In Figure 6, the four most commonly used types

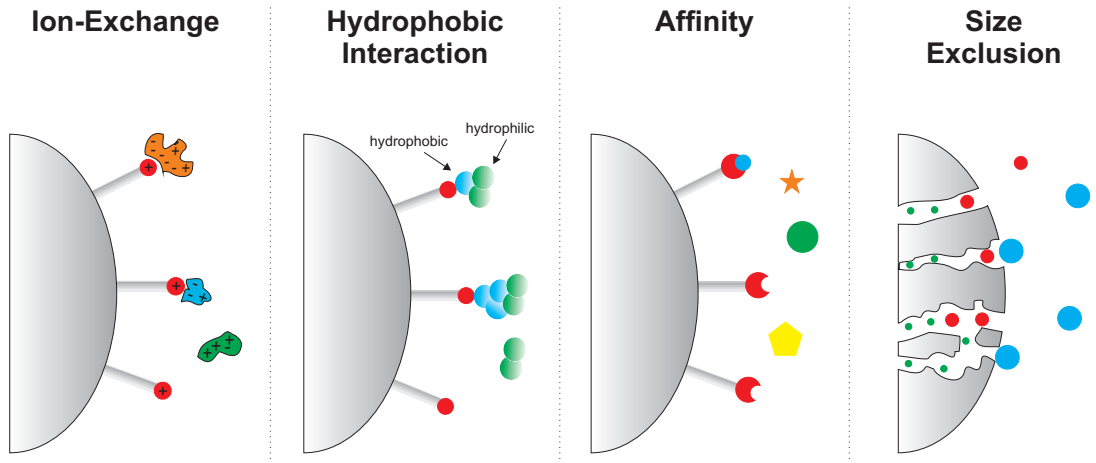

Figure 6: The four most common chromatography types are ion-exchange chromatography (IEX), hydrophobic interaction chromatography (HIC), affinity chromatography (AC), and size exclusion chromatography (SEC). In IEX the charged proteins bind to oppositely charged ligands. HIC is based on hydrophobic interactions of the proteins with the hydrophobic ligands. In AC specific binding of the molecule to the affinity ligand takes places. And in SEC biomolecules are separated due to difference in size.

Table 1: The four most frequently used types of chromatography and their purification mechanisms

Mode of action	Chromatography type	Purification mechanism
Binding	Ion-exchange chromatography	Electrostatic interactions
Binding	Hydrophobic interaction chromatography	Hydrophobic interactions
Binding	Affinity chromatography	Specific affinity interactions
Non-binding	Size exclusion chromatography	Size

of chromatography are illustrated schematically. Table 1 gives a short overview of the purification mechanisms.
Ion-exchange chromatography (IEX) is the most frequently used methodology in the biopharmaceutical industry. Using IEX, the target molecule binds with its charged surface patches to the oppositely charged adsorber ligands under low-salt conditions. When the target molecule is positively charged the cation-exchange (CEX) resin carries a negatively charged ligand. For a negatively charged biomolecule the anion-exchange (AEX) resin is positively charged. Elution is performed by increasing the salt concentration and shielding the electrostatic interactions and displacing the bound biomolecules with salt ions. An alternative can be a pH shift and, thus, changing the net charge of the biomolecule.
Purification via hydrophobic interaction chromatography (HIC) is based on hydrophobic interactions of the target molecules with the hydrophobic adsorber ligands. HIC as the central chromatography type of this thesis is described in more detail in Chapter 1.5.
Affinity chromatography (AC) is a highly specific kind of chromatography. Here, the adsorber ligand is specific to the target molecule and in theory no other molecules can bind. However, it is very complex to find an affinity ligand for the target molecule and the development of a new affinity resin is very expensive.
A chromatography method without any specific interactions is size exclusion chromatography (SEC) / gel filtration. Using SEC, the molecules are separated based on their size only. For this type of chromatography, no binding or interaction of the molecules with the adsorber takes place. The adsorber resin has different pore sizes and thus smaller molecules can diffuse into all pores whereas bigger molecules cannot penetrate each pore and therefore pass the chromatography column faster.

1.5 Hydrophobic Interaction Chromatography

Hydrophobic interaction chromatography (HIC) is one of the most frequently used purification methods in biopharmaceutical industry. Binding is promoted at high salt concentrations and elution is performed by lowering the salt concentration. By the use of kosmotropic salts (see Chapter 1.3.1), hydrophobic interactions are promoted. Due to the high salt concentrations under binding conditions, it can be assumed that electrostatic interactions are eliminated and predominantly hydrophobic interactions are decisive. However, the real mechanism of HIC is not entirely understood so far. Different theories were proposed in the last decades including the preferential interaction theory, the solvophobic, and cavity theory (Arakawa and Timasheff [1984a], Melander and Horváth [1977]). The preferential interaction theory was described in more detail in Chapter 1.3.1. The solvophobic theory (Horváth *et al.* [1976]) describes a correlation between the molal salt concentration, the surface tension of the protein-salt solution and the capacity factor in

HIC (Equation 4; Melander and Horváth [1977]).

$$ln(k') = ln(k'_0) - \frac{Bc^{0.5}}{1 + Cc^{0.5}} - \Lambda c + \Omega\sigma c \tag{4}$$

With $ln(k')$ being the logarithmic retention factor and $ln(k'_0)$ being the retention factor of pure water. B and C are empirical parameters proportional to the protein surface charge. c is the molal concentration. Λ and Ω σ describe salting-in and salting-out constants. σ is the increase in the surface tension that can be determined by Equation 5.

$$\sigma = \frac{\gamma - \gamma_0}{c} \tag{5}$$

With γ being the surface tension of the sample and γ_0 being the surface tension of pure water. According to Melander et al. (Melander and Horváth [1977]) kosmotropic salts increase the surface tension to a higher extent than chaotropic salts. The salt ions are solvated with water molecules (Xia *et al.* [2004]). Cavities are formed and closed around hydrophobic areas on the stationary and mobile phase upon binding (Xia *et al.* [2004]). The formation of cavities is described in the cavity theory (Melander and Horváth [1977]). Surface tension must be overcome to accommodate protein molecules in solution. When a salt, that increases the surface tension (salting-out salt), is present a higher input in energy is required for this mode of action, which is thermodynamically unfavorable. Therefore, protein-protein or protein-ligand interactions are provoked, reducing the surface area and consequently the free energy. However, this theory is neither valid when the salt strongly interacts with the proteins (Xia *et al.* [2004]) nor at low salt conditions. At low salt conditions the electrostatic interactions are not completely shielded and adsorption due to IEX mechanism is promoted (Melander and Horváth [1977]).
Altogether, HIC is an entropy driven process. The hydrophobic surface areas are reduced when proteins bind to hydrophobic ligands. The structured water molecules surrounding the hydrophobic patches are released into the bulk water and the entropy increases.

$$\Delta G = \Delta H - T\Delta S \tag{6}$$

An increase in entropy (S) results in a decrease in the free energy (G) (Equation 6). H is the enthalpy and T is the temperature. The decrease of G due to binding of proteins to hydrophobic ligands is thus thermodynamically favorable (Jungbauer *et al.* [2005]).

1.6 Linking of Protein Phase Behavior and Hydrophobic Interaction Chromatography

Protein phase behavior is the key factor in biopharmaceutical development. The current protein phase state influences each process step and, thus, is mandatory to be controlled. By generating protein phase diagrams, statements on protein phase behavior can be made. The knowledge of the phase behavior is the requirement for using chromatography as purification step. Especially when using hydrophobic interaction chromatography (HIC), the effects of high salt concentrations on the protein phase behavior is important. Thus, HTE can be used to screen for optimal binding conditions for improving binding behavior in HIC under stabilized conditions.

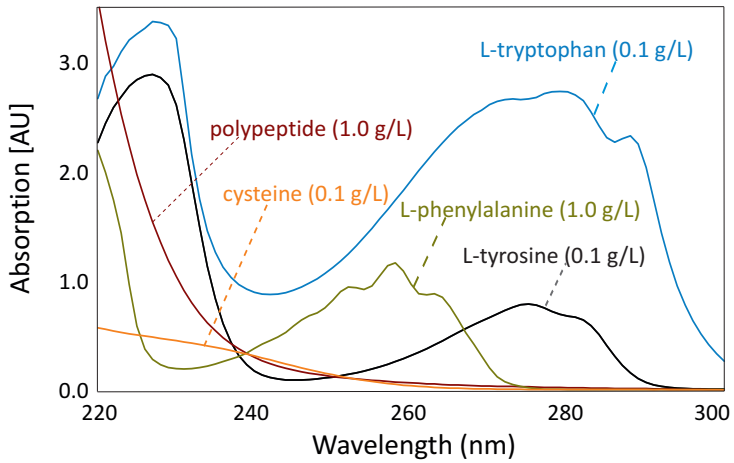

Figure 7: Absorption spectra of amino acids – proteins have different compositions of amino acids resulting in different protein absorption spectra (Hansen *et al.* [2013]).

Additionally, fast analytical methods like surface tension measurements or thermal stability determinations are necessary. When a protein changes its native form and (partially) unfolds, the conformational stability is changed. By unfolding, more hydrophobic patches are exposed and aggregation propensity is also enhanced (colloidal stability). An elegant way to determine the conformational stability is by measuring the melting temperature of proteins. Differential scanning fluorescence is a common way to determine the melting temperature (Goldberg *et al.* [2011]). Here, extrinsic dyes like SYPRO Orange are added to the sample and bind to hydrophobic protein patches. As described above, hydrophobic patches are exposed upon unfolding resulting in a change in the fluorescence signal. A huge disadvantage of this methodology is the insertion of the extrinsic dye which might influence and change the phase behavior of the protein.
For determination of colloidal stability, the aggregation temperature is a good indicator. By using static light scattering in dependence of temperature, the point of aggregation can be measured. A new high-throughput device that combines fluorescence measurement and static light scattering is the Optim®2 system. The big advantage besides the small sample consumption and the possibility of performing parallelized measurements is that no extrinsic dyes are necessary for determining the melting temperatures. Optim®2 measures intrinsic fluorescence evoked by the intrinsic tryptophan residues of the protein. The fluorescence spectrum shifts to red wavelengths during protein unfolding when the environment changes from hydrophobic to hydrophilic in the vicinity of tryptophan residues. This label-free technology prevents from falsified results due to extrinsic dyes.
Other possibilities to investigate conformational and colloidal stability include spectral analysis of protein solutions. Each exposed amino acid contributes to a certain extend to the total protein spectrum (Figure 7). Upon unfolding or aggregation, new residues are exposed or covered, leading to a spectral change.

Summarizing, generating knowledge of protein phase behavior as well as analytical tools for predicting protein stability are desirable to optimize and characterize existing and new processes for biopharmaceutical molecules.

2 Research Proposal

This dissertation is part of the project entitled 'Protein aggregation during production of modern biopharmaceuticals', funded by the German Federal Ministry of Education and Research (BMBF). In this project the big task of protein aggregation is tackled.
During each step of upstream, downstream, and formulation processes it is mandatory to know the current physical state of the molecule of interest. During these steps the protein environment changes constantly: for instance, the pH value is adjusted for virus inactivation or the salt concentration is increased for better binding to a chromatography column. These changes in the environment of the protein affect its phase behavior. For example, pH values near the isoelectric point of the protein or high salt concentrations are known to cause protein aggregation. Unwanted and uncontrolled precipitation or crystallization can lead to clogging of pipes and columns during the purification process. In addition to these processing issues, injection of aggregates, for instance formed during the formulation processes or during storage, could even have lethal consequences for the patient. Thus, it is important to know under which mobile phase conditions the molecule of interest is soluble or changes its phase state. The whole project is focused on the task of aggregation. In Figure 8, the four different parts of the project are shown. There is on part that focuses on the fermentation process and its parameters (P1 & P2). Project

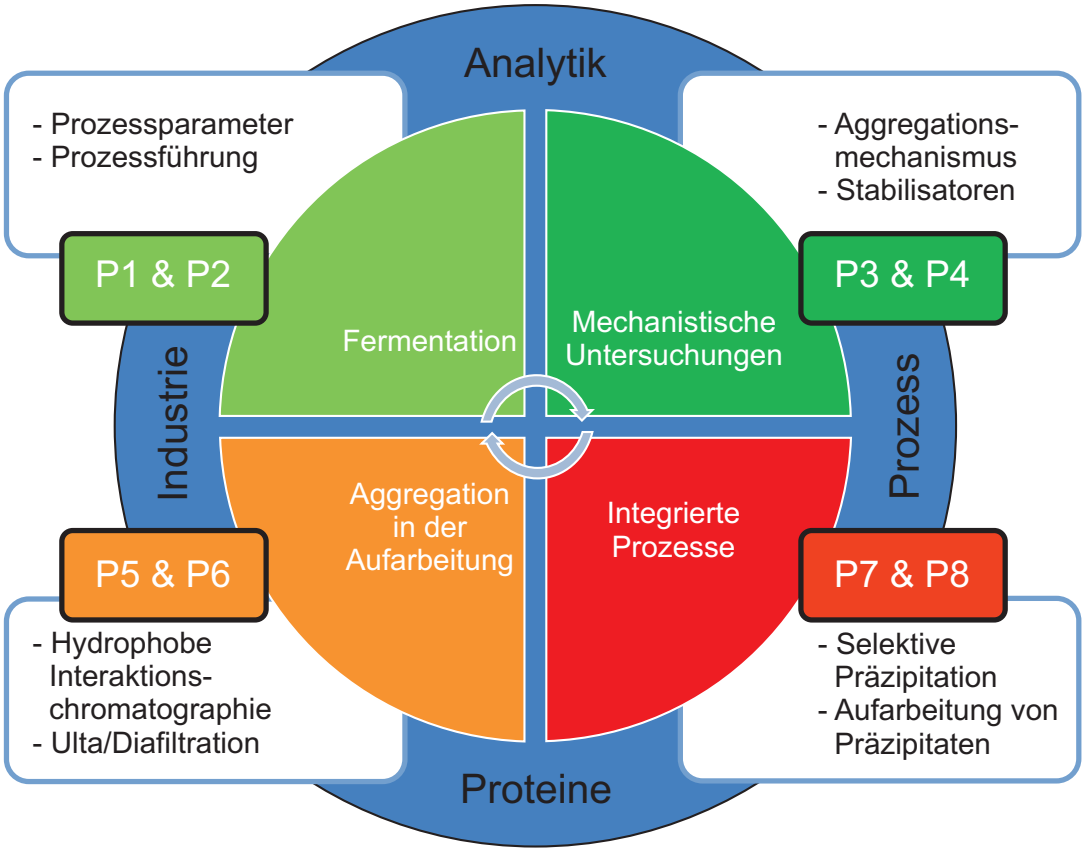

Figure 8: Overview over the project 'Protein aggregation during production of modern biopharmaceuticals'. The project is separated into four different parts: aggregation during fermentation, mechanistic understanding of the aggregation process, aggregation during purification and integrated processes.

P3 & P4 focus on getting an mechanistic understanding of the aggregation processes. P5 & P6 focus on the aggregation during the purification processes and P7 & P8 use aggregation as a selective tool in integrated processes. This thesis deals with project P5, aggregation during purification using hydrophobic interaction chromatography.
In the last decades high-throughput technologies have become state of the art in the biopharmaceutical industry. Using automated robotic platforms, a variety of parameters can be tested in a short time. Due to the 'Time to Market' issue and the low amount of pure and often expensive molecule of interest during early-stage process development, a fast methodology for determining the phase behavior is needed with small target molecule consumption.
Therefore, an automated high-throughput methodology for the generation of protein phase diagrams in μL-scale, to create knowledge of phase behavior in a fast and easy way has to be developed. This methodology offers the basis of environmental conditions in the purification processes. The use of high salt concentrations in the purification of biomolecules with hydrophobic interaction chromatography (HIC) is challenging. Protein solubility is strongly limited. Additionally, the binding capacities of HIC adsorbers are comparatively low. New strategies for finding optimal binding conditions in HIC to increase the binding capacities have to be developed. As HIC is based on hydrophobic interactions, conversely this methodology can assumedly be used to predict protein phase behavior under high-salt conditions. At these conditions electrostatic interactions are shielded and mainly short-range forces like hydrophobic interactions are present. Additionally, other fast analytical tools to estimate protein phase behavior are desirable.

3 Publications & Manuscripts

1. **Determination of protein phase diagrams by microbatch experiments: Exploring the influence of precipitants and pH**

   Kai Baumgartner[‡], Lara Galm[‡],Juliane Nöetzold[‡], Heike Sigloch, Josefine Morgenstern, Kristina Schleining, Susanna Suhm, Stefan A. Oelmeier, Jürgen Hubbuch
   ([‡]: contributed equally)

   International Journal of Pharmaceutics 479 (2015) 28–40
   http://dx.doi.org/10.1016/j.ijpharm.2014.12.027

   This article presents a systematic, automated method for generating phase diagrams in micro-scale format and in high-throughput. The influence of different precipitants on the phase behavior of varying proteins at distinct pH values was investigated. Conditions under which precipitation and crystallization occurred were identified. Additionally, gel formation and liquid-liquid phase separation were observed at certain set-ups. A contribution to the general knowledge of phase behavior was achieved.
   My main contribution to this project was the development of the robotic script for the pipetting of the phase diagrams and the recording of the protein liquid classes. By using this script all protein phase diagrams were generated. Furthermore, I was responsible for the pH stability screenings to ensure constant pH values while mixing of buffer, salt, and protein solutions.

2. **The Influence of Mixed Salts on the Capacity of HIC Adsorbers: A Predictive Correlation to the Surface Tension and the Aggregation Temperature**

   Kai Baumgartner, Sven Amrhein, Stefan A. Oelmeier, Jürgen Hubbuch

   Biotechnology Progress (2015), accepted manuscript
   doi: 10.1002/btpr.2166

   This paper presents a new approach for enhancing the binding capacity in hydrophobic interaction chromatography by mixing salts of kosmotropic and chaotropic nature in different ratios. The aggregation temperature, as a degree of hydrophobic forces, and the surface tension of the protein-salt solution were shown to be fast tools for predicting the binding behavior. A direct correlation between the solubility limit product (ionic strength times salt concentration) and the progression of the binding capacities was identified, making this approach a fast additional tool for predicting binding behavior in HIC.

3. **Influence of Binding pH and Protein Solubility on the Dynamic Binding Capacity in Hydrophobic Interaction Chromatography**

   Pascal Baumann[‡], Kai Baumgartner[‡], Jürgen Hubbuch
   ([‡]: contributed equally)

   Journal of Chromatography A 1396 (2015) 77-85
   doi: 10.1016/j.chroma.2015.04.001

   This study investigates the influence of binding pH and protein solubility on the dynamic binding capacity in hydrophobic interaction chromatography for proteins of acidic, neutral, and alkaline isoelectric points. An increase in the binding capacity close to the solubility limit - and often close to the protein's isoelectric point - was observed. An inverse relationship between the binding kinetics and the binding capacity was discovered, advising a rearrangement of the protein on the adsorber surface during the binding process. Despite increased binding capacities protein integrity after elution was ensured.

4. **Prediction of Salt Effects on Protein Phase Behavior by HIC Retention and Thermal Stability**

   Kai Baumgartner[‡], Steffen Grosshans[‡], Juliane Schütz[‡], Susanna Suhm, Jürgen Hubbuch
   ([‡]: contributed equally)

   Submitted to Journal of Pharmaceutical and Biomedical Analysis (2015)

   This article presents new fast methodologies for estimating protein phase behavior. The determined hydrophobic interaction chromatography (HIC) retention volumes as well as thermal stability measurements were successfully correlated to the phase behavior of glucose isomerase in dependence of precipitant concentration and pH value. By measuring HIC retention times, melting, and aggregation temperatures of glucose isomerase at varied parameters, the protein phase behavior was estimated. Precipitation propensity, crystal size and form, as well as skin formation can be estimated.

Determination of protein phase diagrams by microbatch experiments: Exploring the influence of precipitants and pH

Kai Baumgartner[1,*], Lara Galm[1,*], Juliane Nötzold[1,*], Heike Sigloch[1], Josefine Morgenstern[1], Kristina Schleining[1], Susanna Suhm[1], Stefan A. Oelmeier[1] and Jürgen Hubbuch[1,**]

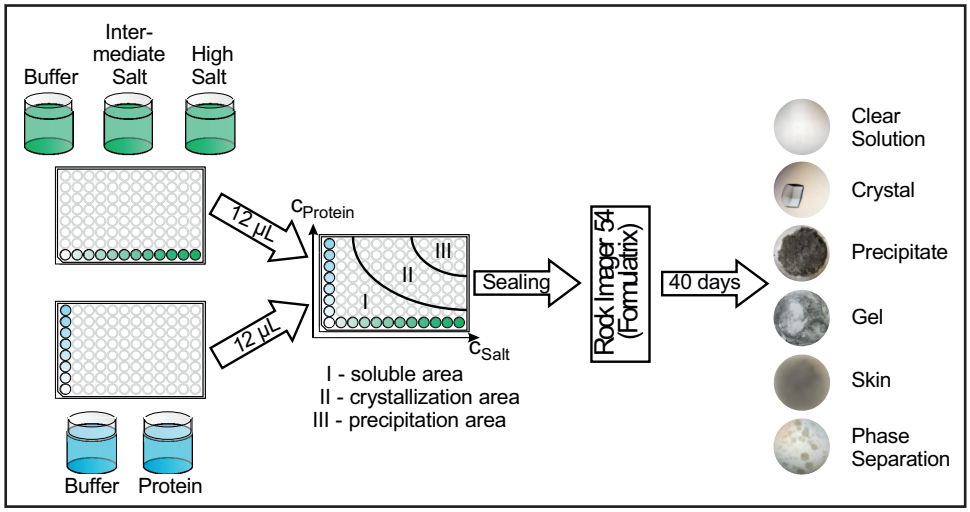

[1] : *Institute of Engineering in Life Sciences, Section IV: Biomolecular Separation Engineering, Karlsruhe Institute of Technology, Engler-Bunte-Ring 1, 76131 Karlsruhe, Germany*

[*] : *Contributed equally to this work*

[**] : *Corresponding author; mail: juergen.hubbuch@kit.edu*

International Journal of Pharmaceutics

Volume 479, (2015), 28-40

Submitted: 2. October 2014
Accepted: 13. December 2014
Available online: 23. December 2014

Abstract

Knowledge of protein phase behavior is essential for downstream process design in the biopharmaceutical industry. Proteins can either be soluble, crystalline or precipitated. Additionally liquid-liquid phase separation, gelation and skin formation can occur. A method to generate phase diagrams in high throughput on an automated liquid handling station in microbatch scale was developed. For lysozyme from chicken egg white, human lysozyme, glucose oxidase and glucose isomerase phase diagrams were generated at four different pH values pH 3, 5, 7 and 9. Sodium chloride, ammonium sulfate, polyethylene glycol 300 and polyethylene glycol 1000 were used as precipitants. Crystallizing conditions could be found for lysozyme from chicken egg white using sodium chloride, for human lysozyme using sodium chloride or ammonium sulfate and glucose isomerase using ammonium sulfate. PEG caused destabilization of human lysozyme and glucose oxidase solutions or a balance of stabilizing and destabilizing effects for glucose isomerase near the isoelectric point. This work presents a systematic generation and extensive study of phase diagrams of proteins. Thus, it adds to the general understanding of protein behavior in liquid formulation and presents a convenient methodology applicable to any protein solution.

Keywords: Protein phase diagram, High throughput, Automated imaging, Protein phase behavior, Microbatch crystallization

1 Introduction

Information on protein phase behavior is important for protein purification and formulation process design. The importance is related both to the avoidance of undesired phase transitions during processing and to the application of phase transitions for purification purposes. Further, protein phase behavior is important where structure determination is conducted via diffraction studies.
A protein phase diagram is a graphical display of the possible phase states of a protein. Hence, a protein phase diagram will provide information on whether crystallization, precipitation, liquid-liquid phase separation or gelation occur under the given conditions [1, 2]. It is generally accepted, that the solubility line divides an undersaturated zone where the protein is soluble, from a supersaturated zone where the protein is potentially either crystalline or precipitated [2, 3]. Phase diagrams can be determined subject to various parameters, e.g. protein concentration, precipitant concentration, temperature and pH. Different precipitants have various influences on protein phase behavior [4, 5], pH-shifts can easily induce supersaturation [3] Temperature as well has a significant but unpredictable impact on the phase behavior as could be shown by Lin et al. [6] for lysozyme, ribonuclease A, ribonuclease S, trypsin, concanavalin A, chymotrypsinogen A, papain, catalase and proteinase K. Commonly, protein phase behavior is visualized as a function of protein and precipitant concentration with all other parameters held constant [1, 2]. The most popular methods to generate protein phase diagrams are via microbatch or vapor diffusion experiments. The latter is conducted by using an undersaturated protein solution in the form of a hanging or a sitting drop. The drop equilibrates against

a reservoir that contains a higher concentration of precipitant than the protein solution [7, 8]. During equilibration the drop volume decreases, leading to an increase of protein and precipitant concentration in the drop. If the supersaturation in the drop is high enough phase transitions like crystallization can occur [8]. In phase diagrams generated by vapor diffusionexperiments, the initial protein concentration is plotted against the initial precipitant concentration [6]. However, the conditions in the protein solution change throughout the equilibration process [7]. Therefore protein and precipitant concentrations at a phase transition cannot be determined exactly. As opposed to vapor diffusion experiments, the solution conditions will remain constant when performing microbatch experiments [7]. Here, the solution is either undersaturated, saturated or supersaturated at the beginning of the experiment. If supersaturation is high enough, crystallization occurs and crystals will grow until the liquid-solid equilibrium, i.e. saturation, is reached [8, 9]. Hence, microbatch experiments not only give a more accurate description of phase states with known protein and precipitant concentration. They also enable determination f solubility by measurement of the protein concentration in the supernatant. Despite these benefits microbatch data can hardly be found in literature.
In addition, crystallization conditions are found mainly by trial–and–error studies using screening methods [5, 10] with sparse-matrix screens being the most popular ones [7]. Until now a systematic approach to map phase diagrams is still missing.
In the present work an experimental method was set up for automated generation of protein phase diagrams with minimized protein consumption. Microbatch experiments were chosen due to the above mentioned advantages. They were conducted in high throughput mode using an automated liquid handling station. Phase diagrams were generated for the four proteins lysozyme from chicken egg white, human lysozyme, glucose isomerase and glucose oxidase. These proteins were selected to cover a broad range in size and isoelectric points. Their phase behavior was investigated at four different pH values 3, 5, 7, 9 using four different precipitants sodium chloride, ammonium sulfate, polyethylene glycol (PEG) 300 and 1000. These precipitants were chosen based on findings in literature [5, 10–13].
The presented work thus demonstrates the use of high throughput experimentation for the generation of phase diagrams. The methodology can be applied to any protein solution and was used herein to generate phase diagrams of model proteins to an unmatched extent.

2 Materials & Methods

2.1 Materials

The used buffer substances were citric acid (Merck, Darmstadt, Germany) and sodium citrate (Sigma-Aldrich, St. Louis, MO, USA) for pH 3, sodium acetate (Sigma-Aldrich, St. Louis, MO, USA) and acetic acid (Merck, Darmstadt, Germany) for pH 5, MOPSO (AppliChem, Darmstadt, Germany) for pH 7 and bis-tris propane (Molekula, Dorset, UK) for pH 9. Sodium chloride was obtained from Merck (Darmstadt, Germany), ammonium sulfate was from VWR (Radnor, PA, USA) and PEG 300 as well as PEG 1000 were purchased from Sigma-Aldrich (St. Louis, MO, USA). Hydrochloric acid and sodium

hydroxide for pH adjustment were obtained from Merck (Darmstadt, Germany). pH adjustment was performed using a five–point calibrated pH–meter (HI-3220, Hanna Instruments, Woonsocket, RI, USA) equipped with a SenTix® 62 pH electrode (Xylem Inc., White Plains, NY, USA) or an InLab® Semi-Micro pH electrode (Mettler Toledo, Greifensee, Switzerland) dependent on the application. All buffers were filtered through 0.2 μm cellulose acetate filters, precipitant solutions through 0.45 μm cellulose acetate filters (Sartorius, Goettingen, Germany).
Lysozyme from chicken egg white (PDB 1LYZ, pI 11.4) (HR7-110) and glucose isomerase from Streptomyces rubiginosus (PDB 3KBS, pI 4.78) (HR7-100) were purchased from Hampton Research (Aliso Viejo, CA, USA). Human lysozyme recombinantly expressed in rice (PDB 1LZ1, pI 11.0) (L1167) and glucose oxidase from Aspergillus niger (PDB 1CF3, pI 4.55) (49,180) were purchased from Sigma-Aldrich (St. Louis, MO, USA). All isoelectric points were calculated using H++ 3.0 [14] for the respective PDB code with protonation at pH 7 and the following parameters: salinity 0.15 M, internal dielectric constant 10, external dielectric constant 80.
Protein solutions were filtered through 0.2 μm syringe filters with PTFE membranes (VWR, Radnor, PA, USA). Size exclusion chromatography was conducted using a HiTrap Desalting Column (GE Healthcare, Uppsala, Sweden) on an AEKTAprime™ plus system (GE Healthcare, Uppsala, Sweden). A subsequent protein concentration step was performed using Vivaspin centrifugal concentrators (Sartorius, Goettingen, Germany) with PES membranes and molecular weight cutoffs of 3 kDa for lysozyme from chicken egg white and human lysozyme, 30 kDa for glucose oxidase and glucose isomerase.
Protein phase diagrams were prepared on MRC under Oil 96 Well Crystallization Plates (Swissci, Neuheim, Switzerland) in microbatch experiments with a Freedom EVO® 100 (Tecan, Maennedorf, Switzerland) automated liquid handling station. Calibration of pipetting for liquid handling of buffers, precipitant solutions and protein solutions were generated using a WXTS205DU analytical balance (Mettler-Toledo, Greifensee, Switzerland). The MRC Under Oil 96 Crystallization Plates were covered with HDclear™ sealing tape (ShurTech Brands, Avon, OH, USA) to prevent evaporation. A Rock Imager 54 (Formulatrix, Waltham, MA, USA) was used as an automated imaging system for protein crystallization. Protein concentration measurements were conducted using a NanoDrop2000c UV-VIS spectrophotometer(Thermo Fisher Scientific, Waltham, MA, USA).

2.2 Methods

2.2.1 Preparation of stock solutions

To set up the buffers and precipitant stock solutions containing sodium chloride, ammonium sulfate, PEG 300 or PEG 1000, all substances were weighed in and dissolved in ultrapure water to 90% of the final buffer volume. pH was adjusted with the appropriate titrant with an accuracy of ±0.05 pH units. After pH adjustment the buffers were brought to their final volume using ultrapure water. All buffers were filtered through 0.2 μm cellulose acetate filters. Precipitant stock solutions were filtered through 0.45 μm cellulose acetate filters. Buffers and precipitant stock solutions were used at the earliest one day after preparation and after repeated pH verification. Buffer capacity was

100 mM for all buffers. Precipitant stock solutions contained 2.5 or 5 M sodium chloride, 1.5 or 3 M ammonium sulfate and 30% (w/V) PEG 300 or PEG 1000 additionally to the corresponding buffer substances.
To set up the protein stock solutions, protein was weighed in and dissolved in the appropriate buffer yielding a concentration of 80 mg/mL for lysozyme from chicken egg white, human lysozyme and glucose oxidase. The crystal suspension of glucose isomerase was diluted with appropriate buffer to redissolve the suspension. The protein solutions then were filtered through 0.2 μm syringe filters to remove particulates and desalted using size exclusion chromatography. Protein concentration was adjusted to 43.5 $\pm$ 1 mg/mL via centrifugal concentrators. A volume of 1 mL of protein stock solution was required for generation of one phase diagram.

2.2.2 pH stability in high concentrated salt solutions

The stability of pH in salt precipitant dilution series was evaluated for the different buffers at a scale of 1 mL. Sodium chloride concentration was varied between 0 and 5 M and ammonium sulfate concentration between 0 and 3 M using the respective buffers including intermediate (2.5 M sodium chloride or 1.5 M ammonium sulfate) and high salt concentration buffers. pH values for the different dilution steps were measured using a five point calibrated pH meter.

2.2.3 Accuracy of automated liquid handling

Calibration of liquid handling is essential for reproducible generation of protein phase diagrams. The method to determine so called liquid classes, including important variables such as plunger volume, aspiration and dispense speed, was described earlier by Oelmeier et al. [15]. The challenge of pipetting different solutions arises due to different viscosities and densities resulting in possibly large errors in automated pipetting. Liquid classes were created for all buffers, precipitant solutions and protein solutions. The calibrated volume range was 7-200 μL.
To create liquid classes the following pipetting parameters were individually adjusted: the aspiration, the dispensing, and the breakoff speeds. Additionally three different air gaps in the pipetting tips which influence the pipetting behavior were adapted. The factors and offsets of regression lines, with which the otherwise incorrect pipetted volumes were corrected automatically, were adjusted individually.

2.2.4 Generation of phase diagrams

Protein phase diagrams were generated on 96 well crystallization plates in microbatch experiments with varying protein and precipitant concentration. The scheme of the following description is shown in Fig. 1. Protein stock solutions were adjusted to 43.5 $\pm$ 1 mg/mL. Eight protein dilution steps between 5 and 43.5 mg/mL for lysozyme from chicken egg white and human lysozyme, glucose oxidase and glucose isomerase were created by mixing of buffer and protein stock solution on a sample plate. Exceptions from this procedure were made for pH values near the isoelectric point of the proteins. Stock solution of glucose oxidase at pH 5 could only be concentrated up to 21.75 $\pm$ 1 mg/mL.

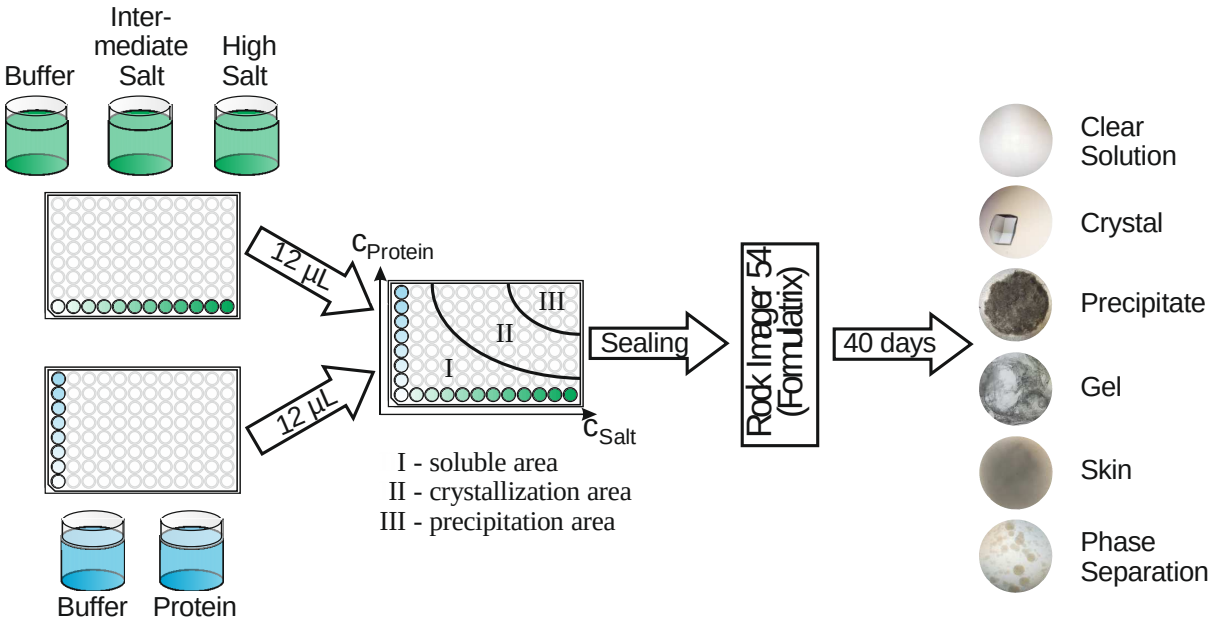

Fig. 1: Schematic illustration of the experimental setup and evaluation of protein phase states for the generation of protein phase diagrams. The soluble (I), crystallization (II) and precipitation (III) area are depicted in the phase diagram.

The purchased crystal suspension of glucose isomerase could not be redissolved in pH 3. At pH 5 glucose isomerase stock solution could only be concentrated up to 30 ± 1 mg/mL. Twelve uniform precipitant dilution steps were created by mixing of buffer and 2.5 M or 2.5 and 5 M sodium chloride stock solution, buffer and 1.5 M or 1.5 and 3 M ammonium sulfate stock solution. For PEG as precipitant buffer and 30% (w/V) PEG 300 stock solution or buffer and 30% (w/V) PEG 1000 stock solution were mixed.
The protein phase diagrams were generated by adding 12 μL of diluted protein solution to 12 μL of diluted precipitant solution on the crystallization plate. Protein concentration was varied per row and precipitant concentration was varied per column. The resulting protein concentration on the crystallization plate ranged between 2.5 and 21.75 mg/mL for lysozyme from chicken egg white, human lysozyme, glucose oxidase and glucose isomerase besides the mentioned exceptions. The corresponding precipitant concentration on the crystallization plate ranged between 0 and 2.5 M for sodium chloride, between 0 and 1.5 M for ammonium sulfate and between 0 and 15% (w/V) for PEG 300 and PEG 1000. Crystallization plates were then centrifuged for 1 min at 1000 rpm to remove air bubbles and covered using optically clear and UV compatible sealing tape.
It has to be noted that microbatch crystallization experiments are normally conducted with a volume of 10 μL and using paraffin oil to cover the solution in order to avoid evaporation [7, 16, 17]. However, DArcy et al. [16] observed that paraffin oil influences crystallization probability. For that reason phase diagrams in this work were determined without paraffin oil, but with a sealing tape to avoid evaporation without influencing phase behavior.
The sealed plates were stored in the Rock Imager for 40 days at 20°C.

2.2.5 Automated imaging

The Rock Imager performed the automated imaging of the crystallization plates. The imaging schedule was as follows: imaging every two hours during the first two days, imaging every six hours from third to ninth day and imaging once a day from tenth to fortieth day. For every well five focus levels were investigated and superimposed to one image. Resolution was 1.2 megapixels. The images were examined after 40 days. Six possible phase states were classified: clear solution, crystallization, precipitation, skin formation, gelation and phase separation. To distinguish between salt and protein crystals, the solution drops were exposed to UV light, exploiting the fluorescence of the aromatic amino acid tryptophan to identify protein crystals. Liquid-liquid phase separation was verified by birefringence of polarized light at 90° [18].

3 Results

3.1 pH stability in high concentrated salt solutions

The issue of pH stability is of high importance to avoid undesired pH deviations in microbatch scale due to used precipitants. Salts are known to shift the pH value [19]. To monitor this shift pH values of different buffers in the applied salt concentration ranges at different dilution steps were measured. The maximum deviation was found to be ±1 pH units. By the use of intermediate salt concentration buffers this deviation could be reduced to ±0.2 pH units.

3.2 Accuracy of automated liquid handling

As described in Section 2.2 different parameters were varied to ensure that correct volumes were pipetted. This provides the reproducible generation of phase diagrams. To reach this high accuracy the volume range was divided into subclasses. The subclasses ranged from 7 to 13 μL, 13.1 to 25 μL, 25.1 to 100 μL and from 100.1 to 200 μL. Within each of these subclasses the pipetting parameters were kept constant. In addition to division into subclasses, liquid handling was optimized for pipetting into air and into liquid.
To determine the quality of the liquid classes the errors of the pipetted volumes in each subclass were calculated according to Eq. (1) [15].

$$r_{av} = \frac{100}{n} \sum \frac{x_{max} - x_{min}}{\overline{x}} \tag{1}$$

r_{av} is the average range, x_{max} is the maximum, x_{min} is the minimum volume in percent of the mean volume pipetted, and n is the number of repetitions. For the buffers and precipitant solutions the r_{av} was always below 2% except for few outliers for the PEG solutions. For protein solutions r_{av} was below 3%.

3.3 Phase diagrams

As stated in Section 2.2 64 protein phase diagrams were determined. Selected phase diagrams of each protein are described in detail in the following. All determined phase

diagrams are shown in the supplementary online material.

3.3.1 Performance

A low volume high throughput method was established to obtain information about the phase behavior of proteins in salt or PEG environment. For the generation of one phase diagram for one protein and one precipitant in microbatch scale at a certain pH value, a total protein mass of less than 150 mg was needed. The total time consumption - for weighing the protein, dissolving it, conducting a buffer change to remove unwanted salts, concentrating the protein solution via centrifugal concentrators to the desired stock solution concentration, pipetting the microbatch plate on the robotic platform, sealing the plate and storing the microbatch plate in the Rock Imager - was around two hours.

3.3.2 Lysozyme from chicken egg white

For lysozyme from chicken egg white phase transitions occurred for sodium chloride and ammonium sulfate as precipitants. Crystallization, precipitation and skin formation could be observed. Crystallization only occurred for sodium chloride as precipitant. Precipitation and skin formation occurred for both precipitants.

Sodium chloride as precipitant For lysozyme from chicken egg white and sodium chloride as precipitant phase transitions occurred over the whole investigated pH range. At pH 3 soluble, crystalline and precipitated phase states were observed. In some cases precipitate was accompanied by skin formation. The phase diagram is illustrated in Fig. 2(A). A soluble region occurred at low protein and precipitant concentrations. Increasing concentrations of both constituents let to crystallization and further increase to simultaneous crystallization and precipitation. At a high protein concentration of for example 21.75 mg/mL a low sodium chloride concentration of 0.45 M was needed to induce crystallization. With increasing sodium chloride concentration the protein concentration needed for induction of crystallization decreased. Three-dimensional crystals, microcrystals and needle-shaped crystals could be observed. Crystal morphology depended on protein and salt concentration. At sodium chloride concentrations of 2.05 M and above and protein concentrations between 5.25 and 21.75 mg/mL skin formation appeared. It always co-occurred with precipitation.
The phase behavior of lysozyme from chicken egg white at pH 5 with sodium chloride as precipitant was similar to the phase behavior with the same precipitant at pH 3. The phase diagram is illustrated in Fig. 2(B). A soluble and a crystalline area were observed, as well as precipitation. However, the soluble area was wider than found at pH 3 and the crystallization area was shifted to higher salt and protein concentrations. Precipitation only occurred for the highest sodium chloride and protein concentration. The morphology of the crystals was similar to pH 3, although no microcrystals occurred at pH 5. Crystals for the same salt and protein concentration were bigger at pH 5 than at pH 3. No skin formation appeared at pH 5 with sodium chloride as precipitant.
At pH 7 sodium chloride induced both crystallization and precipitation. The latter occurred only for the two highest salt and protein concentrations.
At pH 9 sodium chloride induced crystallization. No precipitation or skin formation was

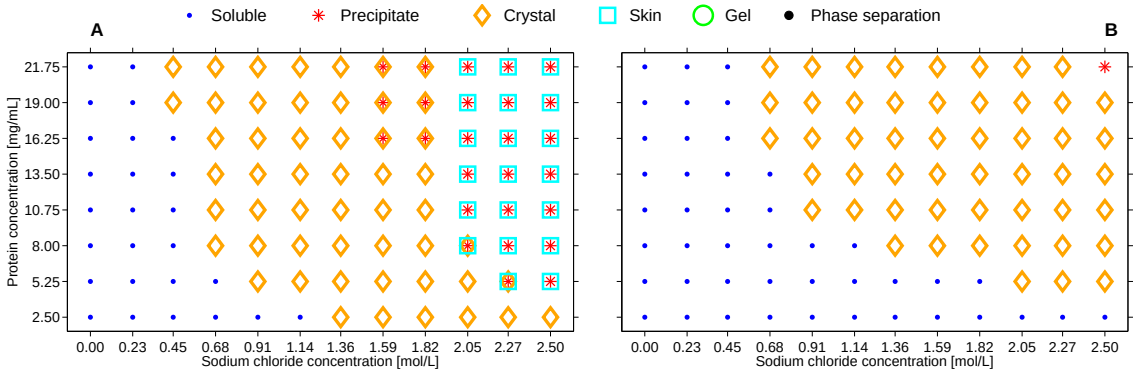

Fig. 2: Phase diagrams of lysozyme from chicken egg white using sodium chloride as precipitant at pH 3 (A) and pH 5 (B).

observed. At pH 7 and pH 9 no clear crystallization area could be defined because it was interspersed by phase states where the protein stayed soluble. However, there were more crystalline phase states at pH 9 than at pH 7. At both pH values isolated, three–dimensional crystals were observed. The crystals were much bigger than at pH 3 and pH 5. Crystal size generally increased with decreasing distance to the isoelectric point.

Ammonium sulfate as precipitant For lysozyme from chicken egg white and ammonium sulfate as precipitant phase transitions occurred only at pH 3 and pH 5. The soluble area of the phase diagram was directly adjacent to the area where skin formation appeared. No crystalline phase states occurred previous to skin formation. Skin formation always co-occurred with precipitation. At pH 3 skin formation appeared for precipitant concentrations between 1.23 and 1.5 M and protein concentrations above 8 mg/mL.
At pH 5 skin formation occurred at 1.5 M ammonium sulfate and the two highest protein concentrations. For pH 7 and pH 9 no phase transition occurred using ammonium sulfate as precipitant.

PEG 300 and PEG 1000 as precipitant No phase transitions of lysozyme from chicken egg white could be observed using PEG 300 or PEG 1000 as precipitant. The solutions stayed soluble over the whole investigated PEG and protein concentration range at each examined pH value.

3.3.3 Human lysozyme

For human lysozyme crystallization, gelation and precipitation were observed. Precipitation occurred predominantly and crystallization always occurred in combination with precipitation or gelation.

Sodium chloride as precipitant Using sodium chloride as precipitant, soluble, crystalline, gelled and precipitated phase states occurred. Crystals always coexisted with gel or precipitate. For human lysozyme at pH 3 (Fig. 3(A)) phase transitions occurred for sodium chloride concentrations higher than 1.14 M. The soluble area was followed by an area where crystallization, gelation and precipitation occurred. The area where

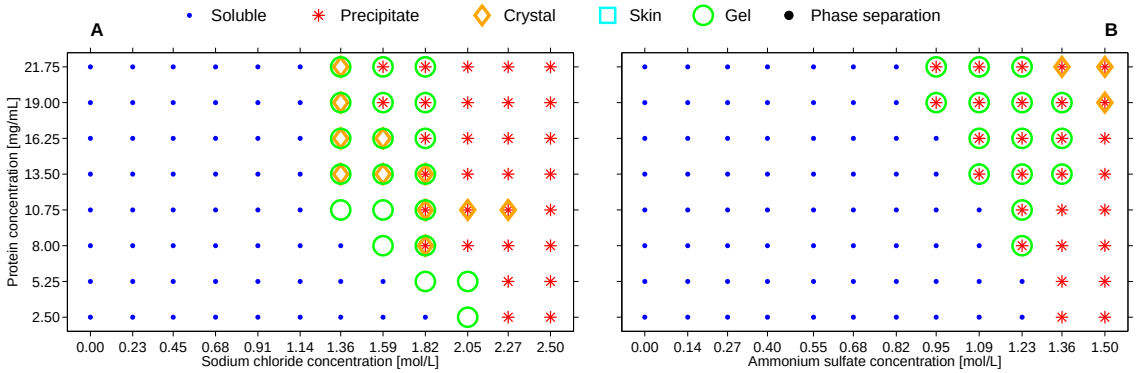

Fig. 3: Phase diagrams of human lysozyme at pH 3 using sodium chloride (A) and ammonium sulfate (B) as precipitant.

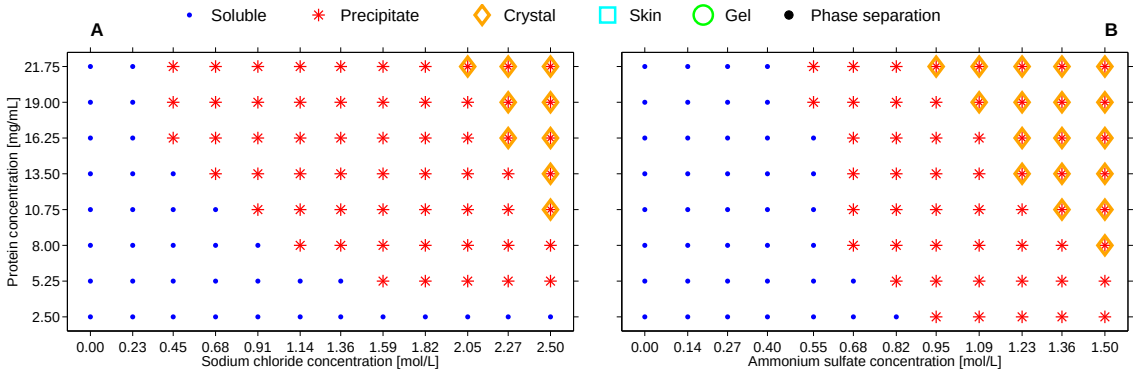

Fig. 4: Phase diagrams of human lysozyme at pH 5 using sodium chloride (A) and ammonium sulfate (B) as precipitant.

gelation appeared in combination with crystallization and/or precipitation was located in a sodium chloride concentration range between 1.36 and 1.82 M. Gelation alone appeared for 1.36-1.59 M sodium chloride and 8-10.75 mg/mL human lysozyme as well as for 1.82-2.05 M sodium chloride and 2.5-5.25 mg/mL human lysozyme. The area where gelation appeared was followed by an area where precipitation occurred. In two cases crystals and precipitated states coexisted.

For human lysozyme at pH 5 using sodium chloride as precipitant (Fig. 4(A)) the precipitation area started at a sodium chloride concentration of 0.45 M and protein concentrations above 13.5 mg/mL. For sodium chloride concentrations from 2.05 M and protein concentrations between 10.75 and 21.75 mg/mL crystallization and precipitation occurred simultaneously.

At pH 7 and pH 9 only a soluble and a precipitated area could be identified, no crystals occurred. At pH 7 the precipitation started at 0.45 M sodium chloride and protein concentrations above 8 mg/mL. At pH 9 it started at 1.59 M sodium chloride and 21.75 mg/mL human lysozyme.

Ammonium sulfate as precipitant Using ammonium sulfate as precipitant, soluble, crystalline, gelled and precipitated phase states occurred. Crystals always coexisted with precipitate. Gelation only occurred at pH 3. For human lysozyme at pH 3

using ammonium sulfate as precipitant (Fig. 3(B)) gelation always co-occurred with precipitation. The combined gelation and precipitation area seems to represent a transfer region to a pure precipitate area. Gelation in combination with precipitation occurred for ammonium sulfate concentrations between 0.95 and 1.36 M and protein concentrations between 8 and 21.75 mg/mL. Precipitation without coexisting gelation occurred at ammonium sulfate concentrations of 1.36 M and 1.5 M and protein concentrations below 13.5 mg/mL or 19 mg/mL, respectively. Crystallization in combination with precipitation at pH 3 occurred for ammonium sulfate concentrations of 1.36 M and 1.5 M with human lysozyme concentrations of 21.75 mg/mL and 19-21.75 mg/mL, respectively.
At pH 5 (Fig. 4(B)) a pure precipitation area and an area with precipitation and crystallization in combination could be identified. Precipitation started at 0.55 M ammonium sulfate and 19 mg/mL human lysozyme. Crystals coexisted with precipitate from 0.95 M ammonium sulfate at 21.75 mg/mL human lysozyme. For ammonium sulfate concentrations above 0.95 M the protein concentration needed to induce crystallization decreased. At 1.5 M ammonium sulfate 8 mg/mL human lysozyme were needed to induce crystallization in addition to precipitation.
At pH 7 precipitation started at 0.4 M ammonium sulfate and 19 mg/mL human lysozyme. Crystals coexisted with precipitate at and above 1.09 M ammonium sulfate and 19 mg/mL human lysozyme. At 1.5 M ammonium sulfate 8 mg/mL human lysozyme were needed to induce crystallization out of the precipitate.
At pH 9 precipitation started at 0.4 M ammonium sulfate and 16.25 mg/mL human lysozyme. Crystals coexisted with precipitate from 1.36 M ammonium sulfate and 21.75 mg/mL human lysozyme. At 1.5 M ammonium sulfate 19 mg/mL human lysozyme were needed to induce crystallization emerging from precipitate.
With decreasing distance to the isoelectric point and while using ammonium sulfate as precipitant the combined precipitated and crystalline area decreased continuously in its size. Only the phase behavior at pH 3 made an exception to this.

PEG 300 as precipitant In the investigated pH range no phase transition of human lysozyme occurred when using PEG 300 as precipitant.

PEG 1000 as precipitant At pH 3 and pH 5 no phase transition of human lysozyme occurred when using PEG 1000 as precipitant. At pH 7 and pH 9 precipitation occurred. Precipitation started at 2.73% (w/V) PEG 1000 and for human lysozyme concentrations from 19 mg/mL in both cases. The effect of PEG on the phase behavior of human lysozyme was thus found to be dependent both on polymer size and pH.
Although phase behavior of human lysozyme at pH 7 and pH 9 with PEG 1000 as precipitant looks very similar there is a difference when considering precipitation kinetics. At pH 7 no spontaneous precipitation occurred. Precipitation evolved over time. At pH 9 spontaneous precipitation immediately after pipetting occurred for 9.55% (w/V) PEG 1000 and 21.75 mg/mL human lysozyme and from 10.91% (w/V) PEG 1000 for human lysozyme concentrations of 16.25 mg/mL and above.

3.3.4 Glucose oxidase

For glucose oxidase only phase transitions to precipitation were observed. It was distinguished between spontaneous precipitation and precipitation of slower kinetics. The former occurred immediately after pipetting, the latter evolved over time. No other phase transitions were found at any of the examined conditions for glucose oxidase.

Sodium chloride as precipitant For glucose oxidase and sodium chloride as precipitant precipitation with different kinetics could be observed for pH 3 and pH 5.
At pH 3 glucose oxidase was stable without salt over the whole protein concentration range and with 0.23 M sodium chloride for 2.5-5.25 mg/mL glucose oxidase. From and above 0.45 M sodium chloride spontaneous precipitation was induced for the highest protein concentration of 21.75 mg/mL. With increasing sodium chloride concentration the protein concentration needed for spontaneous precipitation decreased. In the transition area from soluble to spontaneous precipitation, an area with precipitation formation of slower kinetics existed.
At pH 5 slowly evolving precipitation formation was observed starting from 0.45 M sodium chloride for protein concentrations above 8.13 mg/mL. No spontaneous precipitation was found.
For pH 7 and pH 9 no phase transitions were observed for sodium chloride as precipitant.

Ammonium sulfate as precipitant For glucose oxidase and ammonium sulfate as precipitant at pH 3 (Fig. 5(A)) precipitation occurred starting at 0.14 M. At salt concentrations between 0.14 and 0.4 M this precipitate evolved over time. Ammonium sulfate induced spontaneous precipitation at salt concentrations from 0.4 M ammonium sulfate for a protein concentration of 21.75 mg/mL. At higher salt concentrations lower protein concentrations sufficed for spontaneous precipitation. At 1.5 M ammonium sulfate 2.5 mg/mL glucose oxidase sufficed to induce spontaneous precipitation.
At pH 5 slowly evolving precipitate formation was monitored starting at a salt concentration of 0.27 M ammonium sulfate and protein concentrations of 8.13 mg/mL and above. Hereby it has to be mentioned that the maximum glucose oxidase concentration in the phase diagram for pH 5 was 10.88 mg/mL. At higher salt concentrations above 0.27 M ammonium sulfate lower protein concentrations sufficed for precipitate formation of slower kinetics, with 4 mg/mL glucose oxidase at 1.5 M ammonium sulfate being the lowest. At 1.5 M ammonium sulfate spontaneous precipitation occurred for protein concentrations for 9.5 and 10.88 mg/mL.
For pH 7 no phase transition was monitored.
At pH 9 (Fig. 5(B)) precipitation was found for 0.4 M ammonium sulfate and above starting at 16.25 mg/mL glucose oxidase. For higher ammonium sulfate concentrations lower protein concentrations were needed for precipitate formation. This slow evolving precipitation was followed by spontaneous precipitation at salt concentrations from 0.95 M ammonium sulfate and protein concentrations starting at 16.25 mg/mL. For 1.5 M ammonium sulfate spontaneous precipitation occurred for 5.25 mg/mL glucose oxidase and above.

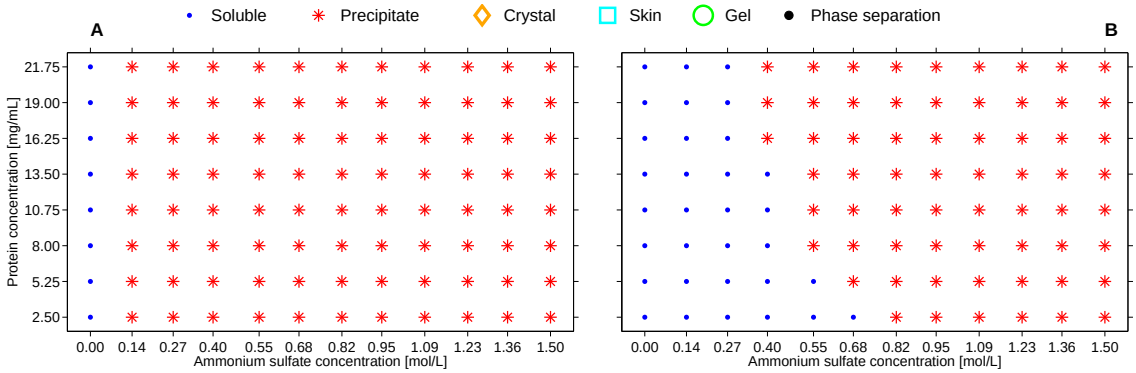

Fig. 5: Phase diagrams of glucose oxidase using ammonium sulfate as precipitant at pH 3 (A) and pH 9 (B).

PEG 300 as precipitant Glucose oxidase showed no phase transitions for PEG 300 in the investigated concentration and pH range.

PEG 1000 as precipitant For PEG 1000 no spontaneous precipitation formation of glucose oxidase occurred. At pH 5, close to the protein's isoelectric point, precipitate evolved over time starting at 9.55% (w/V) PEG 1000 and the highest protein concentration of 10.88 mg/mL. Higher precipitant concentrations let to precipitation starting at lower protein concentrations. This slowly evolving precipitation occurred at 15% (w/V) PEG 1000 for 4 mg/mL glucose oxidase and above.
At pH 3, 7 and 9 all investigated conditions showed no phase transitions for PEG 1000.

3.3.5 Glucose isomerase

For glucose isomerase phase transitions to crystallization, precipitation, liquid-liquid phase separation (LLPS) and skin formation were observed. The precipitate formation was divided into spontaneous and slow evolving precipitation as described above for glucose oxidase.

Sodium chloride as precipitant For glucose isomerase and the precipitant sodium chloride only precipitation and skin formation occurred at pH 5. Here slowly evolving precipitation and additional skin formation occurred independently of salt or protein concentration for all tested conditions.
At pH 7 and pH 9 no phase transitions occurred while using sodium chloride as precipitant.

Ammonium sulfate as precipitant For glucose isomerase and ammonium sulfate as precipitant crystallization, precipitation and skin formation were observed. At pH 5 ammonium sulfate concentrations below 0.82 M let to evolving precipitation and skin formation for all protein concentrations, with 15 mg/mL being the highest determinable glucose isomerase concentration. At one condition within the slow evolving precipitation zone threedimensional crystals occurred additionally (5.52 mg/mL glucose oxidase, 0.68 M ammonium sulfate). At ammonium sulfate concentrations of 0.82 M and above spontaneous protein precipitation with coexisting skin formation occurred. At

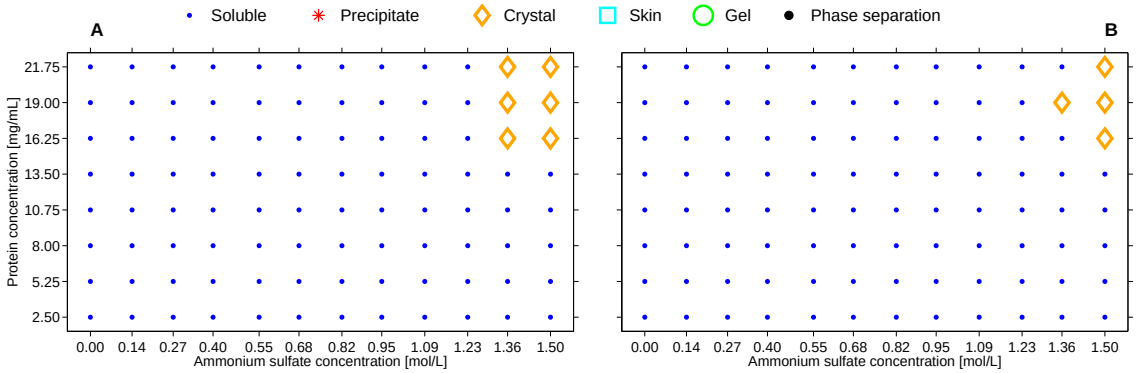

Fig. 6: Phase diagrams of glucose isomerase using ammonium sulfate as precipitant at pH 7 (A) and pH 9 (B).

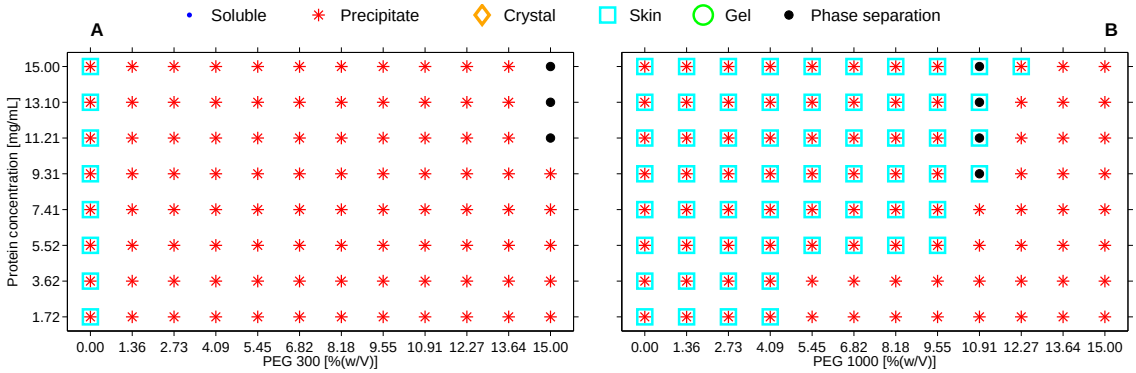

Fig. 7: Phase diagrams of glucose isomerase at pH 5 using PEG 300 (A) and PEG 1000 (B) as precipitant.

1.5 M ammonium sulfate 5.52 mg/mL sufficed to induce spontaneous precipitation.
At pH 7 and pH 9 crystallization of glucose isomerase occurred for ammonium sulfate concentrations of 1.36 M and above (Fig. 6). For pH 7 crystallization of glucose isomerase started from 16.25 mg/mL. For pH 9 the following conditions yielded crystals: 1.36 M ammonium sulfate at 19 mg/mL glucose isomerase and 1.5 M ammonium sulfate at 16.25-21.75 mg/mL glucose isomerase. For pH 9 the soluble area was slightly wider compared to pH 7. All crystals found were three–dimensional.

PEG 300 as precipitant For glucose isomerase and precipitant PEG 300 (Fig. 7(A)) only phase transitions were found at pH 5. Here, the conditions without precipitant showed slowly evolving precipitation with coexisting skin formation. For PEG 300 concentrations starting at 1.36% (w/V) skin formation was suppressed at all investigated protein concentrations. At PEG 300 concentrations of 15% (w/V) LLPS was observed for conditions starting from 11.21 mg/mL protein.
At pH 7 and pH 9 no phase transitions were monitored for PEG 300 as precipitant.

PEG 1000 as precipitant For glucose isomerase and PEG 1000 phase transitions occurred only at pH 5 (Fig. 7(B)). 10.91% (w/V) PEG 1000 let to LLPS for protein concentrations starting from 9.31 mg/mL. At PEG 1000 concentrations starting from 12.27% (w/V) spontaneous precipitation occurred for 9.31 mg/mL glucose isomerase and

above. For 15% (w/V) PEG 1000 7.41 mg/mL glucose isomerase sufficed to induce spontaneous precipitation. For all other conditions slowly evolving precipitate was observed. Additional skin formation was observed for PEG 1000 up to 4.09% (w/V) for all glucose isomerase concentrations. At PEG 1000 concentrations from 5.45% (w/V) and glucose isomerase concentrations below 5.52 mg/mL skin formation was suppressed. At higher PEG concentrations skin formation was suppressed at higher protein concentrations.
At pH 7 and pH 9 no phase transitions occurred with PEG 1000 as precipitant.

4 Discussion

4.1 pH stability in high concentrated salt solutions

When mixing a buffer without salt and a buffer with salt at the same pH the pH value of the buffer mixture can drift. This phenomenon can be described by the DebyeHückel-theory Eq. (2) [19].

$$pK_a^* = pK_a - \frac{1.824 * 10^6}{(\epsilon * T)^{3/2}} |z^+ z^-| \sqrt{I} \tag{2}$$

$pK_a{}^*$ is the corrected pK_a value, ϵ is the dielectric constant of the solution, T is the temperature (K), z is the charge of the ion and I is the ionic strength (M). When the ionic strength I of a buffer is increased the pK_a of the buffer substance changes to $pK_a{}^*$ (Eq. (2)). Thereby the pH value of the buffer solution changes. For polyprotic buffer substances the charge of the buffer ions at the second or third pK_a of the buffer substance is higher than at the first pK_a value. When the ionic strength is increased the pK_a is influenced more strongly at the second or third pK_a value compared to the first pK_a. All pK_a values were obtained from [20]. Citrate (pK_{a1}: 3.13, pK_{a2}: 4.76, pK_{a3}: 6.40) is used at pH 3 at its first of its three pK_a values therefor the change of the ionic strength is not problematic. Acetate (pK_a: 4.76) - used at pH 5 - has only one pK_a and so there is hardly a problem when using three stock solutions with 0 M, 2.5 M and 5 M sodium chloride or 0 M, 1.5 M and 3 M ammonium sulfate. The synthetically manufactured buffer substance MOPSO (pK_a: 6.90) has only one pK_a value at pH 6.9. Hence the buffer pH stays constant in the entire salt concentration range. Bis–tris propane has two pK_a values (pK_{a1}: 8.93, pK_{a2}: 6.59). Bis–tris propane is a basic buffer substance, hence at pH 9 it is used at the first pK_a. The abovementioned discussion demonstrates the importance of carefully choosing buffering components when investigating protein solutions over a wide pH and salt concentration range. Thereby, we were able to rule out any unwanted pH shifts in the samples. Thus, it was possible to create phase diagrams at various pH values with high confidence.

4.2 Accuracy of automated liquid handling

Optimization of liquid handling is an essential step for the reproducible preparation of phase diagrams. This led to pipetting accuracies with errors below 2% for buffers and precipitant solutions and to errors $\leq$3% for protein solutions. Without these optimizations pipetting inaccuracies between 10% and 30% can be expected.
The main difference between pipetting salt buffer in air and pipetting into liquid is, that

the leading air gap - that means the air gap that is dispensed following the buffer - is smaller for pipetting into liquid. The creation of too much air bubbles could be avoided through this adjustment.
With higher viscosities for PEG containing buffers compared to salt buffers the dispensing speed had to be lowered to get accurately pipetted volumes.
The main difference for protein liquid classes compared to precipitant liquid classes is, that for protein solutions no leading air gap was used. Creation of air bubbles, that could probably be critical to the protein, could be avoided.
The optimization procedures described in Section 2.2 ensured that during preparation of phase diagrams correct volumes of each liquid were pipetted and that the specified concentrations are trustworthy. As with the careful selection of buffering components, thorough optimization of liquid handling parameters is critical for generation of high quality data.

4.3 Phase diagrams

4.3.1 Performance

In this paper a method to create phase diagrams in high throughput was established. Two hours and a protein mass of less than 150 mg were needed to cover a broad protein and precipitant concentration range and to determine the phase behavior of the protein. One phase diagram consists of 96 different conditions with variation of protein and precipitant concentration at a constant pH value and at 20°C. It was thus shown, that the developed methodology lends itself well for a standardized approach for phase diagram generation and can easily be ported to other protein and precipitant systems. However, system composition and operating conditions should be taken into consideration carefully.

4.3.2 Lysozyme from chicken egg white

Sodium chloride as precipitant The distance from the isoelectric point and the sodium chloride concentration had an influence on lysozyme solubility, aggregation kinetics and crystal morphology.
The influence on lysozyme solubility was mainly driven by the pH value, i.e. the distance from the isoelectric point. At pH 9 the first phase transition occurred at 0.23 M sodium chloride where lysozyme still stayed soluble at pH 3, 5 and 7. Hence, we assume that for low sodium chloride concentrations up to 0.23 M the solubility increased with increasing distance to the pI. This fits to the commonly accepted observation that for most proteins at low salt concentrations solubility decreases while approaching the pI and is lowest at the pI [21]. For sodium chloride concentrations above 0.23 M phase transitions occurred at lower protein concentrations at lower pH values. Hence, solubility decreased with increasing distance to the pI. In a low-electrolyte region, which was identified to reach up to 0.23 M sodium chloride, the long–range electrostatic protein interactions are significant [22]. These long–range electrostatic forces are repulsive, which means that the higher the protein charge, the higher the repulsion between the equally charged protein molecules. Lysozyme solubility in the low-electrolyte region thus is highest at pH 3 because of the highest electrostatic repulsion and lowest at pH 9. Our experimental results

in the low-electrolyte range can further be supported by second osmotic virial coefficient (B22) measurements of Velev et al. [22]. The B22 values up to 0.1 M sodium chloride are highest at pH 3 and decrease with increasing pH value.
The long–range electrostatic repulsion between charged proteins is reduced by the presence of salt ions. These salt ions screen the electrostatic fields of neighboring proteins and short–range attractive forces become noticeable. The importance of short–range forces in protein interactions and for protein phase behavior was described in literature before [23–26]. Short–range attractive forces can be van der Waals forces, hydrophobic or osmotic forces [27]. Attractive osmotic forces due to a high electrolyte concentration have been described earlier [28–30]. Hydrophobic interactions occur due to hydrophobic patches on the protein surface and are strong at high ionic strengths [21].
For lysozyme from chicken egg white and sodium chloride concentrations above 0.23 M the effect of electrostatic repulsion seems to vanish and short–range forces become increasingly important. At pH values with a higher distance from the pI, lower lysozyme concentrations are needed to induce phase transitions in the high–electrolyte region, beginning with crystallization. In the high–electrolyte region the common belief that solubility is lowest at or near the pI seems not to be valid for lysozyme from chicken egg white with sodium chloride as precipitant.
As mentioned before, the sodium chloride concentration and the distance from the pI also had an influence on the lysozyme aggregation kinetics and crystal morphology. A comparison between the phase diagrams of lysozyme from chicken egg white with sodium chloride as precipitant for different pH values shows that most phase transitions occurred at pH 3. Three-dimensional crystals evolved for sodium chloride concentrations between 0.45 and 1.36 M sodium chloride but crystal size decreased with increasing sodium chloride and protein concentration resulting in needle-shaped crystals and microcrystals. A broad area with precipitation and skin formation occurred, which is a hint for protein denaturation [18]. At pH 5 fewer phase transitions occurred compared to pH 3. Aggregation kinetics also had been slower than at pH 3, resulting in bigger crystal sizes at identic sodium chloride concentrations and the absence of microcrystals and a precipitation area. At pH 7 and pH 9 only isolated phase transitions occurred. Aggregation kinetics were slow resulting in single three-dimensional, big crystals and a crystallization area that was interspersed with conditions where lysozyme stayed soluble. As phase transitions at every investigated pH value happened in a sodium chloride concentration range where long–range electrostatic forces are screened, this shows that the attractive short–range forces causing aggregation need to be pH dependent. The attractive short–range forces increased for lysozyme from chicken egg white with increasing distance to the pI resulting in smaller protein crystals. Attractive short–range forces also increased in strength with increasing sodium chloride concentration. That resulted in accelerated aggregation kinetics and thus altered crystal morphology and caused pronounced precipitation. The intermolecular short–range forces at pH 3 between lysozyme from chicken egg white molecules seem to be strong enough to induce complete or partial protein denaturation resulting in skin formation.
To the best of our knowledge the here proposed and experimentally supported pH dependency of short–range attractive forces was not described in literature earlier.

Ammonium sulfate as precipitant For lysozyme from chicken egg white using ammonium sulfate as precipitant phase transitions only occurred at pH 3 and pH 5 at high ammonium sulfate concentrations. Except of one condition where only precipitation occurred, precipitation and skin formation always coexisted. In general, kosmotropes such as ammonium sulfate are useful for salting-out proteins, i.e. decrease protein solubility, but tend to reduce protein denaturation. Our results showed no salting-out, i.e. amorphous precipitation, up to 1.09 M ammonium sulfate at pH 3 and 1.36 M at pH 5 but induction instead of reduction of protein denaturation for higher ammonium sulfate concentrations. Ries-Kautt and Ducruix [31] found that lysozyme from chicken egg white follows the inverse Hofmeister series for anions where solubility is highest for strong kosmotropes such as ammonium sulfate and lower for sodium chloride. Zhang and Cremer [32] suggested that in general positively charged macromolecular systems should show inverse Hofmeister behavior only at relatively low salt concentrations, but revert to a direct Hofmeister series as the salt concentration is increased.
Up to 1.09 M ammonium sulfate at pH 3 and 1.36 M at pH 5 solutions stayed soluble analogous to the systems with 0 M ammonium sulfate. No statement about solubility enhancement and thus direction of the Hofmeister series in this ammonium sulfate concentration range is possible. But solubility in ammonium sulfate solutions is higher than in sodium chloride solutions at the same concentrations. With increasing ammonium sulfate concentration almost exclusively precipitation along with skin formation, i.e. protein denaturation, occurred. This observation negates the reversion to a direct Hofmeister series for high salt concentrations described by Zhang and Cremer [32].
Attractive short–range forces causing aggregation are pH dependent as it was observed for sodium chloride as precipitant, too. The short–range forces increased with increasing distance to the pI resulting in more phase transitions. Attractive short–range forces also increased in strength with increasing ammonium sulfate concentration what resulted in pronounced precipitation and skin formation.

PEG as precipitant No phase transitions were observed for PEG 300 and PEG 1000 up to 15% (w/V) in the investigated protein concentration and pH range. Hence, PEG 300 and PEG 1000 have no effect on the phase behavior of lysozyme from chicken egg white in the investigated protein concentration range.

4.3.3 Human lysozyme

Sodium chloride as precipitant For human lysozyme with sodium chloride as precipitant at pH 3, a broad gelation area was found. The observed gels were translucent. The development of gelation at pH 3 might be due to the appearance of partial denaturation. For globular proteins denaturation is often considered a prerequisite to gelation [33] and a pH value far away from the isoelectric point might lead to partial or complete denaturation for some proteins [34].
Gelation occurred in a sodium chloride concentration range between 1.36 and 2.05 M. For low human lysozyme concentrations gelation appeared exclusively. Increasing protein concentration led to formation of crystals or precipitate or both of them next to gelation. We assume that crystals and precipitate developed in the supernatant of the gelled phase for human lysozyme concentrations that are high enough for short–range

forces to be effective. At 1.59 M sodium chloride for example crystallization co-occurred to gelation for 13.5-16.25 mg/mL human lysozyme, precipitation co-occurred to gelation for 19-21.75 mg/mL. This shows, that short–range forces either increase or gain more impact with increasing protein concentration. This concurs with the results of Stradner et al. [25] who also described a protein concentration dependency of short–range intermolecular forces. The phase behavior of human lysozyme at pH 5, 7 and 9 showed that aggregation propensity decreased with decreasing distance to the isoelectric point. The short–range attractive forces responsible for aggregation of the protein molecules are pH dependent as it was shown for lysozyme from chicken egg white. Aggregation propensity decreases while the short–range attractive forces decrease.
Amorphous structures emerge if short–range forces are very strong [35] because the protein molecules do not have time to orient themselves into a crystal lattice [36]. Short–range forces have to be strong for human lysozyme at pH 5, 7 and 9 using sodium chloride as precipitant because no crystallization area evolved prior to the precipitation area.
Crystallization could only be observed at pH 5 and the crystals arose from the precipitate. It could not be determined if the crystals evolved in the supernatant of the precipitated solution or through restructuring of amorphous precipitate into a crystal lattice. It is also controversial whether the occurrence of amorphous aggregate hinders or promotes crystal growth, but the formation of amorphous aggregate prior to crystallization is a known phenomenon [24]. Piazza [24] explains the evolution of crystals out of precipitate by restructuring of the protein molecules. Crystal growth out of the supernatant of precipitated solutions might be explained as follows. short–range forces are too strong to enable ordered structures, especially at high protein concentrations, and precipitation occurs. In the supernatant of precipitated protein solutions the protein concentration could be low enough to form ordered structures despite the strong short–ranged attraction. This would mean that short–ranged attraction is also driven by protein concentration and decreases in its effectiveness with decreasing protein concentration. Protein concentration dependency of short–range forces was described by Stradner et al. [25]. The overall strength of the short–range attraction at pH 5 has to be higher than at pH 7 and pH 9 to explain why the reduced short–range force in the supernatant only at pH 5 is high enough to result in crystallization.

Ammonium sulfate as precipitant At pH 3 the soluble area is followed by a gelation area. Protein denaturation is often considered a prerequisite for gel formation [33]. As for human lysozyme in sodium chloride solutions this could be due to the pH value far away from the isoelectric point leading to partial or complete denaturation [34]. In contrast to the phase behavior of lysozyme from chicken egg white at pH 5, 7 and 9, ammonium sulfate had a similar but slightly stronger influence on human lysozyme than sodium chloride. Human lysozyme crystals coexisting to precipitate occurred at pH 5, 7 and 9 when using ammonium sulfate whereas using sodium chloride they occurred only at pH 5. As for sodium chloride, the soluble area was followed by a precipitation area. Precipitation started in a medium to high electrolyte region, which means that repulsive electrostatic forces were not significant. For high salt and protein concentrations crystals coexisted with precipitate. The propensity for crystallization decreased with increasing pH value. Short–range attractive forces, as they were described for lysozyme from chicken egg white and sodium chloride as precipitant, again seem to be pH dependent and were

stronger for pH values with a higher distance to the isoelectric point.
A comparison between the phase behavior of human lysozyme and lysozyme from chicken egg white at pH 5, 7 and 9 shows that also the short–range forces are extremely salt-specific. This was earlier described by Piazza [24] who additionally mentioned that the short–range interparticle potential is closely related to the hydrophilic-hydrophobic 'patching' of the protein surface. Schwierz et al. [37] specified these observations and showed that direct, reversed and also partially reversed Hofmeister series are possible depending on the protein surface charge and surface polarity, i.e. hydrophobic patching. This leads to the conclusion that a reversal or transposition of the salt order in the Hofmeister series does not mainly depend on a pH below or above the isoelectric point as it was suggested by Ries-Kautt and Ducruix [31]. We go along with Piazza [24] and Schwierz et al. [37] as we saw that the short–range forces leading to various aggregation processes are extremely salt- and protein-specific and hardly predictable.

PEG as precipitant PEG 300 has no effect on the phase behavior of human lysozyme whereas PEG 1000 has an influence on the aggregation propensity of human lysozyme at pH 7 and pH 9. PEG 1000 causes a higher depletion attraction than PEG 300 due to its larger size. The origin of this depletion attraction is explained in detail in Section 4.3.5 for glucose isomerase.
The fact that PEG 1000 only influences aggregation propensity at pH 7 and pH 9 could be a hint for a pH dependent hydrophobic force. Lee and Lee [38] found that the magnitude of protein solution destabilization by PEG depends on the average hydrophobicity of proteins. Destabilization was stronger for proteins with a higher extent of hydrophilic residues. This might be explained by binding of PEG to sufficiently large hydrophobic protein surface patches as it was described by Baynes and Trout [39] and by that reduction of attractive hydrophobic forces. This means that the average hydrophobicity of human lysozyme at pH 3 and pH 5 is higher than at pH 7 and pH 9 and solution destabilization, i.e. protein aggregation, at pH 3 and pH 5 is reduced by the presence of PEG. Discussion of the destabilizing effect of PEG on glucose isomerase will additionally show that destabilizing effects through depletion attraction occur when electrostatic repulsion is at its minimum, i.e. near the isoelectric point.
According to Lee and Lee [38] we also conclude that the average hydrophobicity of lysozyme from chicken egg white has to be higher than that of human lysozyme because neither PEG 300 nor PEG 1000 showed a destabilizing effect on lysozyme from chicken egg white.

4.3.4 Glucose oxidase

Sodium chloride as precipitant Glucose oxidase with sodium chloride as precipitant showed only transitions from soluble to precipitated states at pH 3 and pH 5. No crystallization was observed in the transition area between soluble and precipitated states.
In the pH range of pH 3-pH 5, close to the isoelectric point of glucose oxidase, long–ranged repulsive electrostatic forces are at the minimum. This is generally observed to decrease protein solubility in solution in a low-electrolyte region where conductivity is low [21]. The lower obtainable stock solution concentration for glucose oxidase at pH 5 was

found to be in agreement. In higher salt concentrations the shielding of long–ranged electrostatic repulsion strengthens the influence of short–range interactions such as van der Waals, osmotic and hydrophobic interactions as described in Section 4.3.2 for lysozyme from chicken egg white. In the high–electrolyte region the extent of glucose oxidase precipitation with sodium chloride as precipitant was found to be lower at pH 5 compared to pH 3 for similar protein concentrations. This behavior of decreasing solubility with increasing distance to the isoelectric point in the pH range of $pH < pI$ indicates a pH dependency of short–range attractive interactions as proposed for lysozyme from chicken egg white. Further it is assumed that acidic pH values can lead to partial or complete protein denaturation (Wang et al., 2010) which consequently increases hydrophobicity. This is in agreement with our experimentally observed phase behavior and might explain the observed increase of short–range forces at pH 3 leading to destabilization of the protein solution.
At pH 7 and pH 9 glucose oxidase was stable in the presence of sodium chloride as precipitant within the experimental range. In this pH range, $pH > pI$, short–range attractive forces were weak for glucose oxidase molecules, as no phase transitions were observed here.

Ammonium sulfate as precipitant For glucose oxidase with ammonium sulfate as precipitant transitions from soluble to precipitated phase states were found at pH 3, 5 and 9.
At pH 3 the precipitation extend was higher compared to pH 5 at similar protein concentrations as was seen for sodium chloride as precipitant. At pH 7 no phase transition was monitored. But at further distance to the isoelectric point, at pH 9, precipitation was observed in the high–electrolyte region for ammonium sulfate.
This precipitation at increasing distance to the isoelectric point in a high–electrolyte region encourages the assumption that pH depended short–range attractive forces are of significant impact.
Further, our results for glucose oxidase showed salting-out for ammonium sulfate when compared to sodium chloride. This salt specificity of short–range forces, as also seen for human lysozyme, was described earlier by Piazza [24]. The order of salts promoting salting-out of glucose oxidase is in agreement with the Hofmeister series [40]. Kosmotropes, such as ammonium sulfate, are strongly hydrated ions (water structure maker) which can lead to destabilization of the protein hydration layer. Therefore the protein reduces solvent accessible surface area by decreasing solubility. This is in contrast to the mode of action of chaotropes, such as sodium chloride. Chaotropic ions are large monovalent ions of low charge density which are weakly hydrated (water structure breaker). Those ions lead to a stabilized hydration shell around the protein maximizing its solvent accessible surface area. At high chaotrope concentrations this can lead to denaturation/unfolding of the protein molecule [41].

PEG as precipitant PEG 300 had no effect on the phase behavior of glucose oxidase up to 15% (w/V) in the investigated pH range. PEG 1000 triggered precipitation of glucose oxidase at pH 5 at PEG concentration of 9.55% (w/V) and above. The destabilizing mechanism of PEG as precipitant can be explained with depletion effects driven by osmotic pressure as described in Section 4.3.5 for glucose isomerase.

This described PEG destabilization mechanism is in agreement with the results presented here for glucose oxidase and PEG 1000 at pH 5. The observed protein destabilization could only emerge at conditions where electrostatic repulsion between protein molecules is at its minimum, close to its isoelectric point.

4.3.5 Glucose isomerase

Sodium chloride as precipitant For glucose isomerase and sodium chloride as precipitant only phase transitions at pH 5 were observed. At this pH, all conditions were instable and showed evolving precipitation and skin formation independent of sodium chloride concentration. In the low-electrolyte region stabilizing electrostatic forces of repulsive nature are suspected to be low due to the vicinity to the isoelectric point of glucose isomerase. The observed skin formation is an indicator for non-native aggregation [18]. This observed phase behavior is supported by findings of partially folded intermediates at pH 5 with higher hydrophobicity and tendency to form aggregation [42]. This tendency to denaturation at low pH was not found for glucose oxidase, a protein with similar isoelectric point to glucose isomerase. Lysozyme from chicken egg white showed skin formation at pH 3 for both investigated salts and at pH 5 for ammonium sulfate in the high–electrolyte region whereas human lysozyme showed no skin formation but gelation.
At pH 7 and pH 9 no phase transitions occurred for glucose isomerase and sodium chloride. Thus, both the low and high-electrolyte environment was governed by stabilizing effects. In the low-electrolyte region this effect is likely to be caused by electrostatic repulsive forces. The high-electrolyte region the solubility mediating effect of the chaotropic salt sodium chloride is likely to be the dominating effect as described in Section 4.3.4 for glucose oxidase.

Ammonium sulfate as precipitant Ammonium sulfate as precipitant caused more phase transitions of glucose isomerase than sodium chloride in the entire investigated pH range.
At pH 5 additional to the observed evolving precipitation and skin formation without salt and in the low-electrolyte region, spontaneous precipitation was observed for ammonium sulfate in the high-electrolyte region. This leads to the assumption of stronger short–range attractive forces in high-electrolyte region for ammonium sulfate when compared with sodium chloride. This emphasizes the salting-out effect of ammonium sulfate and is in agreement with the Hofmeister series [40].
Crystallization of glucose isomerase was found for pH 5, 7 and 9. At pH 5 one condition within a precipitation zone of evolving precipitation and skin formation occurred. At pH 7 and pH 9 crystallization evolved at high ammonium sulfate concentrations. The soluble area increased with increasing pH value. This is in agreement with findings from Chayen et al. [43] in the pH range of 5.5-6.5 at 1.5 M ammonium sulfate. This observation for glucose isomerase leads to the assumption that short–range attractive interactions are weaker with increasing distance to the isoelectric point. Those attractive interactions are weak enough to form three dimensional crystals. Nonspecific aggregation would appear if attractive interactions are stronger.
Our findings concerning the pH dependency of short–range attractive forces vary for

the investigated alkaline proteins, such as lysozyme from chicken egg white and human lysozyme, and acidic proteins glucose oxidase and glucose isomerase. For the alkaline proteins the short–range forces increase with increasing distance to the isoelectric point whereas for the acidic proteins lower shortrange attractive forces are found in greater distance of the proteins isoelectric point.

PEG as precipitant Polyethylene glycol (PEG) resulted in phase transitions towards precipitation and liquid–liquid phase separation (LLPS) for glucose isomerase at pH 5.

Thus, an influence of PEG was only seen at conditions close to the isoelectric point of the protein where electrostatic repulsive forces are at their minimum. Therefore attractive protein-protein interactions encouraged by PEG are at a maximum where electrostatic repulsion is at its minimum. Phase transitions were found for glucose isomerase and glucose oxidase at pH 5 and human lysozyme at pH 7 and pH 9. No phase transition was found for lysozyme from chicken egg white.

PEG molecules are non-adsorbing and non-polar polymers. PEG influence has previously been described using the depletion attraction mechanism which was first proposed in 1958 by Asakura and Oosawa [44] for colloidal particles in a suspension of macromolecules. The depletion attraction effect appears when the distance between protein molecules becomes smaller than the diameter of the polymer molecules. A concentration gradient of polymer between the inter-protein area and the bulk solution is the result. As a consequence of this 'polymer depletion', water molecules are drawn out of the gap between the protein molecules resulting in an osmotic pressure change and encourages protein–protein interactions [44]. The extent of the depletion effect is dependent on PEG molecular weight and concentration. PEG at higher concentrations and with higher molecular weight induces a stronger depletion effect [45]. Small PEG molecules with molecular size below the distance of two protein molecules can enter into the -protein-protein interspace. This may help to shield possible attractive protein–protein interactions, thus lead to protein solution stabilization.

The consequence of PEG destabilization is protein aggregation in form of crystallization [46] precipitation [47] or liquid–liquid phase separation [48]. The latter is described to be the consequence of PEG destabilization and short–range attractive protein interactions [49]. This metastable phase separation state parts the solution into a dilute protein state and rich 'dense' protein droplets [17].

In agreement with the described theories we found that PEG stabilizing and destabilizing interaction mechanisms are dependent on PEG molecular weight and concentration. The PEG induced attractive protein–protein interactions were only large enough to emerge in solution conditions were long–range electrostatic repulsive forces are at its minimum, close to the isoelectric point, and for the higher molecular weight PEG molecule, PEG 1000. This led to precipitation at high PEG concentration for glucose oxidase at pH 5 and human lysozyme at pH 7 and pH 9.

For glucose isomerase the PEG 1000 effect at pH 5 is more complex. The destabilizing effects are more pronounced: LLPS and spontaneous precipitation occurred at lower precipitant concentration when compared to PEG 300. LLPS occurred in the transition zone just before spontaneous precipitation. This is in agreement with literature describing this phase state as metastable [17]. Skin formation was suppressed at high PEG 1000

concentrations. However, this was likely not a stabilizing effect of the PEG, but rather the results of PEG promoting protein–protein interactions leading to rapid precipitation in the native state rather than denaturing and skin formation. For the lower molecular weight PEG 300 a balance of stabilizing and destabilizing effects was observed for glucose isomerase at pH 5. PEG 300 stabilized the protein solution by suppressing skin formation starting at the lowest examined PEG concentration. Destabilization was observed at the highest PEG concentration of 15% (w/V) where LLPS formation occurred. This balance of stabilizing and destabilizing effects is in agreement with the proposed PEG mechanism at low molecular weight. PEG 300 is small enough to penetrate the inter-protein area. While separating the protein molecules it is proposed to stabilize the native protein structure leading to stabilization whilst suppressing skin formation. At higher PEG 300 concentration this stabilization is obscured by the destabilizing effect due to depletion attraction leading to formation of LLPS.

5 Conclusion

A method to generate protein phase diagrams in high throughput on an automated liquid handling station in microbatch scale was successfully developed. It was shown that thorough optimization of liquid handling parameters is critical for generation of high quality data. Buffering components need to be selected carefully, especially when high salt concentrations are used, in order to prevent unwanted pH shifts in the samples.
The method allowed for realization of an extensive and systematic study of protein phase behavior in a reasonable amount of time. Thereby the general knowledge on phase behavior of proteins, the influence of salts and the understanding of effects of extreme pH values and effects of PEG on protein structure and solution stability could be increased. For the investigated proteins it was possible to induce all known phase transitions. The investigated salts thereby showed various effects on the protein phase behavior. It was shown that extremely acidic pH values induce specific phase transitions such as skin formation and gelation. Gelation and skin formation are assumed to be related to partial or complete protein denaturation.
To the best of our knowledge the here proposed and experimentally supported pH dependency of short–range attractive forces was not described in literature earlier.
It can be supported that the phase behavior with PEG precipitants is dependent on PEG molecular size, concentration and protein charge. For the lower molecular weight PEG 300 stabilizing effects could be found for glucose isomerase. At higher molecular weight, PEG 1000, destabilization was triggered at conditions close to the isoelectric point of glucose oxidase, glucose isomerase and human lysozyme. Here electrostatic repulsion is at its minimum and destabilizing effects due to depletion attraction can resume.

Acknowledgements

We gratefully acknowledge the expertise and support by Sigrid K. Hansen and Florian Dismer. We also gratefully acknowledge the financial support by the Federal Ministry of Education and Research (BMBF) (0315342B).

Appendix A. Supplementary data

Supplementary data associated with this article can also be found, in the online version, at http://dx.doi.org/10.1016/j.ijpharm.2014.12.027.
A total of 64 protein phase diagrams were determined as experimental fundament for this work. Selected phase diagrams of each protein were described in detail in Section 3. in the manuscript. All determined phase diagrams are shown in the following sections.

Lysozyme from chicken egg white Phase diagrams of lysozyme from chicken egg white for pH 3 are shown in Fig. S1, for pH 5 in Fig. S2, for pH 7 in Fig. S3 and for pH 9 in Fig. S4.

Human lysozyme Phase diagrams of human lysozyme for pH 3 are shown in Fig. S5, for pH 5 in Fig. S6, for pH 7 in Fig. S7 and for pH 9 in Fig. S8.

Glucose oxidase Phase diagrams of glucose oxidase for pH 3 are shown in Fig. S9, for pH 5 in Fig. S10, for pH 7 in Fig. S11 and for pH 9 in Fig. S12.

Glucose isomerase Phase diagrams of glucose isomerase for pH 3 are shown in Fig. S13, for pH 5 in Fig. S14, for pH 7 in Fig. S15 and for pH 9 in Fig. S16.

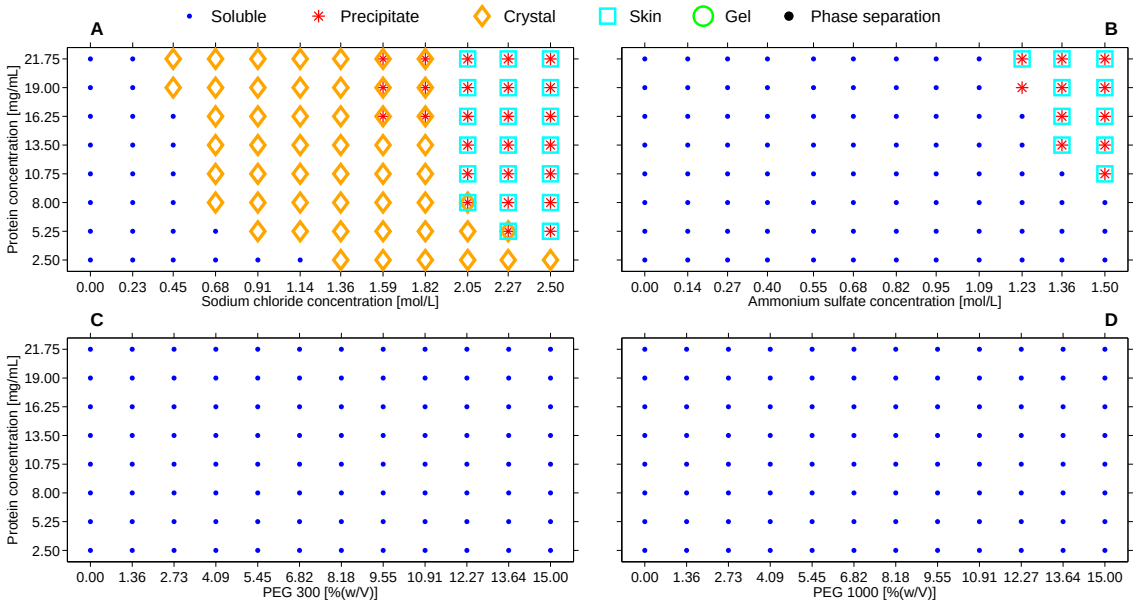

Fig. S1: Phase diagrams of lysozyme from chicken egg white at pH 3 using sodium chloride (A), ammonium sulfate (B), PEG 300 (C) or PEG 1000 (D) as precipitant.

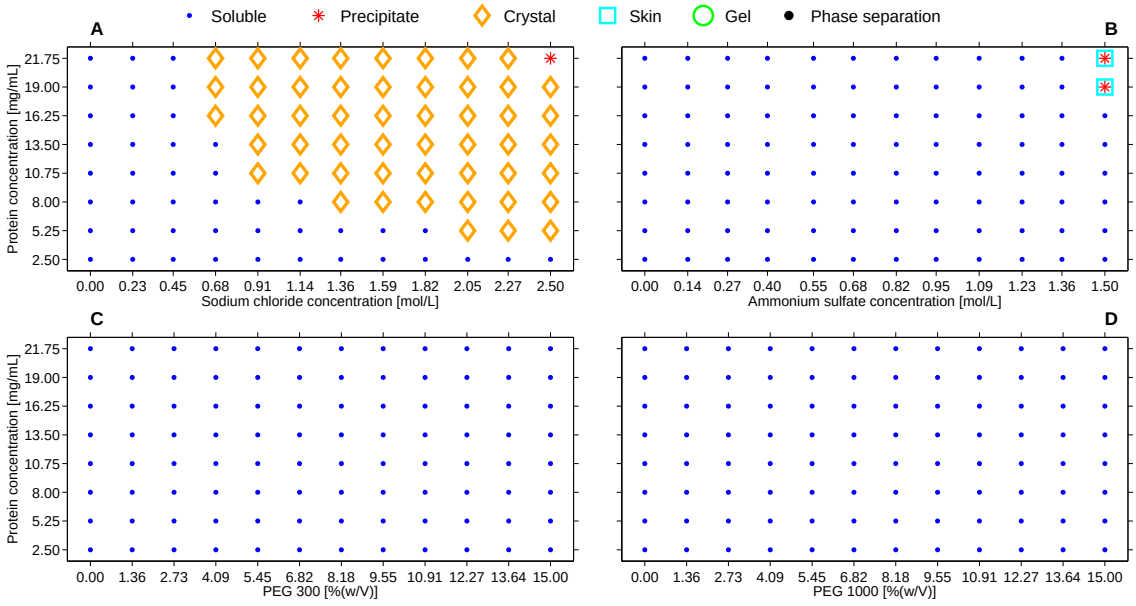

Fig. S2: Phase diagrams of lysozyme from chicken egg white at pH 5 using sodium chloride (A), ammonium sulfate (B), PEG 300 (C) or PEG 1000 (D) as precipitant.

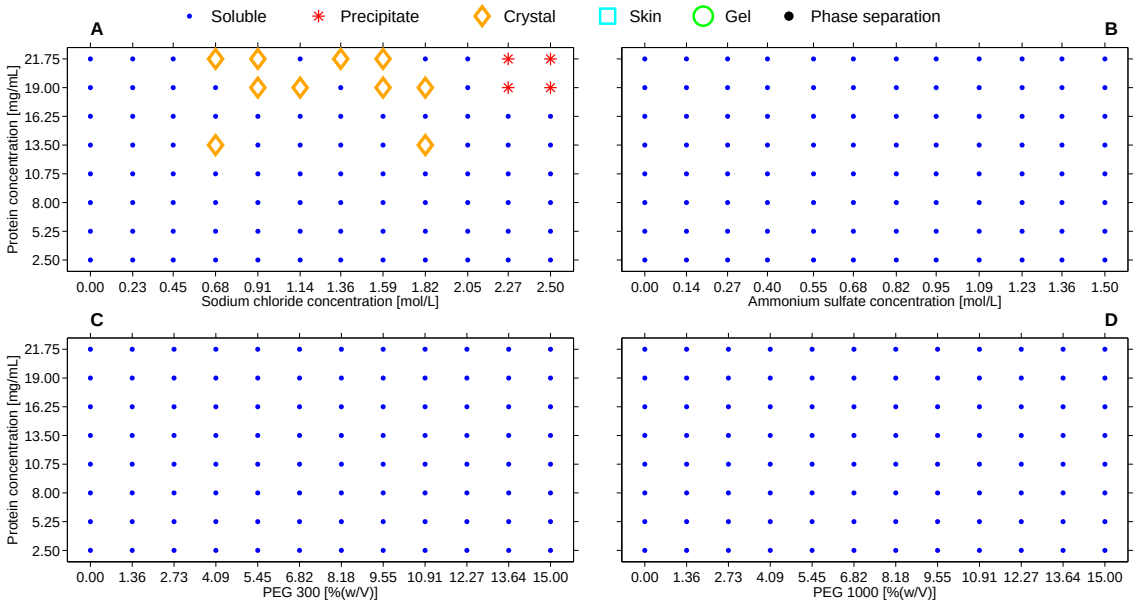

Fig. S3: Phase diagrams of lysozyme from chicken egg white at pH 7 using sodium chloride (A), ammonium sulfate (B), PEG 300 (C) or PEG 1000 (D) as precipitant.

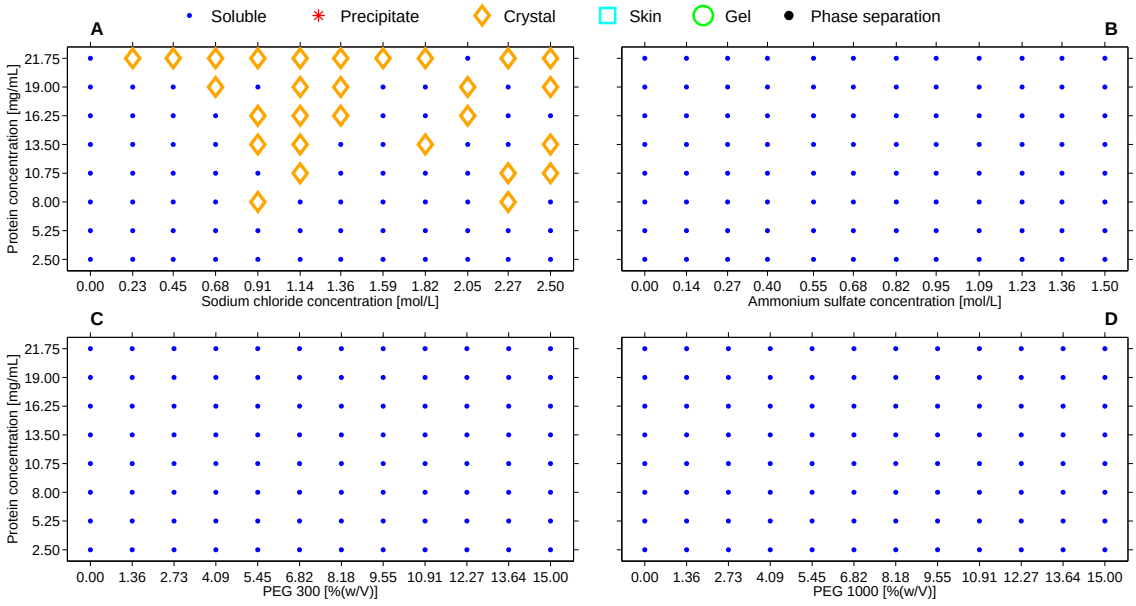

Fig. S4: Phase diagrams of lysozyme from chicken egg white at pH 9 using sodium chloride (A), ammonium sulfate (B), PEG 300 (C) or PEG 1000 (D) as precipitant.

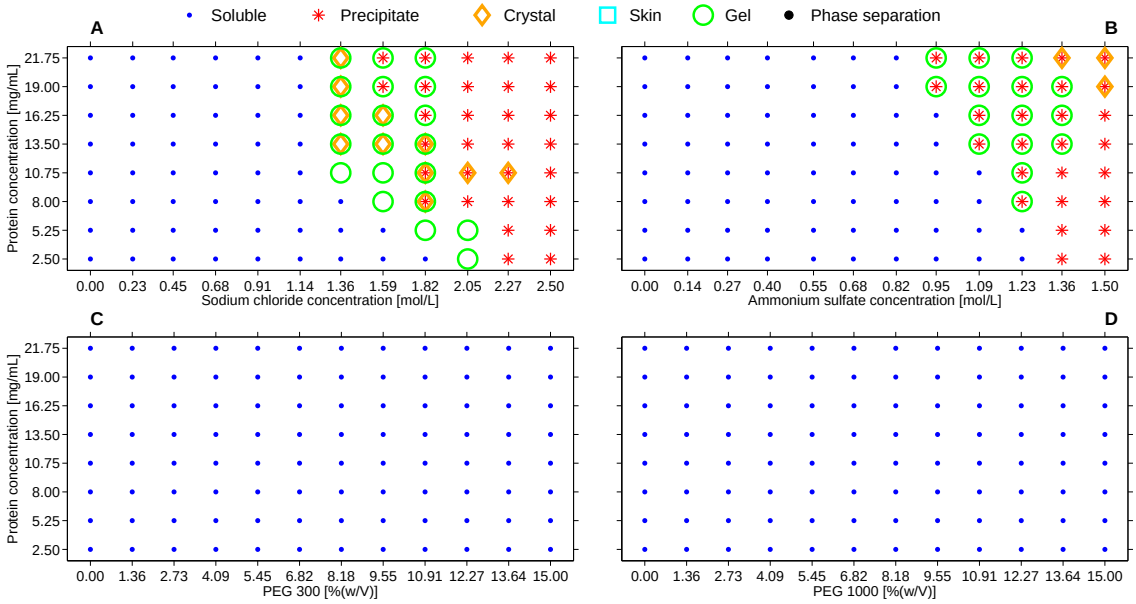

Fig. S5: Phase diagrams of human lysozyme at pH 3 using sodium chloride (A), ammonium sulfate (B), PEG 300 (C) or PEG 1000 (D) as precipitant.

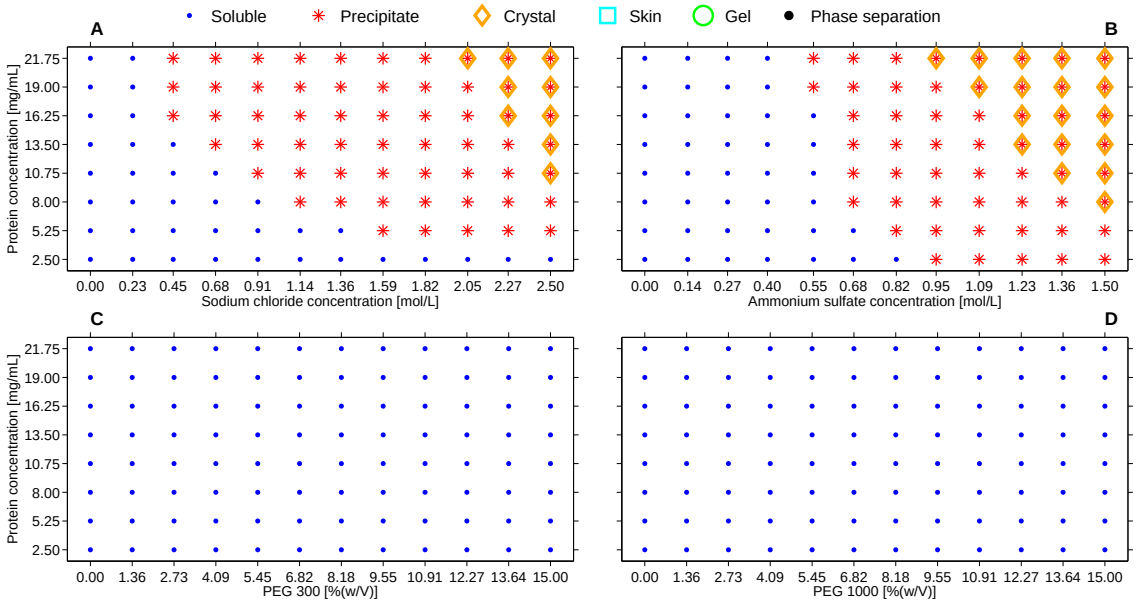

Fig. S6: Phase diagrams of human lysozyme at pH 5 using sodium chloride (A), ammonium sulfate (B), PEG 300 (C) or PEG 1000 (D) as precipitant.

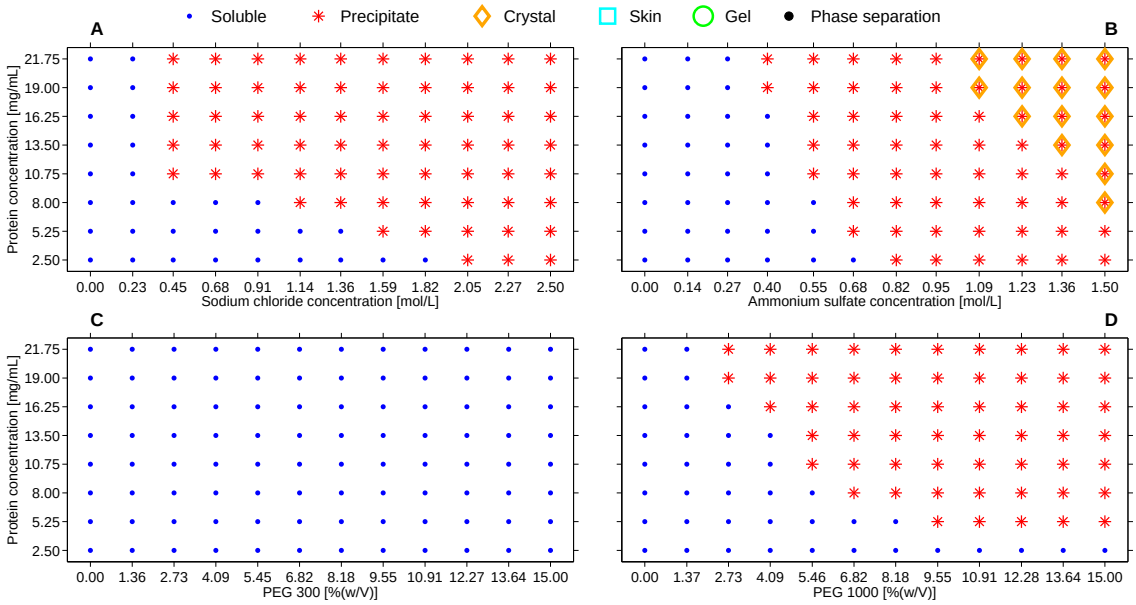

Fig. S7: Phase diagrams of human lysozyme at pH 7 using sodium chloride (A), ammonium sulfate (B), PEG 300 (C) or PEG 1000 (D) as precipitant.

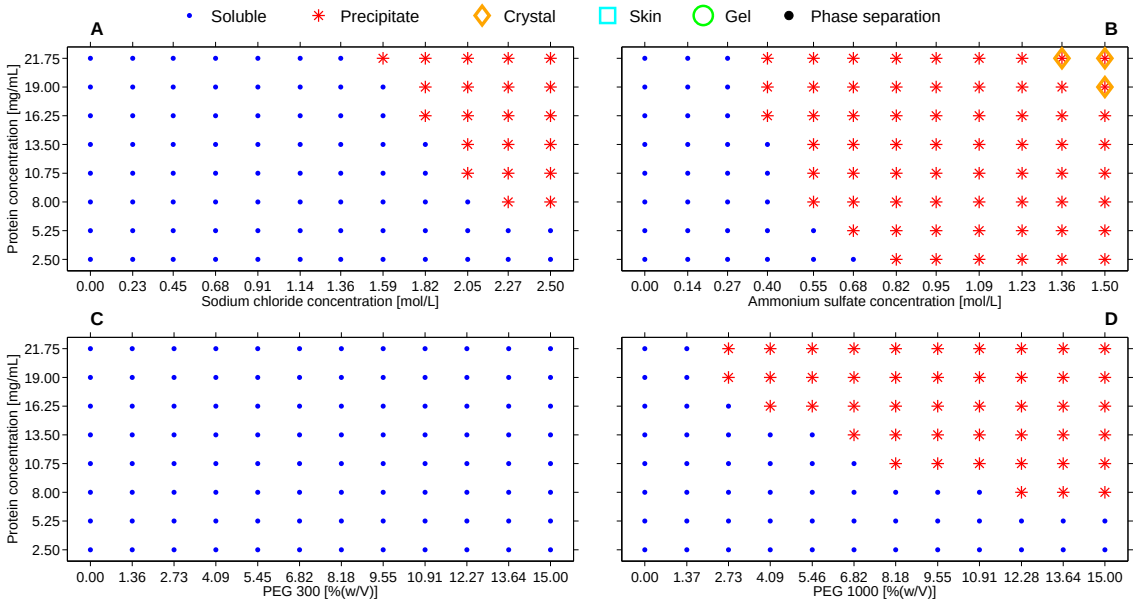

Fig. S8: Phase diagrams of human lysozyme at pH 9 using sodium chloride (A), ammonium sulfate (B), PEG 300 (C) or PEG 1000 (D) as precipitant.

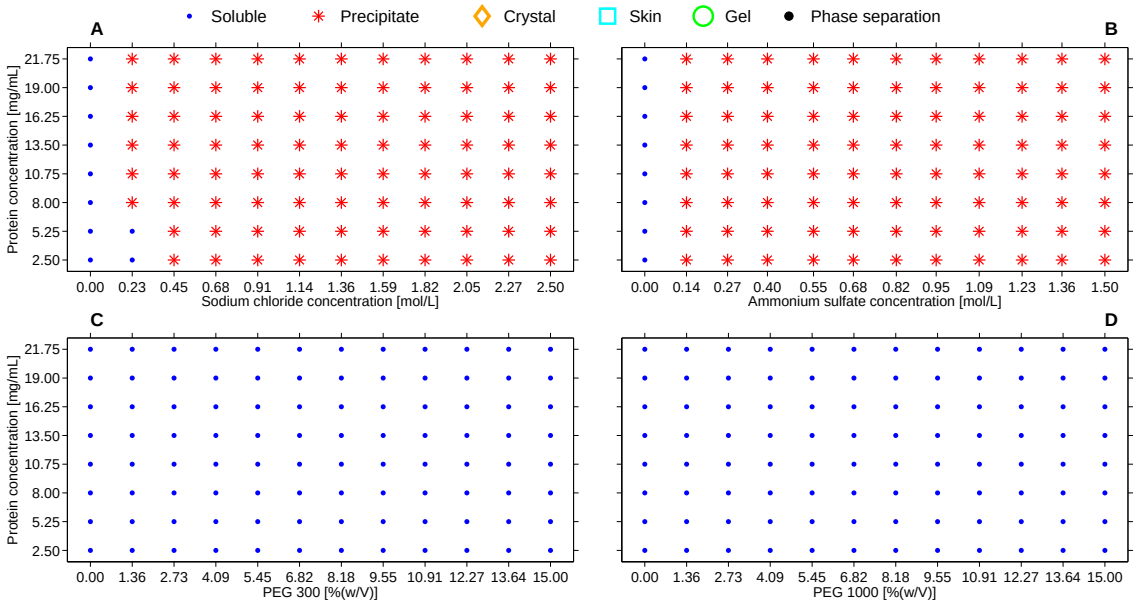

Fig. S9: Phase diagrams of glucose oxidase at pH 3 using sodium chloride (A), ammonium sulfate (B), PEG 300 (C) or PEG 1000 (D) as precipitant.

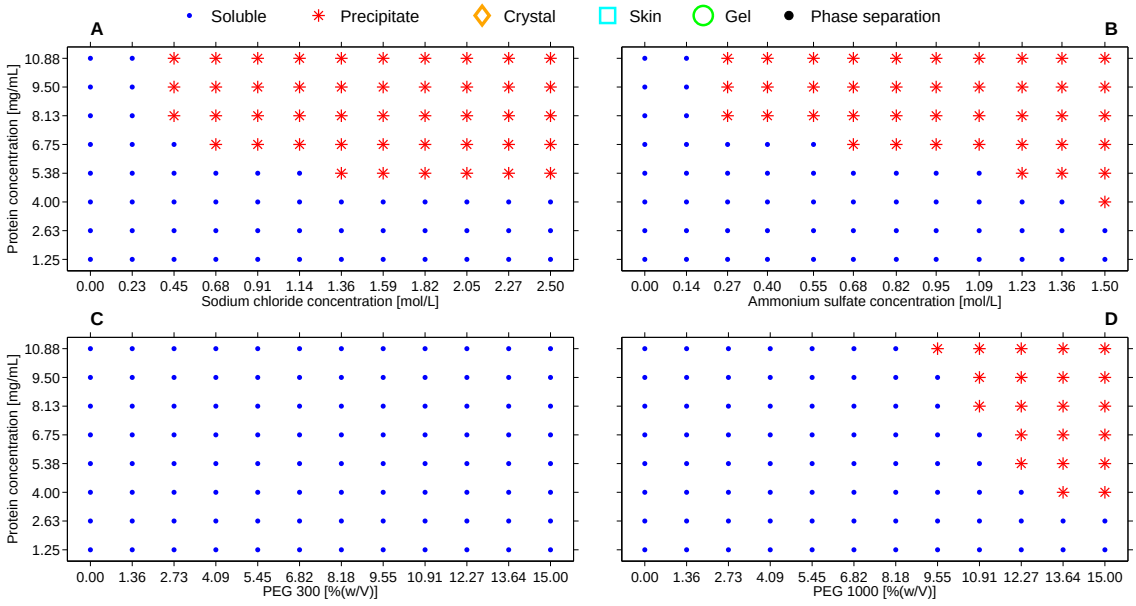

Fig. S10: Phase diagrams of glucose oxidase at pH 5 using sodium chloride (A), ammonium sulfate (B), PEG 300 (C) or PEG 1000 (D) as precipitant.

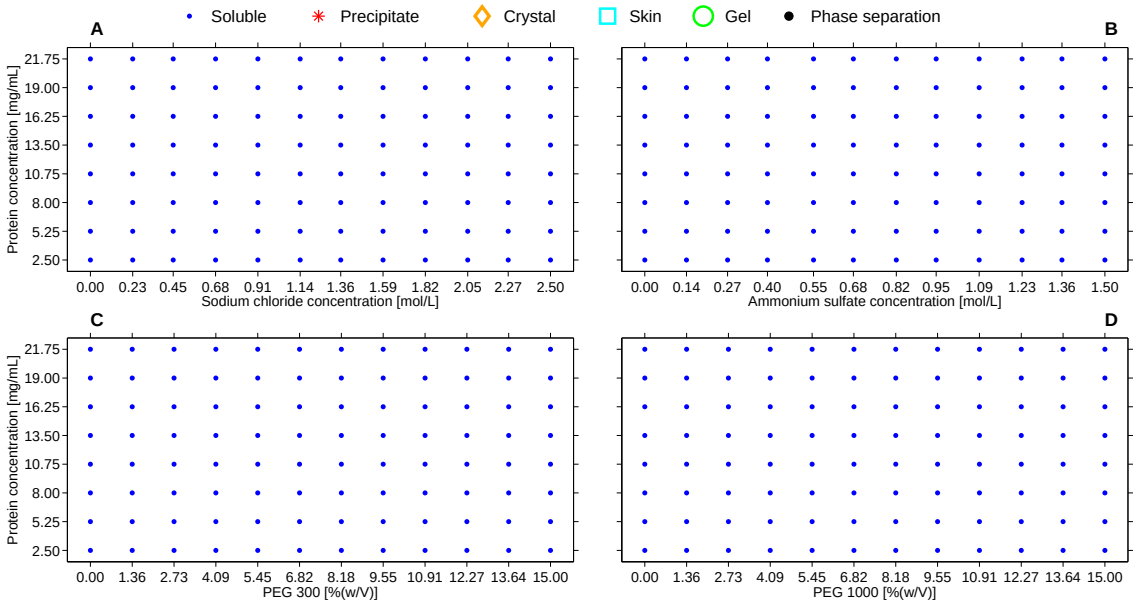

Fig. S11: Phase diagrams of glucose oxidase at pH 7 using sodium chloride (A), ammonium sulfate (B), PEG 300 (C) or PEG 1000 (D) as precipitant.

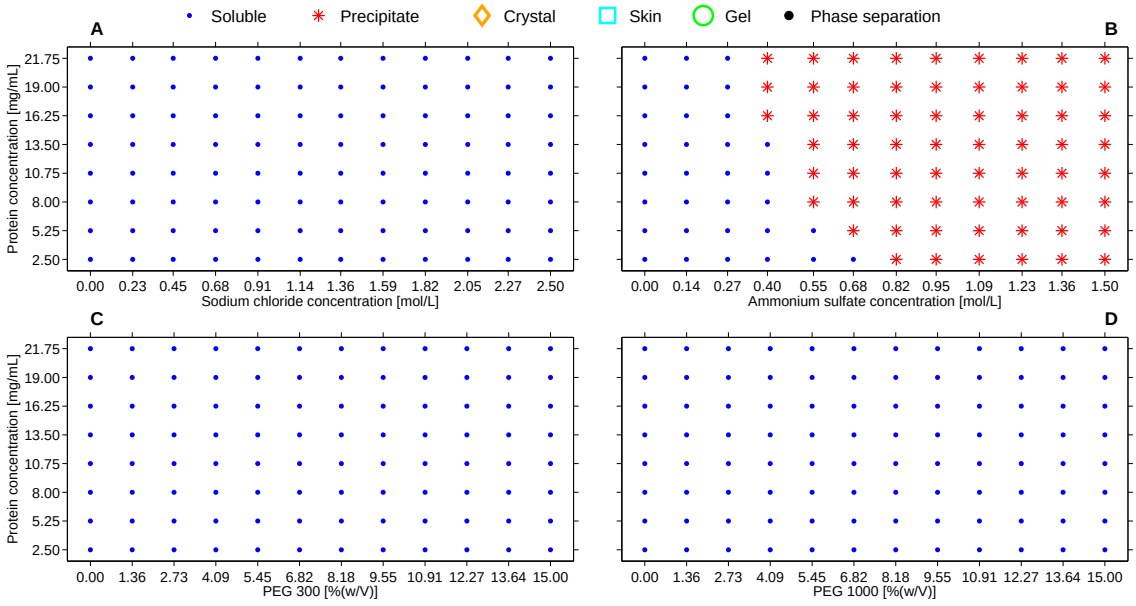

Fig. S12: Phase diagrams of glucose oxidase at pH 9 using sodium chloride (A), ammonium sulfate (B), PEG 300 (C) or PEG 1000 (D) as precipitant.

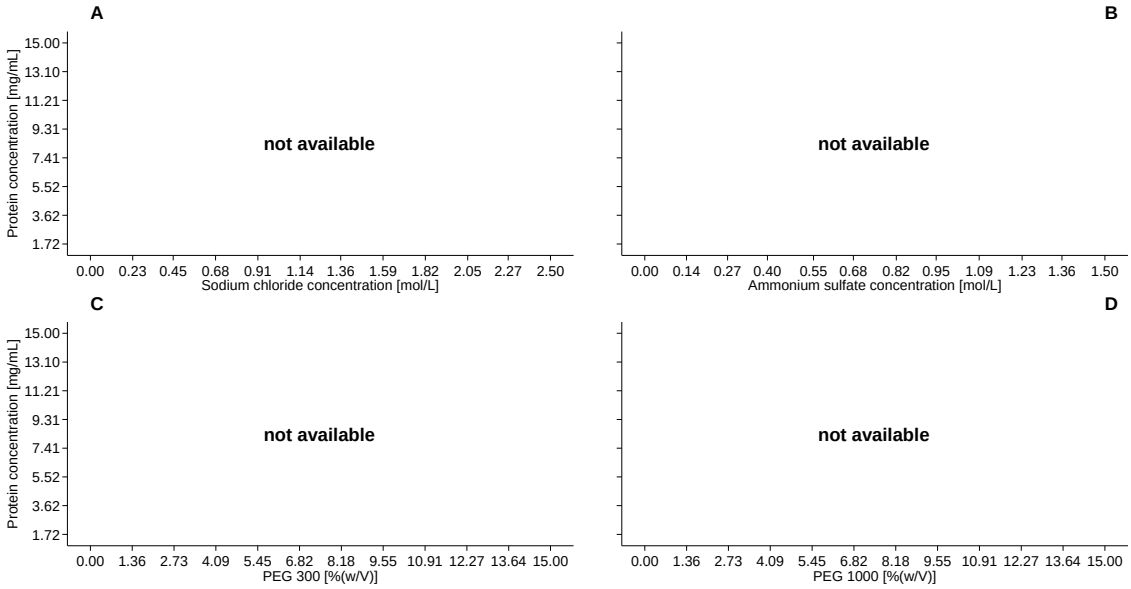

Fig. S13: Phase diagrams of glucose isomerase at pH 3 using sodium chloride (A), ammonium sulfate (B), PEG 300 (C) or PEG 1000 (D) as precipitant.

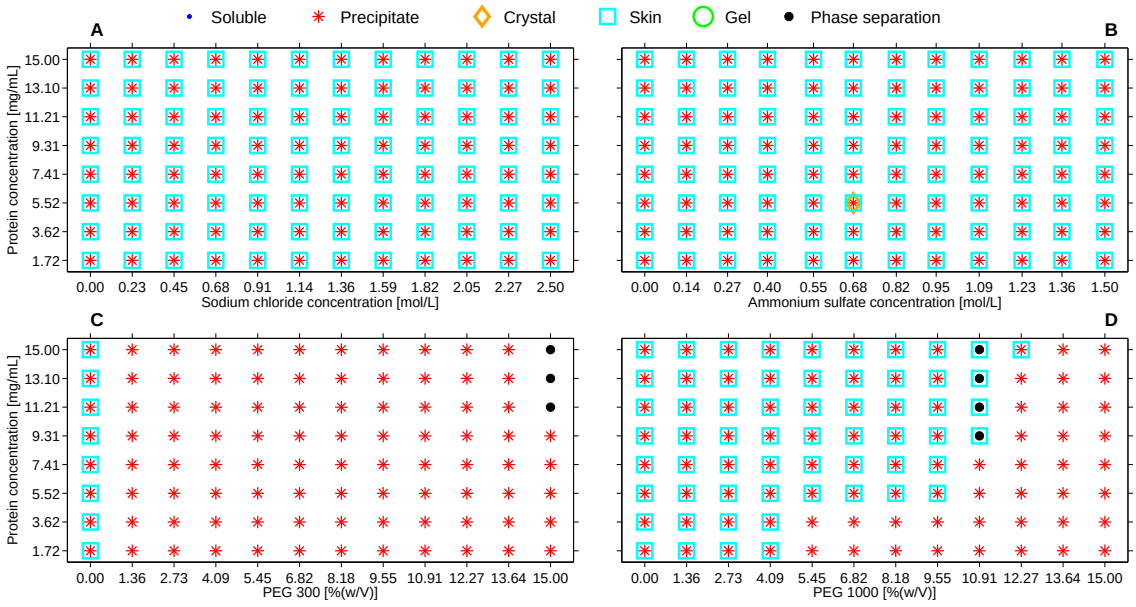

Fig. S14: Phase diagrams of glucose isomerase at pH 5 using sodium chloride (A), ammonium sulfate (B), PEG 300 (C) or PEG 1000 (D) as precipitant.

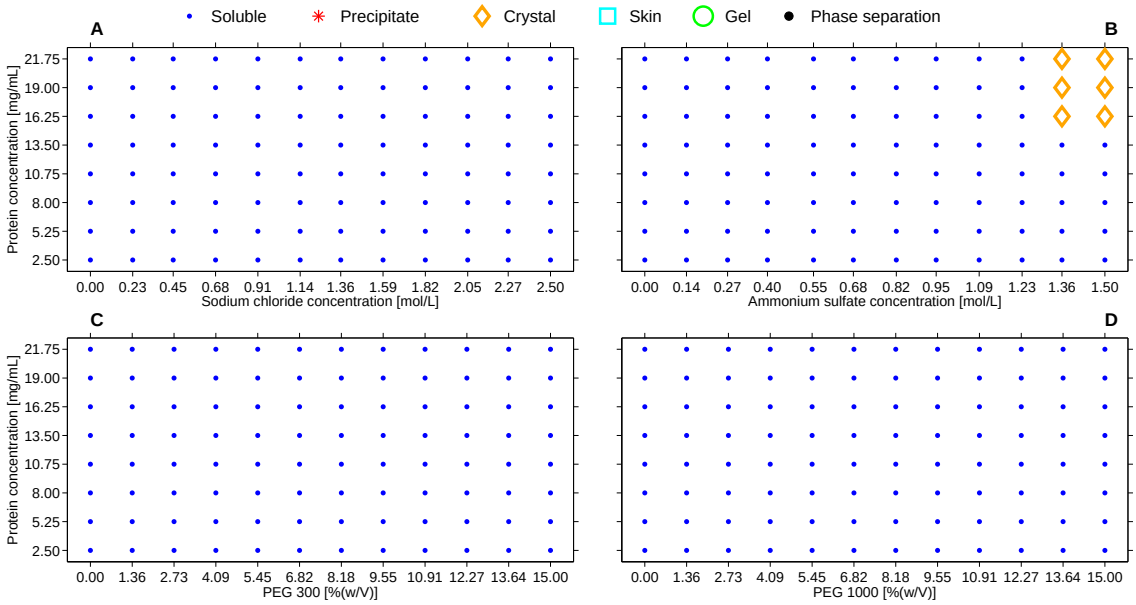

Fig. S15: Phase diagrams of glucose isomerase at pH 7 using sodium chloride (A), ammonium sulfate (B), PEG 300 (C) or PEG 1000 (D) as precipitant.

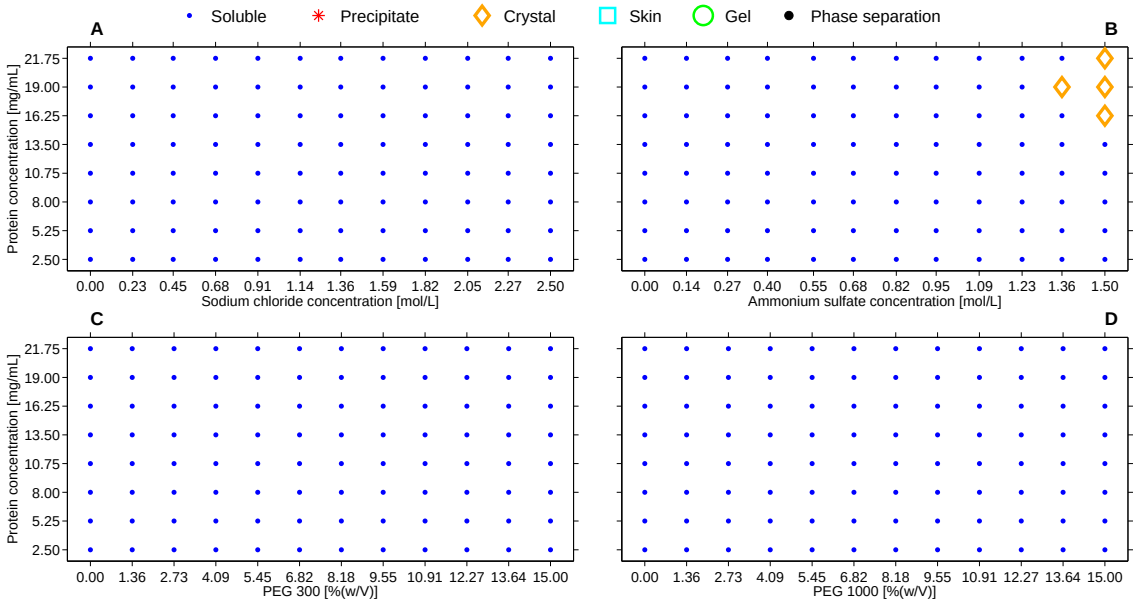

Fig. S16: Phase diagrams of glucose isomerase at pH 9 using sodium chloride (A), ammonium sulfate (B), PEG 300 (C) or PEG 1000 (D) as precipitant.

References

[1] T. Ahamed, B. N. A. Esteban, M. Ottens, G. W. K. van Dedem, L. A. M. van der Wielen, M. A. T. Bisschops, A. Lee, C. Pham, J. Thömmes, Phase behavior of an intact monoclonal antibody, Biophys. J. (2) 610–619. doi:10.1529/biophysj.106.098293.

[2] N. Asherie, Protein crystallization and phase diagrams, Methods (3) 266–272. doi:10.1016/j.ymeth.2004.03.028.

[3] C. Faber, T. J. Hobley, Measurement and Prediction of Protein Phase Behaviour and Protein-Protein-Interactions, Ph.D. thesis (2006).

[4] A. C. Dumetz, A. M. Chockla, E. W. Kaler, A. M. Lenhoff, Comparative Effects of Salt, Organic, and Polymer Precipitants on Protein Phase Behavior and Implications for Vapor Diffusion, Cryst. Growth Des. (2) 682–691. doi:10.1021/cg700956b.

[5] A. McPherson, A comparison of salts for the crystallization of macromolecules, Protein Sci. 10 (2001) 418–422. doi:10.1110/ps.32001.418.

[6] Y.-B. Lin, D.-W. Zhu, T. Wang, J. Song, Y.-S. Zou, Y.-L. Zhang, S.-X. Lin, An Extensive Study of Protein Phase Diagram Modification: Increasing Macromolecular Crystallizability by Temperature Screening, Cryst. Growth Des. (12) 4277–4283. doi:10.1021/cg800698p.

[7] N. E. Chayen, E. Saridakis, Protein crystallization: from purified protein to diffraction-quality crystal, Nat. Methods 5 (2) (2008) 147–153.

[8] J. R. Luft, G. T. DeTitta, Rational Selection of Crystallization Techniques, in: T. M. Bergfors (Ed.), Protein Cryst., 2nd Edition, Internat'l University Line, 2009, Ch. 2, pp. 11–46.

[9] R. Boistelle, J. P. Astier, Crystallization mechanisms in solution, J. Cryst. Growth 90 (1988) 14–30.

[10] A. McPherson, B. Cudney, Searching for silver bullets: an alternative strategy for crystallizing macromolecules., J. Struct. Biol. (3) 387–406. doi:10.1016/j.jsb.2006.09.006.

[11] H. M. Kalisz, H.-J. Hecht, D. Schomburg, R. D. Schmis, Crystallization and preliminary X-ray diffraction studies of a deglycosylated glucose oxidase from Aspergillus niger, J. Mol. Biol. 213 (1990) 207–209.

[12] J. Lu, X.-J. Wang, C.-B. Ching, Effect of Additives on the Crystallization of Lysozyme and Chymotrypsinogen A, Cryst. Growth Des. 3 (1) (2003) 83–87.

[13] M. Sleutel, R. Willaert, C. Gillespie, C. Evrard, L. Wyns, D. Maes, Kinetics and Thermodynamics of Glucose Isomerase Crystallization, Cryst. Growth Des. 9 (1) (2009) 497–504.

[14] R. Anandakrishnan, B. Aguilar, A. V. Onufriev, H++ 3.0: automating pK prediction and the preparation of biomolecular structures for atomistic molecular modeling and simulations., Nucleic Acids Res. (Web Server issue) W537–W541. doi:10.1093/nar/gks375.

[15] S. A. Oelmeier, F. Dismer, J. Hubbuch, Application of an aqueous two-phase systems high-throughput screening method to evaluate mAb HCP separation, Biotechnol. Bioeng. (1) 69–81. doi:10.1002/bit.22900.

[16] A. D'Arcy, A. Mac Sweeney, M. Stihle, A. Haber, The advantages of using a modified microbatch method for rapid screening of protein crystallization conditions, Acta Crystallogr. Sect. D Biol. Crystallogr. (2) 396–399. doi:10.1107/S0907444902022011.

[17] A. C. Dumetz, A. M. Chockla, E. W. Kaler, A. M. Lenhoff, Protein phase behavior in aqueous solutions: crystallization, liquid-liquid phase separation, gels, and aggregates, Biophys. J. (2) 570–583. doi:10.1529/biophysj.107.116152.

[18] J. P. Zeelen, Interpretation of the Crystallization Drop Results, in: T. M. Bergfors (Ed.), Protein Cryst., 2nd Edition, Internat'l University Line, 2009, Ch. 10, pp. 175–194.

[19] P. Debye, E. Hückel, Zur Theorie der Elektrolyte, Phys. Zeitschrift 24 (11) (1923) 185–206.

[20] F. Kröner, J. Hubbuch, Systematic generation of buffer systems for pH gradient ion exchange chromatography and their application., J. Chromatogr. A 78–87doi:10.1016/j.chroma.2013.02.017.

[21] R. K. Scopes, Separation by Precipitation, in: Protein Purif. Princ. Pract., 3rd Edition, Springer-Verlag New York, Inc., 1994, Ch. 4, pp. 71–101.

[22] O. D. Velev, E. W. Kaler, A. M. Lenhoff, Protein interactions in solution characterized by light and neutron scattering: comparison of lysozyme and chymotrypsinogen, Biophys. J. (6) 2682–2697. doi:10.1016/S0006-3495(98)77713-6.

[23] S. Beretta, G. Chirico, G. Baldini, Short-Range Interactions of Globular Proteins at High Ionic Strengths, Macromolecules (23) 8663–8670. doi:10.1021/ma0006171.

[24] R. Piazza, Interactions and phase transitions in protein solutions, Curr. Opin. Colloid Interface Sci. 38–43doi:10.1016/S1359-0294(00)00034-0.

[25] A. Stradner, H. Sedgwick, F. Cardinaux, W. C. K. Poon, S. U. Egelhaaf, P. Schurtenberger, Equilibrium cluster formation in concentrated protein solutions and colloids, Nature (7016) 492–495. doi:10.1038/nature03109.

[26] A. Tardieu, F. Bonneté, S. Finet, D. Vivarès, Understanding salt or PEG induced attractive interactions to crystallize biological macromolecules, Acta Crystallogr. Sect. D Biol. Crystallogr. (10) 1549–1553. doi:10.1107/S0907444902014439.

[27] D. Leckband, J. Israelachvili, Intermolecular forces in biology, Q. Rev. Biophys. (2) 105–267.

[28] R. A. Curtis, J. M. Prausnitz, H. W. Blanch, Protein-protein and protein-salt interactions in aqueous protein solutions containing concentrated electrolytes, Biotechnol. Bioeng. (1) 11–21.

[29] V. Vlachy, H. W. Blanch, J. M. Prausnitz, Liquid-liquid phase separations in aqueous solutions of globular proteins, AIChE J. (2) 215–223. doi:10.1002/aic.690390204.

[30] V. Vlachy, J. M. Prausnitz, Donnan Equilibrium. Hypernetted-Chain Study of One-Component and Multicomponent Models for Aqueous Polyelectrolyte Solutions, J. Phys. Chem. 96 (15) (1992) 6465–6469.

[31] M. M. Ries-Kautt, A. F. Ducruix, Relative effectiveness of various ions on the solubility and crystal growth of lysozyme, J. Biol. Chem. (2) 745–748.

[32] Y. Zhang, P. S. Cremer, The inverse and direct Hofmeister series for lysozyme, Proc. Natl. Acad. Sci. U. S. A. (36) 15249–15253. doi:10.1073/pnas.0907616106.

[33] G. R. Ziegler, E. A. Foegeding, The Gelation of Proteins, in: J. E. Kinsella (Ed.), Adv. Food Nutr. Res., Academic Press, 1990, pp. 203–298.

[34] W. Wang, N. Li, S. Speaker, External Factors Affecting Protein Aggregation, in: W. Wang, C. J. Roberts (Eds.), Aggreg. Ther. Proteins, 1st Edition, John Wiley & Sons, 2010, Ch. 4, pp. 119–204.

[35] A. George, W. W. Wilson, Predicting protein crystallization from a dilute solution property, Acta Crystallogr. D. Biol. Crystallogr. (Pt 4) 361–365. doi:10.1107/S0907444994001216.

[36] R. A. Curtis, J. Ulrich, A. Montaser, J. M. Prausnitz, H. W. Blanch, Protein-protein interactions in concentrated electrolyte solutions, Biotechnol. Bioeng. (4) 367–380. doi:10.1002/bit.10342.

[37] N. Schwierz, D. Horinek, R. R. Netz, Reversed anionic Hofmeister series: the interplay of surface charge and surface polarity, Langmuir (10) 7370–7379. doi:10.1021/la904397v.

[38] J. C. Lee, L. L. Y. Lee, Preferential solvent interactions between proteins and polyethylene glycols, J. Biol. Chem. (2) 625–631.

[39] B. M. Baynes, B. L. Trout, Rational design of solution additives for the prevention of protein aggregation, Biophys. J. (3) 1631–1639. doi:10.1529/biophysj.104.042473.

[40] F. Hofmeister, Zur Lehre von der Wirkung der Salze, Arch. für Exp. Pathol. und Pharmakologie 25 (1) (1888) 1–30.

[41] K. D. Collins, Ions from the Hofmeister series and osmolytes: effects on proteins in solution and in the crystallization process, Methods (3) 300–311. doi:10.1016/j.ymeth.2004.03.021.

[42] S. A. Pawar, V. V. Deshpande, Characterization of acid-induced unfolding intermediates of glucose/xylose isomerase, Eur. J. Biochem. (21) 6331–6338.

[43] N. Chayen, J. Akins, S. Campbell-Smith, D. M. Blow, Solubility of glucose isomerase in ammonium sulphate solutions, J. Cryst. Growth 90 (1988) 112–116.

[44] S. Asakura, F. Oosawa, Interaction between Particles Suspended in Solutions of Macromolecules, J. Polym. Sci. 33 (126) (1958) 183–192.

[45] D. Vivarès, L. Belloni, a. Tardieu, F. Bonneté, Catching the PEG-induced attractive interaction between proteins., Eur. Phys. J. E. Soft Matter (1) 15–25. doi:10.1140/epje/i2002-10047-7.

[46] A. McPherson, Crystallization of Proteins from Polyethylene Glycol, J. Biol. Chem. 251 (20) (1976) 6300–6303.

[47] D. H. Atha, K. C. Inghamg, Mechanism of Precipitation of Proteins by Polyethylene Glycols, J. Biol. Chem. 256 (23) (1981) 12108–12117.

[48] O. Annunziata, N. Asherie, A. Lomakin, J. Pande, O. Ogun, G. B. Benedek, Effect of polyethylene glycol on the liquid-liquid phase transition in aqueous protein solutions, Proc. Natl. Acad. Sci. U. S. A. (22) 14165–14170. doi:10.1073/pnas.212507199.

[49] M. H. J. Hagen, D. Frenkel, Determination of phase diagrams for the hard-core attractive Yukawa system, J. Chem. Phys. (5) 4093–4097. doi:10.1063/1.467526.

The Influence of Mixed Salts on the Capacity of HIC Adsorbers: A Predictive Correlation to the Surface Tension and the Aggregation Temperature

Kai Baumgartner[1], Sven Amrhein[1], Stefan A. Oelmeier[1] and Jürgen Hubbuch[1,*]

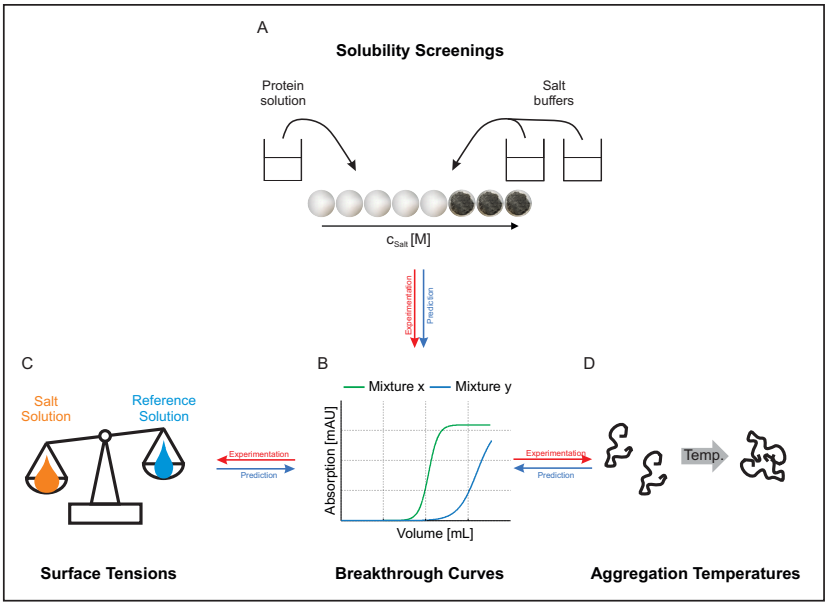

[1] : *Institute of Engineering in Life Sciences, Section IV: Biomolecular Separation Engineering, Karlsruhe Institute of Technology, Engler-Bunte-Ring 3, 76131 Karlsruhe, Germany*

[*] : *Corresponding author; mail: juergen.hubbuch@kit.edu*

Biotechnology Progress

Volume 1396, (2015), 77-85

Submitted: 26. June 2015
Accepted: 2. September 2015
Available online: 11. September 2015

Abstract

Hydrophobic interaction chromatography (HIC) is one of the most frequently used purification methods in downstream processing of biopharmaceuticals. During HIC, salts are the governing additives contributing to binding strength, binding capacity, and protein solubility in the liquid phase.
A relatively recent approach to increase the dynamic binding capacity (DBC) of HIC adsorbers is the use of salt mixtures. By mixing chaotropic with kosmotropic salts, the DBC can strongly be influenced. For salt mixtures with a higher proportion of chaotropic than kosmotropic salt, higher DBCs were achieved compared to single salt approaches. By measuring the surface tensions of the protein salt solutions, the cavity theory – proposed by Melander and Horváth –, that higher surface tensions lead to higher DBCs, was found to be invalid for salt mixtures. Aggregation temperatures of lysozyme in the salt mixtures, as a degree of hydrophobic forces, were correlated to the DBCs. Measuring the aggregation temperatures has proven to be a fast analytical methodology to estimate the hydrophobic interactions and thus can be used as a measure for an increase or decrease in the DBCs.

Keywords: Hydrophobic Interaction Chromatography, Mixed Salts, Dynamic Binding Capacity, Surface Tension, Aggregation Temperature

1 Introduction

Hydrophobic interaction chromatography (HIC) is a frequently used purification method in the biopharmaceutical industry [1, 2, 3, 4]. This purification technique is based on interactions of hydrophobic surface patches of proteins and hydrophobic adsorber ligands. The major challenge of HIC are the low binding capacities of the adsorber resins compared to IEX resins [5]. In addition, the use of high concentrations of kosmotropic salt leads to reduced protein solubility. In HIC, adsorption is promoted by high concentrations of predominantly kosmotropic salts [6]. In 1888, Franz Hofmeister arranged different salts based on their propensity of precipitating proteins [7]. There are two groups into which salts can be classified. Kosmotropic salts, as class one, are salting-out salts. They promote protein-protein or protein-ligand interaction due to their ability of changing the water structure [8]. The number of highly ordered water molecules surrounding the hydrophobic surface patches of the proteins decreases and the hydrate shell around the protein is diminished. This leads to an increase in the hydrophobic interactions and thus a decreased protein solubility [9, 10]. Class two, chaotropic salts, are salting-in salts which increase the solubility of proteins by weakening the hydrophobic interactions and thus prevent the accumulation of proteins [11, 12].
In 2009, Senczuk et al. introduced a new methodology using salt mixtures in HIC [13]. By mixing two kosmotropic salts, an increase in the solubility of proteins as well as an increase in the dynamic binding capacities (DBCs) was achieved. However, the authors used Fc-fusion proteins only and annotated that the observed behavior might be specific to these proteins. In 2013, Müller et al. [14] pursued this topic, expanded it to salt mixtures of kosmotropic and chaotropic salts, and proposed a rule of thumb: By mixing a constant salt concentration of around 1 M of the kosmotropic salt with varying

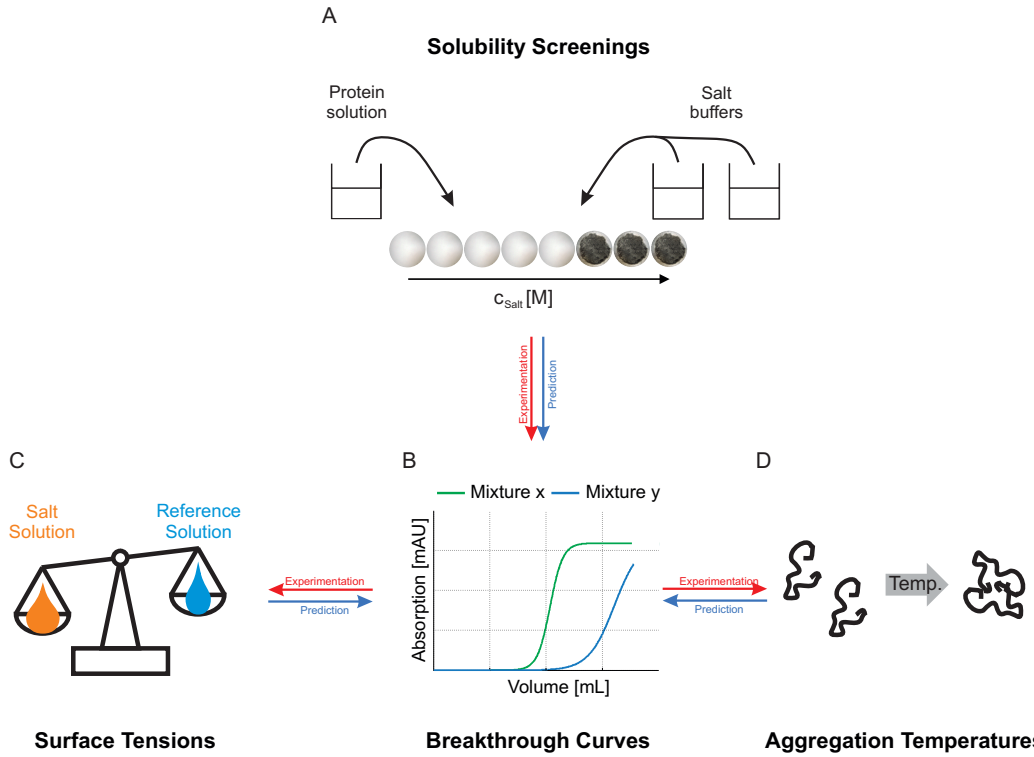

Figure 1: Schematic drawing of screening methodology: A: Solubility screenings: Salt concentration was increased in small steps determining soluble and precipitated conditions, B: Breakthrough curves were determined using 90% of the critical salt concentration from A, C: With a stalagmometric method, the surface tensions of the protein salt solutions were determined with water as a reference solution, D: Aggregation temperatures were determined using an Optim2 system. With the help of surface tensions, aggregation temperatures, and solubility screenings predictions of the binding behavior were made (blue arrows).

amounts of a chaotropic salt, the DBCs of HIC adsorbers could be increased significantly. Nevertheless, the authors remarked that it is necessary to expand this rule of thumb by extended screenings. Müller et al. also referred to the cavity theory originally proposed by Melander and Horváth [15] and also mentioned by Senczuk et al. [13]. This theory describes that higher surface tensions, caused by kosmotropic salts, induce higher DBCs of HIC adsorbers, whereas chaotropic salts lead to inverse trends. Müller et al. [14] described that mixing a kosmotropic and a chaotropic salt should lead to an intermediate surface tension. Nevertheless, this assumption has not been experimentally verified so far. Werner et al. [16] also used salt mixtures of kosmotropic and chaotropic salts for increasing the static binding capacities of HIC adsorbers in batch mode with the main focus on differences between lysozyme and PEGylated lysozyme. For this issue, the authors developed a mathematical model. Werner et al. used a constant overall ionic strength for all of their experiments leading to low-salt concentrations for polyvalent ions, commonly not applied in the biopharmaceutical industry. Thus, a thorough investigation of the influence of the mixing ratios of kosmotropic and chaotropic salts on the dynamic binding capacities of HIC adsorbers as well as a predictive insight based on new straightforward measurement techniques like stalagmometric methods and aggregation temperature is needed.

In this paper, the approach of mixing kosmotropic and chaotropic salts for increasing

the dynamic binding capacities of HIC adsorbers and the important impact of the mixing ratios on the DBCs are investigated in more detail. New straightforward methods are used to get predictive knowledge on the binding behavior of HIC adsorbers. As a model protein, lysozyme from chicken egg white was used. Using lysozyme as a model protein can show a special behavior because of its high isoelectric point. However, lysozyme is a commonly used model protein and good for developing screening methodologies and predictive tools. Additionally, Müller et al. [14] and Werner et al. [16], who set the basis for this work, also used this protein and Müller et al. confirmed that a similar behavior was discovered for an antibody. A schematic drawing of the screening methodology is shown in Figure 1. Solubility screenings of this protein in different salt mixtures were performed on a liquid handling station by TECAN for boundary conditions of the breakthrough curve experiments. After obtaining the solubility limits, dynamic binding capacities were determined using an ÄKTA^{TM} Purifier System by GE Healthcare on a medium hydrophobic Toyopearl Phenyl-650M and strongly hydrophobic Toyopearl Butyl-650M adsorber. These column experiments were conducted at salt concentrations close to the protein's solubility limit to exploit the maximal design space and work efficiently. To investigate the validity of the cavity theory for mixed salts, surface tension measurements were conducted using an in-house-developed stalagmometric methodology [17]. Additionally, as a degree of hydrophobic forces, the aggregation temperatures in the different salt mixtures were determined using an Optim®2 by Avacta Analytical and were correlated to the DBCs.

2 Materials and Methods

2.1 Materials

2.1.1 Chemicals & Disposables

The model protein lysozyme from chicken egg white was purchased from Hampton Research (USA). The sodium phosphate buffer components and the salt ammonium sulfate were bought from VWR Prolabo (USA). The salt sodium chloride was purchased from Merck Millipore (USA). The salt sodium sulfate was bought from Fluka BioChemika (Switzerland). All buffers were prepared with ultra-pure water and a buffer capacity of 20 mM sodium phosphate. The pH of all buffers was adjusted to pH 7 using hydrochloric acid or sodium hydroxide (Merck, Germany), respectively. The low-salt buffers were filtered using 0.2 μm cellulose acetate membrane filters provided by Sartorius Stedim Biotech (Germany). The high-salt buffers were filtered using Supor-450 0.45 μm membrane filters (Pall Life Sciences, Mexico). All low-salt protein solutions were filtered using 0.2 μm syringe filters, all high-salt protein solutions using 0.45 μm syringe filters with PTFE membranes (VWR, Germany).
High-throughput robotic precipitation experiments and UV measurements were carried out in 96-well flat-bottom UV-Star full-area micro plates (Greiner Bio-One, Germany). The plates were sealed with non-sterile Platemax aluminum sealing films (Axygen Scientific, USA).
For the breakthrough experiments, 0.5 mL hydrophobic interaction chromatography Mini Chrom columns, filled with Toyopearl Phenyl-650M or Butyl-650M, were purchased from

Atoll (Germany).
For the surface tension measurements, 1 mL 96-round-DeepWell plates supplied by Thermo Scientific Nunc (USA) were used.
Aggregation temperature measurements were carried out in multi-cuvette arrays in Optim® MCA frames with spare silicone seals by Avacta Analytical (UK).

2.1.2 Instrumentation & Software

For pH adjustment of all buffers, a five-point calibrated HI-3220 pH meter (Hanna Instruments, USA) equipped with a SenTix 62 pH electrode (Xylem Inc., USA) was used. The instrument was calibrated using high-precision standards by Hanna Instruments (USA). The exact determination of protein concentrations was carried out in a NanoDrop2000c UV-Vis spectrophotometer operated with the Nanodrop measurement software version 1.4.2 (Thermo Fisher Scientific, USA).
The automated solubility screenings were conducted using a Freedom EVO 200 liquid handling station controlled by Evoware 2.5 supplied by Tecan (Germany). The system is equipped with eight fixed pipetting tips, a plate-moving arm, and an orbital shaker. Absorption measurements were carried out in an integrated Infinite M200 UV plate spectrometer operated with the software Magellan 7.1 (Tecan, Germany). Also, a Rotanta 46RSC centrifuge (Hettich, Germany) is integrated in the robotic system. For protein incubation for up to 24 hours in 96-well plates, a Heidolph Reax 2 overhead shaker (Germany) was applied.
The determination of the dynamic binding capacities was carried out with an ÄKTA™ Purifier system by GE Healthcare (USA). The operating software package for the system control and data analysis was Unicorn 5.1 (GE Healthcare, USA). The ÄKTA™ Purifier is equipped with an UV detector and a conductivity cell.
The surface tension screenings were performed using a Freedom Evo 100 operated by Evoware 2.5 supplied by Tecan (Germany).
The aggregation temperatures were determined in an Optim®2 operated with the Optim® Client and Optim® Analysis softwares by Avacta Analytical (UK).
Data processing and creation of figures was performed in Matlab® R2014a (MathWorks, USA) and CorelDRAW® Graphics Suite X5 (Corel Corporation, Canada).

2.2 Experimental Setup

2.2.1 Solubility Screenings with Single Salts and Mixed Salts

To define the experimental design space for the dynamic binding capacity determination experiments, solubility screenings were carried out on a Freedom Evo 200 liquid handling station supplied by Tecan. The aim of the screenings was to determine the single salt concentrations (c_{crit}) at which 10 mg/mL lysozyme start to precipitate at pH 7. As a threshold criterion for precipitation conditions, a recovery below 90% of the initial protein concentration was defined. 20 mM sodium phosphate buffer was used as a low-salt buffer (buffer without additional salt) in all experiments. The protein stock solutions consisted of the same buffer with 30 mg/mL lysozyme from chicken egg white added. The deployed protein concentration was determined exactly with a NanoDrop2000c by Thermo Fisher Scientific. High-salt buffer stock solutions for the screenings using sodium

chloride consisted of low-salt buffer with additional 2.5 M or 5.0 M sodium chloride. The high-salt stock solutions for the precipitation screenings using ammonium sulfate consisted of low-salt buffer with 1.5 M or 3.0 M ammonium sulfate. As a third salt type, sodium sulfate was investigated using a stock solution of low-salt buffer and buffer with 1.5 M and – due to its solubility limit – 2.5 M sodium sulfate. Mixing low-salt buffer and high-salt buffer with high amounts of additional salt (> 2 M) can result in pH shifts [18, 19]. Thus, intermediate salt stock solutions were used to get a constant pH value over the whole salt concentration range.
Different volumes of low and high-salt buffer with a total volume of 200 μL were pipetted into a 96-well UV-Star micro plate and mixed in an orbital shaker. 100 μL of the 30 mg/mL lysozyme stock solution were added to each well and mixed with the respective salt solution to get a final protein concentration of 10 mg/mL in every approach. The different salt buffer volumes combined with the protein stock solution resulted in salt concentrations in the range of 0 M to 2.8 M for sodium chloride, 0 M to 2.0 M for ammonium sulfate, and 0 M to 1.6 M for sodium sulfate. The 96-well UV-Star plate was sealed with non-sterile Platemax aluminum sealing films and incubated at room temperature for 24 hours in an overhead shaker. Next, the micro plate was centrifuged for 10 min at 4000 rpm to ensure a supernatant free of precipitate. After centrifugation, the seal was removed and 15 μL of supernatant were transferred to a 96-well UV-Star plate pre-filled with 285 μL low-salt buffer. After mixing, the protein concentration in the supernatant was determined at a wavelength of 280 nm in an Infinite M200 photometer provided by Tecan. The maximum salt concentration (c_{crit}) at which 10 mg/mL lysozyme are soluble (schematic drawing: Figure 1 A) was calculated based on a predetermined calibration curve.
The screenings for the maximum salt concentrations ($c_{crit,total}$) of salt mixtures at which 10 mg/mL lysozyme are soluble was performed analogously as described for the single salts. For the mixed salts experiments, 4 salt buffer stock solutions had to be prepared for each screening. The salt concentrations of each salt buffer were the intermediate 1.5 M and the 3.0 M, to avoid pH shifts. By varying high and low-salt buffer volumes, different salt concentrations and salt ratios could be adjusted. With these experiments and the single salt experiments, the critical total salt concentrations (c_{crit} and $c_{crit,total}$) at which 10 mg/mL lysozyme are soluble were identified at 9 different compositions as explained in Table 1.

2.2.2 Determination of Dynamic Binding Capacities

For determination of the dynamic binding capacities (DBCs) of the two investigated adsorber resins (Toyopearl Phenyl-650M and Toyopearl Butyl-650M) as a function of the salt mixing ratios, 0.5 mL MiniChrom columns by Atoll were used on an ÄKTA™ Purifier system as shown by example in Figure 1 B. To have a safety margin against protein precipitation, the DBCs were determined at conditions using salt buffers with 90% of the critical ionic strength (IS_{crit}) as determined in the solubility screenings. Using 90% ($IS_{crit,90}$) of the solubility limit instead of an overall constant ionic strength was considered to be more practical and more economical. An overall constant ionic strength would lead to low-salt concentrations for e.g. polyvalent salts. The protein was dissolved in low-salt buffer to a concentration of 30 mg/mL and diluted with respective

Table 1: Ratio of kosmotropic salt and the corresponding composition in the salt mixture. Sodium chloride was used as a chaotropic salt, ammonium sulfate and sodium sulfate were used as kosmotropic salts.

Ratio $c_{chao} : c_{kosm}$	Proportion kosmotropic salt	$\text{Part}_{chaotrope}$	$\text{Part}_{kosmotrope}$
1:0	0	1	0
7:1	1/8	7	1
3:1	1/4	3	1
5:3	3/8	5	3
1:1	1/2	1	1
3:5	5/8	3	5
1:3	3/4	1	3
1:7	7/8	1	7
0:1	1	0	1

salt buffer mixtures to a final protein concentration of 10 mg/mL and the predetermined salt concentration. After equilibration of the column with 5 column volumes (CV) of correspondingly high-salt buffer, a 15 CV protein sample application followed, ensuring protein breaking through. After a low-salt wash step of 10 CV, a wash step with 10 CV of ultra-pure water followed. Finally, the columns were cleaned with 10 CV of 20% ethanol for storage. By detecting the 280 nm UV signal, the DBCs could be calculated at a breakthrough of 10% of the initial protein concentration. Respective absorption values were determined by a protein calibration curve. The DBCs were calculated considering the column bed volume. All experiments were performed as duplicates.

2.2.3 Determination of Surface Tension

The surface tensions of 10 mg/mL lysozyme in the different salt buffers were measured using an in-house-developed stalagmometric method. By measuring the mass of a drop of a sample and comparing it to the mass of a drop of water with known surface tension as a reference (schematic drawing Figure 1 C), the surface tension of the sample was calculated. A detailed description of the used method can be found in the publication by Amrhein et al. [17].

2.2.4 Measuring the Aggregation Temperature

As a degree of the strength of hydrophobic interactions, the aggregation temperatures of 10 mg/mL lysozyme in the different salt mixtures were measured using an Optim®2 from Avacta Analytical (Figure 1 D). To avoid dust, known to cause heterogeneous nucleation, the pipetting of 9 μL of each sample into a multi-cuvette array as well as the sealing were performed on a clean bench. In the Optim®2 system, a stepped temperature ramp with 0.25°C steps from 20°C to 95°C was performed. By measuring the scattered light signal at each temperature step at 266 nm, the temperature at which 10 mg/mL of lysozyme start to aggregate was determined.

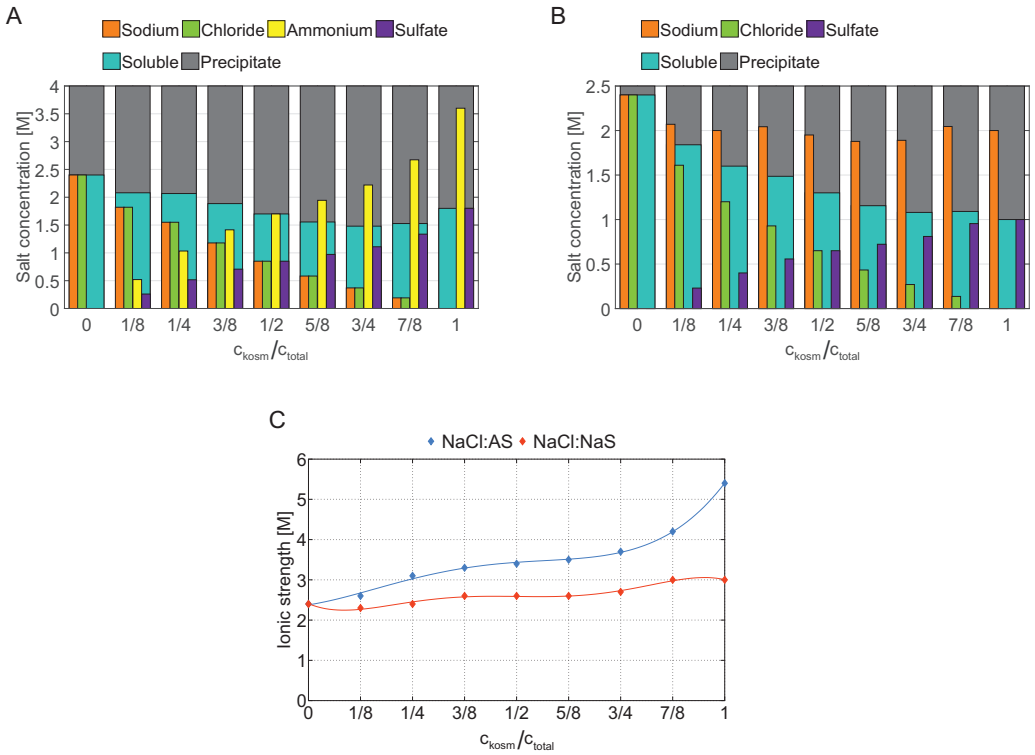

Figure 2: $c_{crit,total}$ [M] with the salt mixtures of A: Sodium chloride and ammonium sulfate, B: Sodium chloride and sodium sulfate, C: Last soluble total ionic strength [M] at which 10 mg/mL lysozyme were soluble as a function of the ratio of the kosmotropic salt concentration to the total salt concentration. Salt mixtures of sodium chloride and ammonium sulfate are shown in blue, salt mixtures of sodium chloride and sodium sulfate are shown in red. The results are fitted with fifth-degree polynomials.

3 Results

3.1 Solubility Screenings with Single Salts and Mixed Salts

Solubility screenings of 10 mg/mL lysozyme were performed for single salts (sodium chloride, ammonium sulfate, sodium sulfate), as well as for salt mixtures of sodium chloride with ammonium sulfate, and of sodium chloride with sodium sulfate. Sodium chloride is a chaotropic salt, whereas ammonium sulfate and sodium sulfate are kosmotropic salts. In Figure 2 A (salt mixtures of sodium chloride and ammonium sulfate) and Figure 2 B (salt mixtures of sodium chloride and sodium sulfate), the $c_{crit,total}$ at which 10 mg/mL lysozyme were soluble are shown as a function of the mixing ratios of the chaotropic and the kosmotropic salts, as well as the ion concentrations of sodium, chloride, ammonium and sulfate. A molar ratio for c_{chao}:c_{kosm} of 1:7 for example represents one part of the chaotropic salt (sodium chloride) and seven times its molar concentration of the kosmotropic salt (ammonium sulfate or sodium sulfate) (see Table 1). c_{crit} of the pure chaotropic salt sodium chloride was determined to be 2.4 M. c_{crit} of the kosmotropic single salts were lower, with 1.8 M for ammonium sulfate and 1.0 M for sodium sulfate. $c_{crit,total}$ for the salt mixtures at which 10 mg/mL lysozyme are soluble were between 2.08 M and 1.48 M for the mixtures of sodium chloride and ammonium sulfate. For the mixtures of sodium chloride and sodium sulfate, $c_{crit,total}$ were between c_{crit} of the single salts and varied between 1.84 M and 1.08 M. For both experimental design spaces, it was shown

that a higher amount of kosmotropic salt in the salt mixture results in a lower $c_{crit,total}$. For the ratio of 1:7, a slight increase in $c_{crit,total}$ was observed compared to the 1:3 ratio mixture. When looking at the ion concentrations for the mixtures of sodium chloride with ammonium sulfate, it can be seen that the concentration of sodium as well as chloride decreases constantly and the concentration of ammonium and sulfate increases. The ammonium concentration increases twice as fast as the sulfate concentration because in ammonium sulfate, two ammonium ions are present. For the mixtures of sodium chloride with sodium sulfate, the sodium concentration stays constant around 2 M whereas the chloride concentration decreases constantly and the sulfate concentration increases with an increasing ratio of sodium sulfate.
Using the determined salt concentrations the ionic strength was calculated by using equation 1:

$$IS = \frac{1}{2} \sum cz^2 \tag{1}$$

with c being the concentration of the ions and z being the valence (single or double charged). The calculated IS_{crit} of these salt mixtures (Figure 2 C) are between the IS_{crit} of the single salts alone. The IS_{crit} increases towards salt mixtures with an increasing ratio of kosmotropic salt, resulting in the highest ionic strengths for the pure kosmotropic salts with 5.4 M for ammonium sulfate and 3.0 M for sodium sulfate.

3.2 Determination of Dynamic Binding Capacities

The 10% dynamic binding capacities (DBCs) of 10 mg/mL lysozyme in the different mixed salts buffers were determined on two different HIC adsorber resins (Toyopearl Phenyl-650M and Toyopearl Butyl-650M) using an ÄKTA™ Purifier system. Figure 3 illustrates the influence of salt mixtures on the DBC of lysozyme on HIC adsorbers. In this figure, the dynamic binding capacities are scaled to the DBC obtained with pure sodium chloride, as this salt is used in both design spaces. It is evident that by mixing sodium chloride with ammonium sulfate, an increase in the dynamic binding capacity of up to 23.1% ± 0.8% can be achieved on the Toyopearl Phenyl-650M adsorber resin and of up to 11.4% ± 2.2% on the Butyl-650M resin. For both adsorbers, a ratio of 5:3 (see Table 1) led to the highest DBC. With this mixing ratio, the dynamic binding capacity was even higher compared to pure ammonium sulfate – a strong kosmotropic salt. For a salt mixture with a ratio of 3:5 of sodium chloride to ammonium sulfate on the Butyl-650M resin, the DBC was decreased by 33.0% ± 0.0% compared to the DBC determined with pure sodium chloride. The maximal decrease of the DBC on the Phenyl-650M adsorber was 21.3% ± 1.2% for the 1:3 ratio.
For sodium chloride and sodium sulfate mixtures (Figure 3 B), a similar behavior as for mixtures of sodium chloride and ammonium sulfate was observed with the highest DBCs in the region with a lower ratio of kosmotropic salt. In this design space, the ratio of 7:1 led to the highest DBCs on both adsorber resins. For these two salts, an overall trend of decreasing DBC with increasing amount of sodium sulfate was detected, with a minimum of −45.9% ± 3.8% for the Phenyl adsorber and −25.1% ± 3.7% for the Butyl adsorber with pure sodium sulfate, each.

In Figure 4 A (for sodium chloride and ammonium sulfate mixtures) and Figure 4 B (for sodium chloride and sodium sulfate mixtures), the relative DBCs are plotted as a

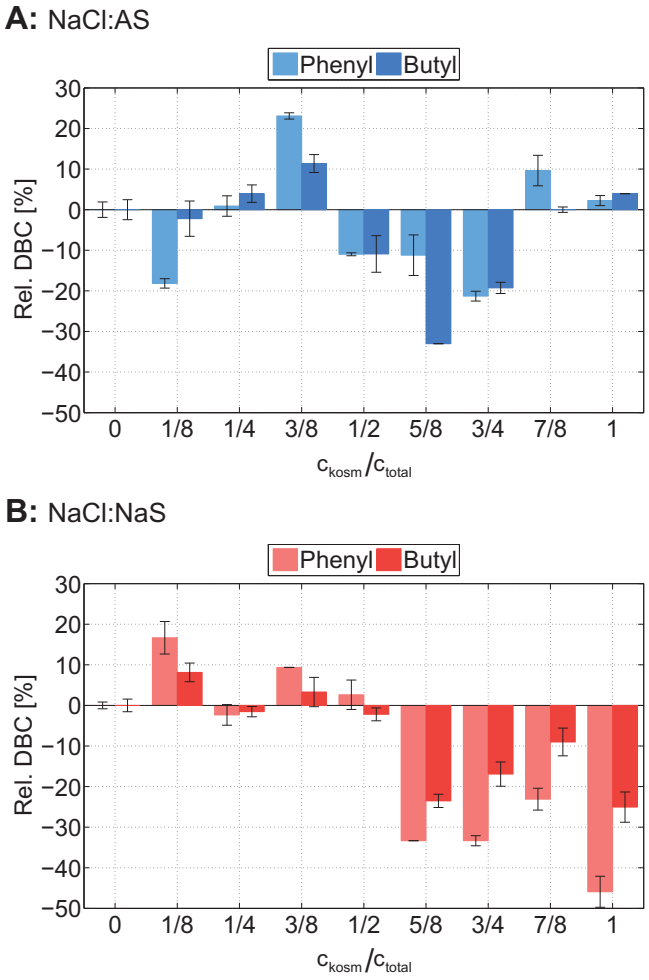

Figure 3: Relative dynamic binding capacity (Rel. DBC) of 10 mg/mL lysozyme for Toyopearl Phenyl-650M (lighter color) and Toyopearl Butyl-650M (darker color) in % scaled to the DBC of 10 mg/mL lysozyme with pure sodium chloride as a function of the ratio of the kosmotropic salt concentration to the total salt concentration. A: Ammonium sulfate as kosmotropic salt, B: Sodium sulfate as kosmotropic salt.

function of the ratio of the kosmotropic salt overlaid with the product of 90% of $c_{crit,total}$ ($= c_{crit,total,90}$) and its corresponding IS_{crit} ($= IS_{crit,90}$). For salt mixtures with $\geq 50\%$ kosmotropic salt, the values of the products are lower than in the region with a higher ratio of chaotropic salt. The highest values are in the region with a lower ratio of kosmotropic salt with a maximum of 5.2 M^2 for the 3:1 (and for the 1:7) mixture of sodium chloride with ammonium sulfate and 3.4 M^2 for the 7:1 mixture of sodium chloride and sodium sulfate. For the salt mixtures of sodium chloride with ammonium sulfate, the values decrease from the 3:1 mixture to the 3:5 mixture (4.41 M^2) and then increase to 5.2 M^2 for the 1:7 ratio. For the salt mixtures of sodium chloride with sodium sulfate, the product of the $c_{crit,total,90}$ and its $IS_{crit,90}$ decreases constantly with an increasing ratio of sodium sulfate and again a slight increase for the 1:7 mixture. The actual values of the product of $c_{crit,total,90}$ and the corresponding $IS_{crit,90}$, however, seem to be irrelevant. The important information is the progression of the product curve. These curves and the progression of the relative DBCs show the same behavior. When the solubility product increases, the DBC increases and vice versa.

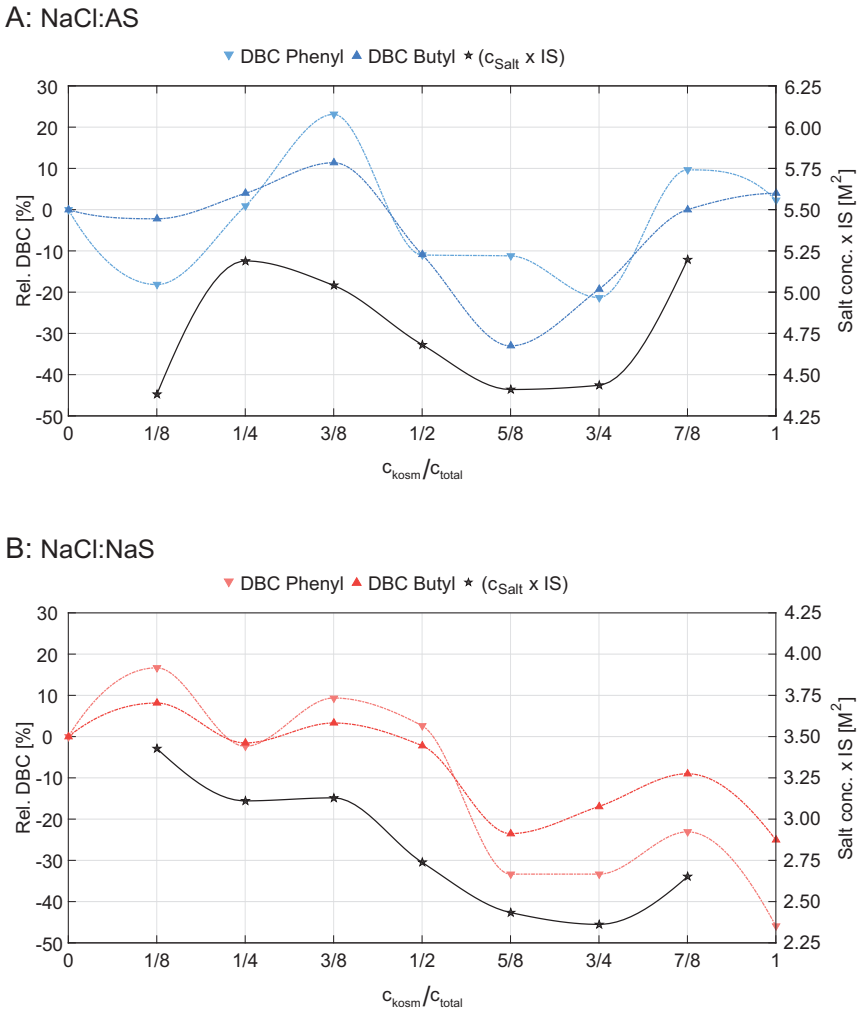

Figure 4: Relative dynamic binding capacity (Rel. DBC) of 10 mg/mL lysozyme for Toyopearl Phenyl-650M (lighter color) and Toyopearl Butyl-650M (darker color) in % scaled to the DBC of 10 mg/mL lysozyme with pure sodium chloride as a function of the ratio of the kosmotropic salt concentration to the total salt concentration. A: Ammonium sulfate as kosmotropic salt, B: Sodium sulfate as kosmotropic salt. Product of $c_{crit,total,90}$ [M] and its corresponding $IS_{crit,90}$ [M], at which 10 mg/mL lysozyme were soluble as a function of the ratio of the kosmotropic salt concentration to the total salt concentration. The results are fitted with splines.

3.3 Determination of Surface Tensions

In Figure 5, the measured surface tensions of 10 mg/mL lysozyme in the different salt buffers are shown as a function of the ratio of the kosmotropic salt for the salt mixtures of sodium chloride with ammonium sulfate (blue) and sodium chloride with sodium sulfate (red). The surface tension of the chaotropic salt (sodium chloride) was determined to be 73.7 mN/m ± 0.08 mN/m. The surface tension of pure kosmotropic salt (sodium sulfate) was almost similar with 73.6 mN/m ± 0.04 mN/m and much higher with 75.0 mN/m ± 0.05 mN/m for ammonium sulfate. The surface tensions of the salt mixtures of sodium chloride with ammonium sulfate were between 73.5 mN/m ± 0.10 mN/m for the mixture with the lowest amount of kosmotropic salt and 74.1 mN/m ± 0.10 mN/m for the mixture with the highest amount of kosmotropic salt. However, the surface tension

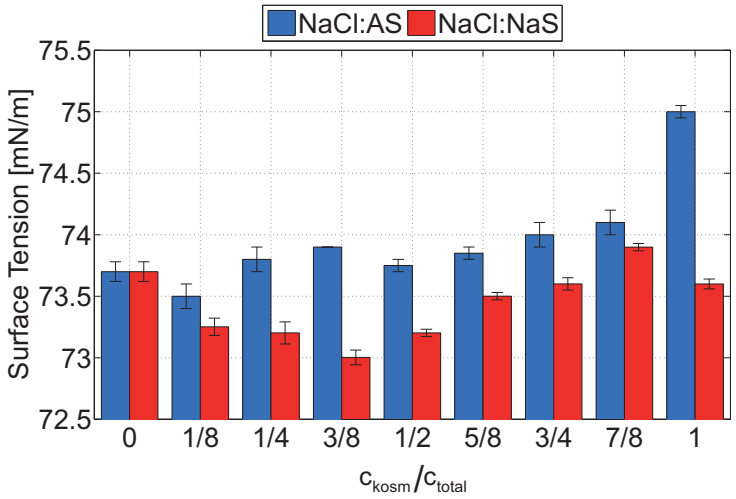

Figure 5: Determined surface tensions of 10 mg/mL lysozyme as a function of the ratio of the kosmotropic salt concentration to the total salt concentration (blue: ammonium sulfate; red: sodium sulfate) with sodium chloride as chaotropic salt.

seems to be more influenced by the chaotropic salt in this scenario. The surface tension values of the salt mixtures are similar to the surface tension determined for sodium chloride.
For the salt mixtures of sodium chloride with sodium sulfate, this observation is more pronounced. Here, the surface tensions of the mixtures with lower ratios of kosmotropic than chaotropic salt were between 73.0 mN/m ± 0.06 mN/m and 73.25 mN/m ± 0.07 mN/m whereas the surface tensions of the mixtures with higher ratios of kosmotropic salt were between 73.5 mN/m ± 0.03 mN/m and 73.9 mN/m ± 0.03 mN/m. It is noteworthy that despite the almost similar surface tensions of the pure salts, the surface tensions of the salt mixtures of sodium chloride and sodium sulfate differ.

3.4 Measuring the Aggregation Temperature

With the Optim®2 system by Avacta Analytical, the aggregation temperatures were determined (Figure 6). The lowest aggregation temperature for 10 mg/mL lysozyme with the salt mixtures of sodium chloride with ammonium sulfate (blue) was determined to be 69.6°C ± 0.4°C for the lowest ratio of ammonium sulfate. With an increasing amount of the kosmotropic salt, the aggregation temperature increased with its overall maximum of 72.1°C ± 0.4°C for the mixture with the second highest ratio of chaotropic to kosmotropic salt (1:3). The aggregation temperatures for the salt mixtures with a higher ratio of ammonium sulfate than sodium chloride were even higher than the aggregation temperature with pure ammonium sulfate (70.8°C ± 0.3°C). The overall lowest aggregation temperature in this design space was determined for sodium chloride resulting in 68.6°C ± 0.1°C.
For the salt mixtures of sodium chloride with sodium sulfate (red), the overall lowest aggregation temperature was determined for a ratio of chaotropic to kosmotropic salt of 5:3 with around 68.0°C ± 0.2°C. Again, for lower amounts of kosmotropic than chaotropic salt, the aggregation temperatures were lower than for a higher ratio of kosmotropic salt. The highest aggregation temperature was determined for the 1:3 ratio with

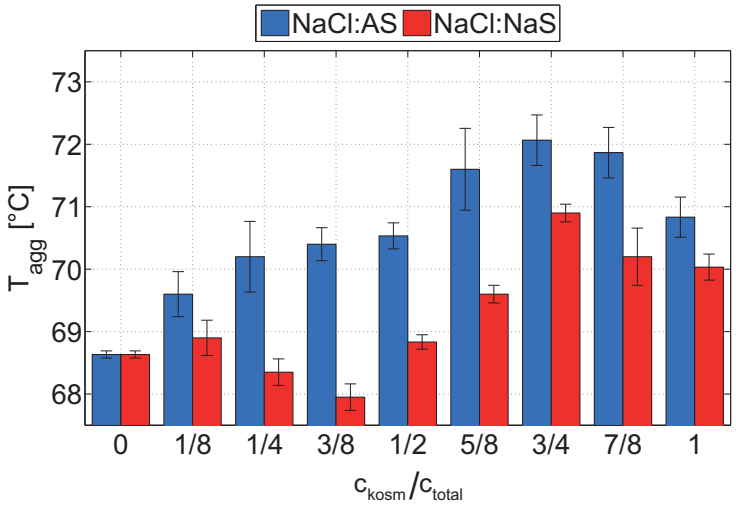

Figure 6: Aggregation temperatures [°C] of 10 mg/mL lysozyme as a function of the ratio of the kosmotropic salt concentration to the total salt concentration (blue: ammonium sulfate; red: sodium sulfate) with sodium chloride as chaotropic salt.

70.9°C ± 0.1°C. The aggregation temperature of 10 mg/ml lysozyme with pure sodium sulfate was 70.0°C ± 0.2°C, which is again lower than for some of the salt mixtures.

4 Discussion

4.1 Solubility Screenings with Single Salts and Mixed Salts

The solubility limit based on salt concentrations for 10 mg/mL lysozyme was higher for sodium chloride than for ammonium sulfate (Figure 2 A) and sodium sulfate (Figure 2 B). Hence, more sodium chloride can be added to a constant protein concentration until protein precipitates. This correlates with the Hofmeister series [7]. Here, the salts are classified as chaotropic salts (salting-in salts) that increase the solubility of proteins and as kosmotropic salts (salting-out salts) that decrease the protein's solubility [15]. As sodium chloride is a chaotropic salt, and ammonium sulfate and sodium sulfate are kosmotropic salts, this solubility behavior of the pure salt species was expected. With an increasing ratio of kosmotropic salt in the salt mixtures, the $c_{crit,total}$ decreased implying a lower solubility for these conditions. This is conform with the previously mentioned classification that kosmotropic salts decrease the solubility of proteins.
By adding a chaotropic salt to a kosmotropic salt, a higher total salt concentration compared to pure kosmotropic salt could be applied to the protein without causing precipitation. Hence, an increase in protein solubility could be achieved.
IS_{crit} of the salt mixtures were between the IS_{crit} of the single salts with an increase in the ionic strength towards the pure kosmotropic salt (Figure 2 C). This behavior inverse to the salt concentration can be explained by the fact that sulfate is a doubly negatively charged ion, and ammonium and sodium, in this chemical compound, are present twice, and thus increase the ionic strength more strongly than single-charged chloride ions or single present sodium ions in sodium chloride. For ammonium sulfate and sodium sulfate, the ionic strength thus equals three times its salt concentration.

4.2 Influence of Salt Mixtures on the DBC

Pure ammonium sulfate, as a kosmotropic salt that increases the protein ligand interaction, was expected to generate higher dynamic binding capacities compared to the chaotropic salt sodium chloride (Figure 3 A). Nevertheless, the dynamic binding capacities with sodium chloride and ammonium sulfate differed by around 2% on the Phenyl adsorber and around 4% on the Butyl adsorber only. This behavior can be explained by the deployed salt concentrations determined with the solubility screenings. The sodium chloride concentration used was around 0.5 M higher than the ammonium sulfate concentration, making the difference in the salting-out effect apparently negligible. Looking at the DBC of pure sodium sulfate, it is even 45% lower than the DBC with pure sodium chloride (Figure 3 B). Again, the used salt concentration of pure sodium chloride was much higher ($> +1.2$ M) than the used sodium sulfate concentration.
In both investigated designs of the salt mixtures of sodium chloride with ammonium sulfate and sodium chloride with sodium sulfate, the highest DBCs were achieved in the region with a lower ratio of kosmotropic salt. This behavior is quite counterintuitive as in HIC, usually kosmotropic salts are needed to reach high DBCs. However, the observed behavior is in agreement with the observations made by Müller et al. [14]. It seems that increasing the protein's solubility by a higher amount of chaotropic salt increases the DBC and only a smaller amount of kosmotropic salt is needed to actually bind protein to the HIC adsorber.
In Figures 4 A and B, a direct correlation between the product of the solubility limit ($c_{crit,total,90}$ times $IS_{crit,90}$) and the DBCs becomes obvious. The progression of the fitted curves of the solubility limits of the salt mixtures and the corresponding DBCs are almost identical. When the product of $c_{crit,total,90}$ and $IS_{crit,90}$ increases compared to the previous mixture, the DBC also increases and vice versa. For example for ammonium sulfate as kosmotropic salt (Figure 4A) the maxima of the curve, when plotting the product of salt concentration and ionic strength, are at ratios of chaotropic to kosmotropic salt of 3:1, 5:3, and 1:7. At the same mixing ratios also maxima of the DBCs were observed. The same observations can be made for the minima at 7:1, 3:5, and 1:3. These minima were found for the salt-product-curve as well as for the DBCs. The authors could not find any satisfying explanation for this behavior. However, this finding might be exploited for HIC optimization studies.

4.3 Correlation of Surface Tension to DBC

The cavity theory, published by Melander and Horváth [15], describes a direct correlation of the surface tension and the dynamic binding capacity. Salts causing high surface tensions (kosmotropic salts) are said to yield higher dynamic binding capacities compared to salts causing lower surface tensions (chaotropic salts). Müller et al. [14] observed that this phenomenon does not apply to salt mixtures from the point of view that mixing a chaotropic and a kosmotropic salt should decrease the surface tension compared to pure kosmotropic salt. However, the authors apparently did not actually measure the surface tensions of the salt mixtures. As described in 3.3, the surface tensions of all used buffer mixtures with 10 mg/mL lysozyme were measured using a stalagmometric method. The surface tension of 10 mg/mL lysozyme in the pure sodium chloride buffer was lower than the surface tension of the protein ammonium sulfate solution (Figure 5). Also, the DBC

with the buffer including pure sodium chloride was lower compared to the DBC with pure ammonium sulfate confirming the cavity theory for these two salts. The DBC with the single salt sodium sulfate was lower than the DBC with sodium chloride, but also the surface tension determined for the sodium sulfate buffer was lower. This contradicts the theory of yielding higher surface tensions with kosmotropic compared to chaotropic salts. An explanation for this observation is that the used concentration of sodium sulfate was, due to its solubility limit, nearly 60% lower than the used concentration of sodium chloride. When comparing the two salts at the same salt concentration, the surface tension of the sodium sulfate buffer was higher than the surface tension of the sodium chloride buffer (data not shown), and therefore agreeing with literature.
The surface tensions of the salt mixtures of sodium chloride and ammonium sulfate varied in a range of 73.5 mN/m and 74.1 mN/m only, with a slight increase towards the mixtures with a higher ratio of the kosmotropic salt. This behavior correlates with the above-mentioned theory that kosmotropic salts increase the surface tension. The same trend was observed for the mixtures of sodium chloride and sodium sulfate with the lowest surface tensions occurring in the low kosmotropic salt region.
Nevertheless, the DBCs with the salt mixtures were highest at rather low surface tensions. This observation contradicts the cavity theory. Concluding from this, the cavity theory is not valid for salt mixtures.

4.4 Correlation of Aggregation Temperature to DBC

s a degree of hydrophobic interactions, the aggregation temperatures of 10 mg/mL lysozyme in the different salt buffers were measured (Figure 6). The high salt concentrations used shielded electrostatic repulsions and thus exposed predominantly hydrophobic interactions as was described by De Young et al. [20]. A lower aggregation temperature correlates with an earlier aggregation and thus implies stronger hydrophobic interactions. When comparing the aggregation temperature of the setup of pure ammonium sulfate with the setup of pure sodium sulfate, a lower aggregation temperature was determined for the sodium sulfate conditions, even though the used sodium sulfate concentration was almost 50% lower than the used ammonium sulfate concentration. These findings agree with the observations made by Lin et al. [21] that sodium sulfate enhances the hydrophobic interactions of lysozyme stronger than ammonium sulfate.
For the salt mixtures, the lowest aggregation temperatures were determined in the design space with lower amounts of kosmotropic salt indicating stronger hydrophobic interactions in this region. This behavior is confirmed when looking at the DBCs. In the region with the lowest aggregation temperatures, the DBCs were highest.

5 Conclusions and Outlook

The screening results presented in this paper confirmed and expanded the observations made by Müller et al. [14]. By mixing kosmotropic and chaotropic salts in a certain ratio, the dynamic binding capacity of HIC adsorbers could be increased for lysozyme from chicken egg white as a model protein. But mixing of salts can also have negative effects on the DBC. Originating from the solubility limits, salt mixtures with a higher amount of chaotropic compared to kosmotropic salt mainly increased the DBCs whereas

higher ratios of kosmotropic salt decreased the binding capacities even compared to single salt experiments. The product of $c_{crit,total,90}$ and its corresponding $IS_{crit,90}$ determined by solubility screenings shows the same progression as the trend of the DBCs, making it a fast possibility to roughly estimate the behavior of the DBCs.
By mixing a higher amount of chaotropic with a lower amount of kosmotropic salt, an increase in the solubility of lysozyme from chicken egg white was achieved. Concluding from this, the amount of kosmotropic salt was reduced drastically yielding higher DBCs. The decrease in the amount of kosmotropic salt also reduces the waste disposal of the ammonium, known to be environmentally harmful. It is possible to reduce the overall ionic strength for the salt mixtures with more chaotropic than kosmotropic salt and still achieve the same DBCs compared to experiments applying pure kosmotropic salt.
The cavity theory proposed by Melander and Horváth [15] is not valid for salt mixtures, as was shown by the surface tension measurements, using lysozyme as a model protein. Additionally, the enhanced hydrophobic interactions leading to increased DBCs could roughly be estimated by the lower aggregation temperatures for salt mixtures with lower amount of kosmotropic compared to chaotropic salt.
In summary, the use of mixed salts with a higher ratio of chaotropic than kosmotropic salt is a promising and gentle approach to rectifying the problem of the low dynamic binding capacities of HIC adsorbers and even reduce the amount of salt needed as indicated for lysozyme as a model system. Additionally, the measurement of the aggregation temperatures is a fast analytical method to roughly estimate the hydrophobic interactions and thus approximately predict an increase or a decrease in binding in HIC processes.
The phenomena described in this paper for lysozyme from chicken egg white have to be verified for other proteins and salts. Good examples might be proteins of acidic or neutral isoelectric points. In this study ammonium sulfate, sodium chloride, and sodium sulfate were used, as these are the most commonly used salts in HIC. These salts were used for exploring the effects, adapting screening methodologies, and discovering predictive tools. In the future, additional salts like acetate, glycine, and citrate have to be investigated. The discovered correlation between the product of the salt concentration and its corresponding ionic strength with the progression of the dynamic binding capacities has to be investigated in more detail with other salts and also with other proteins. By that the empiric description of the trend investigated in this study can be generalized.

Acknowledgments

The authors would like to thank Katharina Christin Bauer and Lara Galm for extensive validation of the stalagmometric method, used in this publication. This authors would also thank Susanna Suhm, Marc Hoffmann, and Sylvius Willerich for contributing to this work as well as Dr. Egbert Müller and Judith Vajda for coming up with the initial idea. Furthermore, the authors would like to thank Pascal Baumann for enlightening discussions and proofreading of the manuscript. Also, the authors are grateful for the financial support by the German Federal Ministry of Education and Research (BMBF) - funding code 0315342B. The authors bear the complete responsibility for the content of the publication. The authors have declared no conflict of interest.

Abbreviations

c_{crit}	critical salt concentration
$c_{crit,90}$	90% of critical salt concentration
$c_{crit,total}$	critical total salt concentration for salt mixtures
$c_{crit,total,90}$	90% of critical total salt concentration for salt mixtures
IS_{crit}	critical ionic strength
$IS_{crit,90}$	90% of critical ionic strength

References

[1] J. Chen, S. Cramer, Protein adsorption isotherm behavior in hydrophobic interaction chromatography, Journal of Chromatography A 1165 (2007) 67–77.

[2] A. Jungbauer, C. Machold, R. Hahn, Hydrophobic interaction chromatography of proteins III. Unfolding of proteins upon adsorption, Journal of Chromatography A 1079 (2005) 221–228.

[3] R. Hahn, K. Deinhofer, C. Machold, A. Jungbauer, Hydrophobic interaction chromatography of proteins II. Binding capacity, recovery and mass transfer properties, Journal of Chromatography B 790 (2003) 99–114.

[4] M. M. Diogo, D. M. F. Prazeres, N. Pinto, J. a Queiroz, Hydrophobic interaction chromatography of homo-oligonucleotides on derivatized sepharose CL-6B. Using and relating two different models for describing the effect of salt and temperature on retention, Journal of Chromatography A 1006 (2003) 137–148.

[5] J. Chen, J. Tetrault, A. Ley, Comparison of standard and new generation hydrophobic interaction chromatography resins in the monoclonal antibody purification process, Journal of Chromatography A 1177 (2008) 272–281.

[6] B. To, A. Lenhoff, Hydrophobic interaction chromatography of proteins. II. Solution thermodynamic properties as a determinant of retention, Journal of Chromatography A 1141 (2007) 235–243.

[7] F. Hofmeister, Zur Lehre von der Wirkung der Salze, Archiv für Experimentelle Pathologie und Pharmakologie 24 (1888) 247–260.

[8] G. Carta, A. Jungbauer, Chromatography Media, Wiley-VCH Verlag GmbH & Co. KGaA Weinheim, 2010, Ch. 3, pp. 85–124.

[9] K. D. Collins, Ions from the Hofmeister series and osmolytes: effects on proteins in solution and in the crystallization process, Methods 34 (2004) 300–311.

[10] M. E. Lienqueo, A. Mahn, J. C. Salgado, J. A. Asenjo, Current insights on protein behaviour in hydrophobic interaction chromatography, Journal of Chromatography B 849 (2007) 53–68.

[11] T. Arakawa, S. Timasheff, Mechanism of protein salting in and salting out by divalent cation salts: balance between hydration and salt binding, Biochemistry 23 (1984) 5912–5923.

[12] J. Queiroz, C. Tomaz, J. Cabral, Hydrophobic interaction chromatography of proteins, Journal of Biotechnology 87 (2001) 143–159.

[13] A. Senczuk, R. Klinke, T. Arakawa, G. Vedantham, Y. Yigzaw, Hydrophobic interaction chromatography in dual salt system increases protein binding capacity, Biotechnology and bioengineering 103 (2009) 930–935.

[14] E. Müller, J. Vajda, D. Josic, T. Schröder, R. Dabre, T. Frey, Mixed electrolytes in hydrophobic interaction chromatography, Journal of separation science 36 (2013) 1327–1334.

[15] W. Melander, C. Horváth, Salt Effects on Hydrophobic Interactions in Precipitation and Chromatography of Proteins: An Interpretation of the Lyotropic Series, Archives of Biochemistry and Biophysics 183 (1977) 200–215.

[16] A. Werner, H. Hasse, Experimental study and modeling of the influence of mixed electrolytes on adsorption of macromolecules on a hydrophobic resin, Journal of Chromatography A 1315 (2013) 135–144.

[17] S. Amrhein, K. Bauer, L. Galm, J. Hubbuch, Non-Invasive High Throughput Approach for Protein Hydrophobicity Determination Based on Surface Tension, Biotechnology and Bioengineering (2015) –.

[18] P. Debeye, E. Hückel, Zur Theorie der Elektrolyte, Physikalische Zeitschrift 24 (1923) 185–206.

[19] K. Baumgartner, L. Galm, J. Nötzold, Determination of protein phase diagrams by microbatch experiments: Exploring the influence of precipitants and pH, International Journal of Pharmaceutics 479 (2015) 28–40.

[20] L. R. De Young, A. L. Fink, K. A. Dill, Aggregation of Globular Proteins, Accounts of Chemical Research 26 (1993) 614–620.

[21] F.-Y. Lin, W.-Y. Chen, M. T. W. Hearn, Microcalorimetric Studies on the Interaction Mechanism between Proteins and Hydrophobic Solid Surfaces in Hydrophobic Interaction Chromatography: Effects of Salts, Hydrophobicity of the Sorbent, and Structure of the Protein, Analytical Chemistry 73 (2001) 3875–3883.

Influence of Binding pH and Protein Solubility on the Dynamic Binding Capacity in Hydrophobic Interaction Chromatography

Pascal Baumann[1,*], Kai Baumgartner[1,*] and Jürgen Hubbuch[1,**]

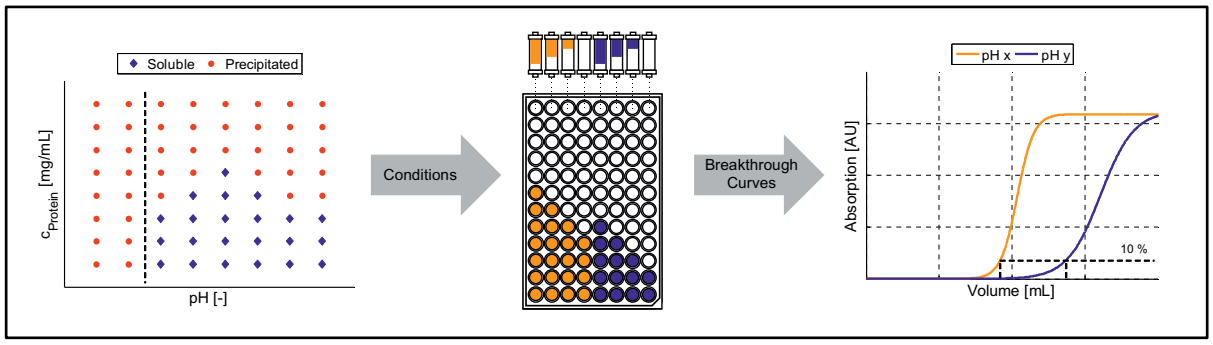

[1] : *Institute of Engineering in Life Sciences, Section IV: Biomolecular Separation Engineering, Karlsruhe Institute of Technology, Engler-Bunte-Ring 1, 76131 Karlsruhe, Germany*

[*]: *Contributed equally to this work*

[**] : *Corresponding author; mail: juergen.hubbuch@kit.edu*

Journal of Chromatography A

Volume 1396, (2015), 77-85

Submitted: 5. February 2015
Accepted: 1. April 2015
Available online: 11. April 2015

Abstract

Hydrophobic interaction chromatography (HIC) is one of the most frequently used purification methods in biopharmaceutical industry. A major drawback of HIC, however, is the rather low dynamic binding capacity (DBC) obtained when compared to e.g. ion-exchange chromatography (IEX). The typical purification procedure for HIC includes binding at neutral pH, independently of the protein's nature and isoelectric point. Most approaches to process intensification are based on resin and salt screenings.
In this paper a combination of protein solubility data and varying binding pH leads to a clear enhancement of dynamic binding capacity. This is shown for three proteins of acidic, neutral, and alkaline isoelectric points. High-throughput solubility screenings as well as miniaturized and parallelized breakthrough curves on MediaScout®RoboColumns®(Atoll, Germany) were conducted at pH 3 to pH 10 on a fully automated robotic workstation. The screening results show a correlation between the DBC and the operational pH, the protein's isoelectric point and the overall solubility. Also, an inverse relationship of DBC in HIC and the binding kinetics was observed. By changing the operational pH, the DBC could be increased up to 30% compared to the standard purification procedure performed at neutral pH. As structural changes of the protein are reported during HIC processes, the applied samples and the elution fractions were proven not to be irreversibly unfolded.

Keywords: Hydrophobic Interaction Chromatography, Dynamic Binding Capacity, Protein Solubility, Binding Kinetics, Multi-variate Data Analysis

1 Introduction

Hydrophobic interaction chromatography (HIC) is a widely applied technique for the intermediate purification and polishing of biomolecules in biopharmaceutical industry. The low dynamic binding capacity compared to e.g. ion-exchange chromatography (IEX) demands for a deeper process understanding and optimization. For IEX, several strategies for process design were reported [1, 2, 3, 4], whereas HIC process development still relies on heuristics and rules of thumb. So far, optimization strategies mostly have been based on the fundamentals of HIC, namely, the salting-out effect of different salts and the stoichiometric displacement of water under entropically favored conditions during protein binding [5, 6]. Considering those two principles, strategic studies mainly focus on screening to identify suitable resins, salt types, and ideal salt concentrations [7].
In [8, 9] the HIC binding mechanism was described in more detail, including additional sub-processes determined by microcalorimetric studies:
a. Dehydration/ deionization of the protein and adsorber surface.
b. Van-der-Waals forces between protein and resin.
c. Structural changes of the protein.
d. Rearrangement of excluded water molecules in solution.
Especially the structural changes and rearrangements of the protein during the binding process is an important factor to be considered. Various studies have shown, that proteins undergo a partial unfolding during the hydrophobic binding process which can be irreversible especially at higher protein concentrations [10, 11]. In [12, 13], distinct elution peaks were detected which were correlated to the same protein species but of different

conformations. In [14] high protein pore concentrations, as found during the elution step, were found to stabilize the structure of α-lactalbumin. Jones et al. [15] proposed that changes in selectivity for stable proteins can be explained by orientational rearrangement on the adsorber surface, whereas unstable proteins like α-lactalbumin exhibit structural changes during binding to the HIC surface. Both aspects of rearrangement and structural change open up new approaches for HIC optimization strategies. In that context, not only the type of salt or adsorber should be considered, but also the physical state of the protein. Related properties include the protein's compressibility, molecular weight and the solute pH [16].
Although, the pH was identified earlier to be a parameter influencing HIC [17, 18, 19], to the best of our knowledge, the dynamic binding capacity as a function of pH and solubility has never been systematically screened, as was shown for IEX [1, 2, 3]. Still, the gold standard for HIC is using an operational pH in the neutral pH range of pH 6 to 8. Examples are the purification of the cystic fibrosis plasmid vector (operational pH 8), the enrichment of proteins from *Haemophilus influenzae* (pH 7), and the separation of single-, double-stranded, and supercoiled nucleic acids (pH 8) [20, 21, 22]. For antibody purification, varying pH values were considered, resulting in a modified retention behavior. However, the studies covered a range of pH 6 to 8.5 only [18]. Kramarczyk et al. [23] introduced a high-throughput strategy for solubility screenings in dependence of pH, salt type as well as salt concentration and HIC binding experiments for a monoclonal antibody. Nevertheless, all subsequent binding experiments were conducted at the solubility optimum at pH 7, only. A thorough investigation into pH effects as a determining factor for protein solubility and adsorbent interactions under typical HIC conditions is needed. In this study, a high-throughput strategy is developed correlating protein solubility and pH to the dynamic binding capacity (DBC) in HIC. The screening methodology is shown in Fig. 1. Salt type and concentration are kept constant to exclude influences of salt nature and altered isotherm binding effects. High-throughput solubility screenings are performed at pH 3 to pH 10 for proteins of acidic, neutral, and alkaline isoelectric points. pH values of instant protein denaturation are excluded from the following breakthrough curves determined in miniaturized robotic chromatography column experiments. DBCs as well as binding kinetics are subsequently correlated to the protein's pI and solubility data. As protein binding is supposed to vary due to reversible structural changes in the protein, the elution samples of increased DBC need to be investigated for protein integrity. This is done by principal component analysis (PCA) of native and denatured protein spectra of selected setups.

2 Materials & Methods

2.1 Materials

2.1.1 Chemicals & Disposables

The following buffer substances were used: Citric acid monohydrate (Merck, Germany) for pH 3 and 4, sodium acetate trihydrate (Fluka BioChemika, Switzerland) for pH 5, MES monohydrate buffer grade (AppliChem, Germany) for pH 6, sodium dihydrogenphosphate monohydrate (Merck, Germany) for pH 7, TAPS buffer grade (AppliChem,

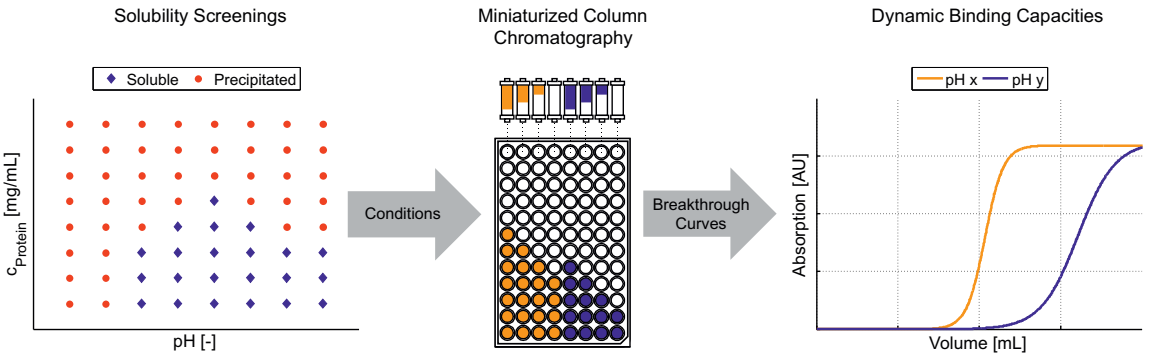

Figure 1: Schematic overview of the HIC pH screening methodology. The solubility screenings determine the feasible pH conditions for the miniaturized column chromatography experiments. Determined breakthrough curves can then be evaluated in terms of dynamic binding capacities, defined as 10% of product breakthrough.

Germany) for pH 8, CHES (AppliChem, Germany) for pH 9, and CAPSO (SantaCruz Biotechnology Inc, USA) for pH 10. All buffers were prepared with a buffer capacity of 40 mM and an additional sodium sulfate (Fluka BioChemika, Switzerland) concentration of 1.875 M. The pH of all buffers was adjusted using hydrochloric acid or sodium hydroxide (Merck, Germany). All buffers were filtered using Supor-450 0.45 μm membrane filters (Pall Life Sciences, Mexico).

Three proteins of different isoelectric points (acidic, neutral, and alkaline) were investigated. All protein solutions were filtered using 0.2 μm syringe filters with PTFE membranes (VWR, Germany). Buffer exchange and protein concentration steps were carried out in Vivaspin®centrifugal concentrators (Sartorius, Germany) equipped with PES membranes and molecular weight cutoffs of 5 kDa. Lysozyme from chicken egg white (PDB 1LYZ, HR7-110) was purchased from Hampton Research (USA). A purified single domain antibody was obtained from the industrial partner (BAC, Netherlands) at a concentration of 17.18 mg/mL. Glutathione-S-Transferase (GST) with Cherry-Tag™ (Delphi genetics, Belgium) was produced in *Escherichia coli* SE1. The cultivation, cell disruption, and purification process was performed according to [24]. Capillary gel electrophoresis (CGE) was performed in a Caliper LabChip®GX II system (Perkin Elmer, USA) using an HT Protein Express & Pico LabChip®and an HT protein express reagent kit (Perkin Elmer, USA). Sample preparation for the CE was conducted in skirted 96-well twin.tec®PCR plates (Eppendorf, Germany). Lysozyme served as an internal standard of known concentration. Protein denaturation as a negative control for protein spectra was accomplished using trichloroacetic acid BioChemica (AppliChem, Germany) combined with acetone for liquid chromatography (Merck, Germany) and urea (Fluka BioChemika, Switzerland).

High-throughput robotic precipitation experiments and UV measurements were carried out in 96-well flat-bottom UV-Star®half-area and full-area microplates (Greiner Bio-One, Germany). The plates were sealed with non-sterile Platemax aluminum sealing films (Axygen®Scientific, USA). For the high-throughput chromatography experiments, 600 μL MediaScout®RoboColumns®(Atoll, Germany) filled with Toyopearl®Phenyl-650M adsorber (Tosoh Bioscience, Germany) were used. Buffers and protein solutions for the robotic chromatography experiments were prepared in 8-row reservoir plates

(Axygen®Scientific, USA).

2.1.2 Instrumentation & Software

For pH adjustment of all buffers, a five-point calibrated HI-3220 pH meter (Hanna Instruments, USA) equipped with a SenTix®62 pH electrode (Xylem Inc., USA) was used. The instrument was calibrated using high-precision standards by Hanna Instruments (USA). Concentration and purity measurements of the protein stock solutions were carried out by capillary gel electrophoresis (CGE) in a Caliper LabChip®GX II (Perkin Elmer, USA). For data processing and analysis, the LabChip®GX 3.1 software (PerkinElmer, USA) was used. A NanoDrop™ 2000c UV-Vis spectrophotometer operated with the NanoDrop™ measurement software version 1.4.2 (Thermo Fisher Scientific, USA) served as a fast tool for the determination of protein concentrations. All isoelectric points were calculated using GPMAW (Lighthouse Data, Denmark) for the respective amino acid sequence derived from the protein data bank (PDB).
Solubility screenings and robotic chromatography experiments were conducted on a Freedom EVO®200 robotic platform operated with the Freedom EVOware®2.5 software (Tecan, Germany). The platform is equipped with a liquid handler with eight fixed pipette tips, a robotic moving arm for transportation of plates, a plate stacker module for storage of plates, a Te-Chrom Bridge for RoboColumns®, and an orbital shaker. Centrifugations were conducted in an integrated Rotanta 46 RSC centrifuge made by Hettich (Germany). Absorption measurements were performed in an integrated infinite M200 Pro spectrophotometer operated with the software Magellan™ 7.1 from Tecan (Germany). Principal component analysis (PCA) of protein spectra was performed in Simca (Umetrics, Sweden). Data processing and creation of figures was performed in Matlab®R2014a (MathWorks, USA).

2.2 Experimental Setup

As temperature is an influencing factor on protein solubility, pH and the binding behavior in HIC [25, 5] all experiments were performed in a temperature-controlled laboratory (constant temperature of 23 °C). All used buffers were adjusted to respective pH values after equilibration to room temperature. Chromatography columns were stored at room temperature over night for temperature adjustment. Thus, temperature related effects were eliminated.

2.2.1 Protein Solubility Screenings

The protein stock solutions were applied at a concentration of 60 mg/mL in ultra-pure water. Lysozyme was obtained as crystalline powder and was directly dissolved in ultra-pure water. Cherry-GST and the single domain antibody (V_HH), by contrast, were stored in the elution buffer from the purification procedures. Buffer exchanges and concentrating procedures were performed using Vivaspin®centrifugal concentrators (Sartorius, Germany) with a cutoff of 5 kDa to the final concentration of 60 mg/mL. With a NanoDrop™ 2000c by Thermo Fisher Scientific, the protein concentration was determined exactly using absorption coefficients derived from capillary gel electrophoresis (data not shown). Theoretical isoelectric points of the investigated proteins were determined based on the

primary protein structure in the GPMAW software. The calculations resulted in pI = 5.2 for Cherry-GST, pI = 7.4 for the V_HH, and pI = 10.9 for lysozyme. Hence, the experiments covered a range of acidic, neutral, and alkaline proteins. As high-salt stock solutions, 40 mM buffers of pH 3 to 10 at a sodium sulfate (NaS) concentration of 1.875 M were prepared.
Protein solubility screenings were carried out on a liquid handling station of the type Freedom EVO®200 (Tecan, Germany). A total volume of 300 μL was pipetted into each well of the 96-well UV-Star®plate. Each mixture consisted of 200 μL 40 mM high-salt (1.875 M NaS) buffer and 100 μL of protein solution in ultra-pure water (3 times the final protein concentration of the screening), resulting in an effective NaS concentration of 1.25 M. The real concentrations of the applied protein solutions were determined using the NanoDrop™ system. The microplates were sealed and incubated in an overhead shaker for two hours. The plates were then centrifuged for 10 min at 4000 rpm for removal of potential precipitate. The supernatant was transferred to a 96-well flat-bottom UV-Star®full-area plate, measured at 280 nm (414 nm for Cherry-GST) in an Infinite M200 Pro photometer by Tecan and the amount of protein recovery was determined. Data processing to determine the protein phase behavior was performed in Matlab®. As a threshold criterion for precipitation conditions, a recovery below 90% was stated. A protein calibration curve in the range from 0 to 1 mg/mL served as a reference.
The initial screenings were performed in a protein concentration range from 0 to 20 mg/mL in 5 mg/mL increments as duplicates. The regions of protein aggregation were subsequently investigated in more detail for each pH in 1 mg/mL steps. For conditions where 20 mg/mL of protein were still soluble, the initial protein concentration was further increased. For those setups, the concentration of the protein stock solution was increased, accordingly. Data points with a relative standard deviation larger than 10% were removed from the evaluation.

2.2.2 Determination of Dynamic Binding Capacities

3 mg/mL of each protein solution were prepared in buffers of the respective pH, including 1.25 M sodium sulfate, as described above and filled into 8-row reservoir plates. The 1.25 M NaS equilibration and wash buffers were applied to the deck of the robotic workstation in the same way.
Dynamic binding capacities were determined using 600 μL Toyopearl®Phenyl-650M Robo-Columns®(Atoll, Germany) in an automated liquid handling station (Tecan, Germany). The miniaturized columns were washed with 6 column volumes (CV) of ultra-pure water for removal of the storage solution. Following 12 CV equilibration with 1.25 M high-salt buffer of the respective pH, protein sample loading was performed. During the sample loading procedure, the liquid droplets from the column outlets were fractionated in 96-well UV-Star®plates. The fraction volume was 150 μL for experiments with half-area plates and 300 μL for experiments with full-area plates. Each experiment was performed in quadruplicate. For a better curve resolution, sample loading was performed interlaced. Prior to the breakthrough experiment, column 2 was loaded with 0.25 CV, column 3 with 0.5 CV, and column 4 with 0.75 CV of protein solution, resulting in slightly shifted elution pools. A schematic illustration is given in Fig. 1 (center). In total, 15 CV of protein solution were applied to each column for experiments using half-area plates. For

conditions of higher DBCs, a second method for applying 30 CV of protein sample was developed using full-area plates. For both methods, the elution was carried out by applying 3 CV (6 CV for full-area plates) of ultra-pure water after a high salt wash step of 3 CV. After another wash of 6 CV of ultra-pure water, the columns were cleaned with 6 CV of ethanol for storage. As eight robotic columns were used simultaneously, two pH setups could be investigated in one run as an interlaced quadruplicate for a higher resolution.
Data processing and the calculation of the DBCs were performed in Matlab®. The variances in sample volume per fractionation due to droplet collection from the RoboColumns®were corrected by 990 nm and 900 nm measurements as described in [26]. The real concentrations of the applied protein solutions were determined in the NanoDrop™ system and were used in the Matlab®evaluation software. 10% of protein breakthrough were defined as the DBC threshold. The respective absorption values were determined by a protein calibration curve in the range from 0 to 1 mg/mL. Finally, the DBCs were calculated considering the fraction volumes and column bed volume.

2.2.3 Determination of HIC Binding Kinetics

The measured 280 nm absorption signals of the breakthrough curves were fitted to a logistic function in Matlab®as shown in Eq. (1). The fitting was carried out using 'Trust region' optimization in the internal Matlab®*curve fitting* toolbox. a, b, and c are the coefficients of the respective fit and V represents the fractionated volume of the droplets.

$$UV_{280nm} = \frac{a}{1 + 10^{b \cdot (c - V)}} \tag{1}$$

The maximum of the derivatives of these fits were calculated and used as a measure of the binding kinetics.

2.2.4 Protein Unfolding Procedures

As HIC protein binding is supposed to be based on reversible partial unfolding, selected samples of increased DBC were investigated for structural integrity after elution by analysis of protein spectra (section 2.2.5). The experiments were performed with lysozyme, as it was obtained with the highest purity (98%) of all investigated proteins to exclude deviations in the spectra due to impurities. Denatured lysozyme spectra were prepared as negative controls. One sample was directly prepared in 6 M urea solution. A second sample was treated with trichloroacetic acid (TCA). For this purpose, 1 mL of 0.3 mg/mL lysozyme solution in ultra-pure water was mixed with 50 μL of 100% (w/v) TCA solution and stored on ice for 10 min. After a centrifugation cycle at 4000 rpm for 5 min, the supernatant was discarded and the pellet was washed twice with 1 mL of 100% cold acetone. The remaining acetone in the protein pellet was evaporated under a vent for at least 4 h. The dried pellets were then resuspended in 1 mL 6 M urea solution for 2 h at 40 °C.

2.2.5 Principal Component Analysis of Protein Spectra

To obtain spectra in a linear range of the spectrophotometer, the protein samples needed to be diluted to a concentration of 0.3 mg/mL. Setups of pH 5, pH 7, and pH 10 were

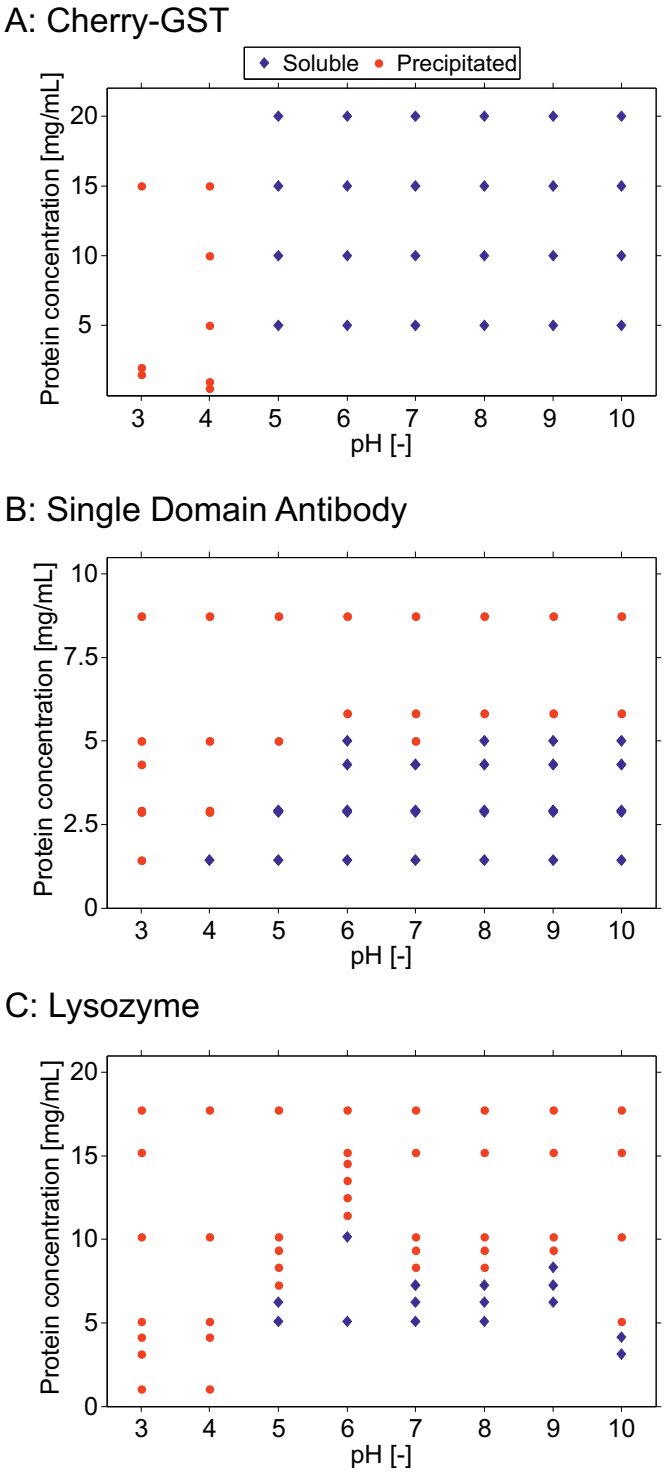

Figure 2: Solubility screenings of three different proteins of acidic, neutral, and alkaline pI in a range from pH 3 to pH 10 in full pH steps, including 1.25 M sodium sulfate. Conditions of soluble proteins are indicated by blue diamonds, precipitated proteins are marked by red circles. A: Cherry-GST (pI = 5.2), B: single domain antibody (V_HH) (pI = 7.4), C: Lysozyme (pI = 10.9).

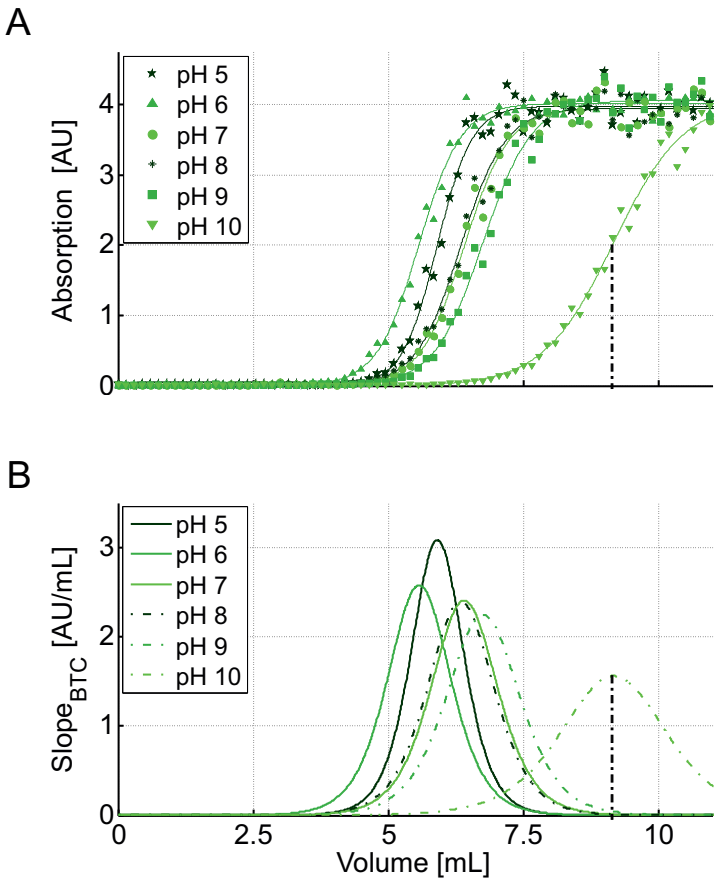

Figure 3: Fitted breakthrough experiments for lysozyme using miniaturized chromatography columns on a robotic workstation (A) and corresponding derivatives of the breakthrough curves (BTCs) (B). The dash-dotted line indicates the maximum of the slope curve, which equals the inflexion point of the BTC shown as an example for pH 10.

investigated. The chosen range covered the boundary conditions of the breakthrough experiments as well as the standard operational neutral pH condition. For each setup, blanked protein spectra were determined in a range from 240 to 300 nm in 2 nm steps. All determined spectra were then analyzed in SIMCA by performing a principal component analysis (PCA). The mean centered data matrix consisted of 31 variables (wavelengths from 240 nm to 300 nm in 2 nm steps) and 9 objects (1 urea and 2 TCA denatured lysozyme samples as well as 6 lysozyme samples before and after chromatography binding at pH 5, 7, and 10). The sample clusters in the score scatter plot were used as a measure of a change in protein integrity.

3 Results

3.1 Protein Solubility Screenings

The results of the protein solubility screenings are illustrated in Fig. 2. All precipitation screenings were carried out in buffers of pH 3 to pH 10 using full pH steps and increasing protein concentrations. The buffers included 1.25 M sodium sulfate. Conditions at which the protein stays soluble are indicated by blue diamonds, whereas conditions of

precipitation are marked by red circles.
For Cherry-GST (pI = 5.2), all reaction mixtures of pH 3 and pH 4 resulted in instant product precipitation even at concentrations below 1 mg/mL (Fig. 2A). For all other pH values, the protein was found to be stable even up to concentrations above 80 mg/mL. Starting from pH 11, Cherry-GST showed a behavior analogous to that at pH 3 and pH 4 (data not shown).
The single domain antibody (V_HH) (pI = 7.4) was not stable above a concentration of 5 mg/mL for all investigated setups (Fig. 2B). pH 3 resulted in an instant precipitation of the product even at a concentration of 1 mg/mL. At pH 4, the V_HH was found to be stable up to 1.25 mg/mL. Starting from pH 5, an almost constant solubility limit in a range from 4 to 5 mg/mL was observed. The maximal solubility was achieved for pH 6, 8, 9, and 10 (5 mg/mL), whereas a decline in solubility was determined for pH 7.
Lysozyme (Fig. 2C), as the most alkaline of the investigated proteins (pI = 10.9), was not stable at pH 3 and pH 4 analogously to Cherry-GST. The solubility maximum was determined to be up to 10 mg/mL for pH 6 and the protein could be kept soluble up to 6 mg/mL at pH 5. Starting from pH 7, lysozyme was found to be stable in the range from 7 to 8 mg/mL. At pH 10, a sharp decline in solubility was observed, with a maximal soluble protein concentration of 4 mg/mL. For pH 11, lysozyme showed a behavior analogous to that at pH 3 and pH 4 (data not shown).
Due to these results, the DBC experiments were carried out in a range from pH 5 to pH 10 only. The protein concentration for the DBC determinations was set to 3 mg/mL for lysozyme and Cherry-GST. Due to the comparably low solubility of the V_HH, the respective experiments were carried out using 2 mg/mL protein solutions.

3.2 Dynamic Binding Capacities (DBCs)

In Fig. 3A the breakthrough curves of lysozyme are exemplarily shown for all investigated pH values. The DBCs were calculated at a breakthrough of 10% of the initial protein concentration, as described above. In Fig. 4A the calculated relative dynamic binding capacities (DBCs) of the three investigated proteins are shown at varying binding pH on the Toyopearl®Phenyl-650M adsorber. The DBCs were normalized to the DBC at pH 7 as the standard procedure. For all investigated proteins, the DBCs show a strong pH dependence.
For Cherry-GST (Fig. 4A - red), the minimal DBC was observed for pH 6, with the DBC being 8.2% ± 0.8% smaller than under standard pH 7 binding conditions. Towards acidic conditions (pH 5), an increased DBC of 12.8% ± 2.4% was observed. Towards the alkaline pH region, higher DBCs were investigated with a maximum increase of 23.4% ± 1.3% at pH 9. Overall, the lowest DBCs were found for the neutral pH conditions (pH 6 to 8), while acidic and alkaline buffers increased protein binding by up to more than 23%.
The single domain antibody (Fig. 4A - blue) revealed the highest DBC under the standard operating conditions at pH 7. The lowest DBC was observed for pH 9, the value being 13.8% ± 2.4% smaller than under the standard pH 7 binding conditions. Towards acidic as well as alkaline conditions, the DBC decreased compared to pH 7, with the impact being more pronounced in the alkaline region.
For lysozyme from chicken egg white (Fig. 4A - green), the maximal DBC was observed for pH 10 with an increase of 28.3% ± 1.0% compared to pH 7. Overall, a trend to-

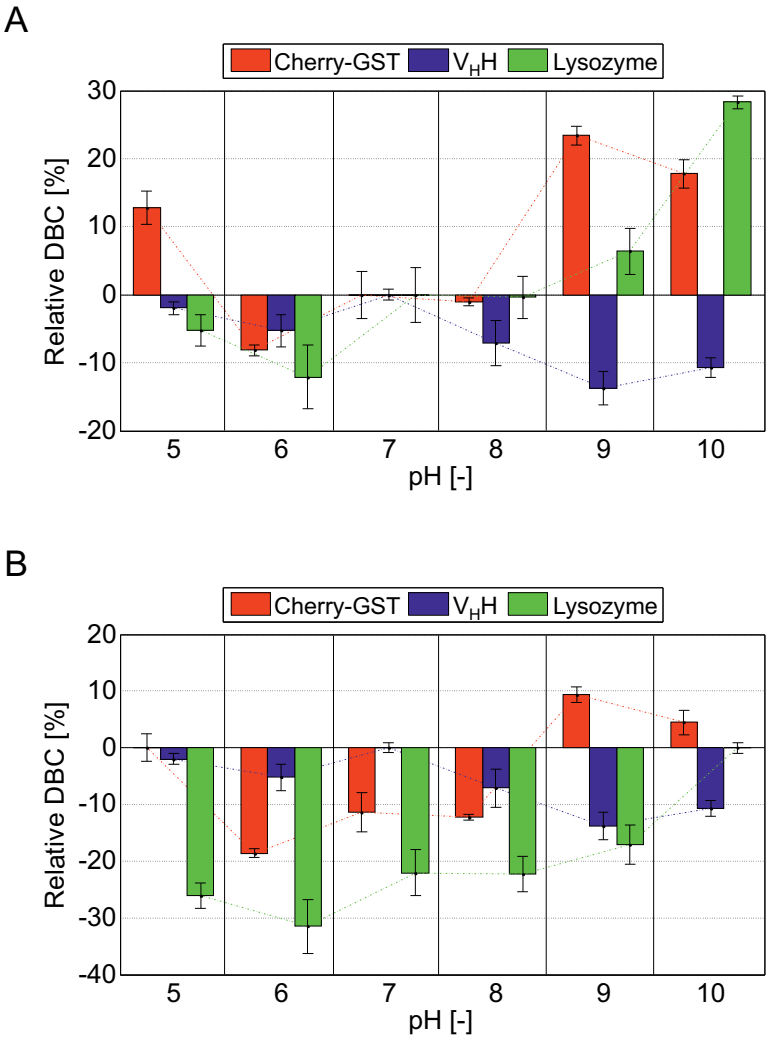

Figure 4: Relative dynamic binding capacities (DBCs) of the three investigated proteins: Cherry-GST (pI = 5.2) is shown in red, the single domain antibody V_HH (pI = 7.4) in blue and lysozyme (pI = 10.9) in green. A: DBC scaled to the typical operational condition at pH 7. B: DBC scaled to the respective isoelectric points.

wards increased protein binding was found under alkaline operational conditions. This observation is clarified in the chromatograms shown in Fig. 3A. Here, the curves of latest breakthrough correspond to the experiments at pH 9 (squares) and pH 10 (downward triangles). Acidic conditions, by contrast, resulted in a decrease in DBC of up to 12.2% ± 4.7% at pH 6. In summary, a continuous increase of DBC was observed for lysozyme from acidic towards alkaline binding conditions on the Toyopearl®Phenyl-650M adsorber.

In Fig. 4B the DBCs are scaled to the values of the respective protein pI's. Except for Cherry-GST at pH 9 and pH 10 all residual conditions yielded in negative relative DBCs. Thus, the isoelectric point was found to be the system point of maximal DBC of almost all investigated conditions.

Fig. 5 shows the correlation between the protein's relative solubility limit (scaled to the solubility maximum) and the corresponding relative DBC (scaled to the maximal investigated DBC) for the single domain antibody (Fig. 5A) and lysozyme (Fig. 5B). Both

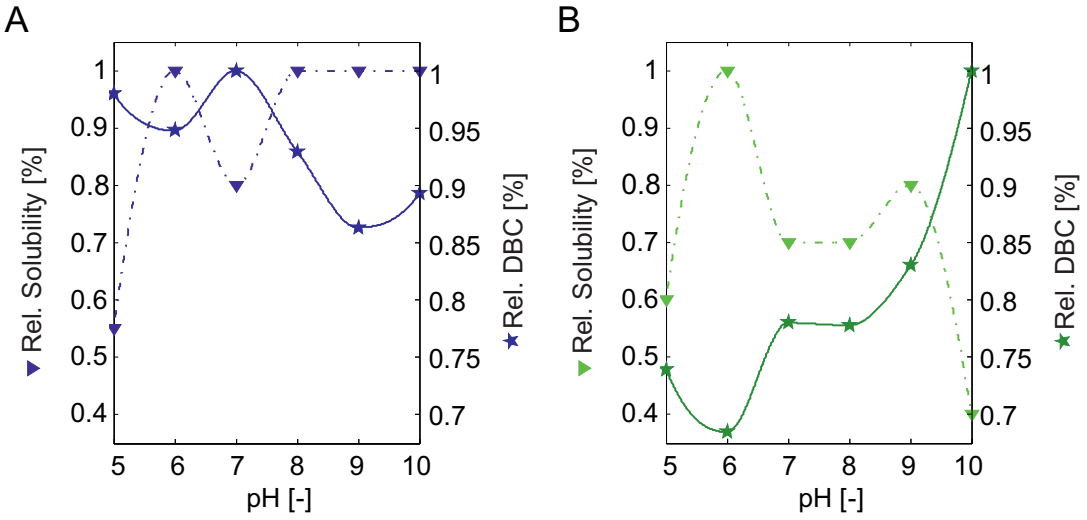

Figure 5: Correlation of relative (scaled to the maximum) protein solubilities (dash-dotted line) and relative (scaled to the maximum) dynamic binding capacities (solid line) of the single domain antibody V_HH (A) and lysozyme (B) in dependence of the operational pH value.

proteins show an inverse trend of relative solubility and relative DBC, most pronounced at pH 6 and pH 10 for lysozyme (Fig. 5B). For Cherry-GST no solubility limit could be determined making such a figure for this protein obsolete.

3.3 Determination of HIC Binding Kinetics

The derivatives of the breakthrough curves (BTCs) are shown as an example for all lysozyme setups in Fig. 3B. The maxima of the derivatives describe the binding kinetics and mark the inflexion points of the BTCs as highlighted by the dash-dotted lines in Fig. 3. In Table 1 the maximal slopes of the fitted breakthrough curves are listed under all investigated conditions. For Cherry-GST, the highest binding kinetics were determined in the range from pH 6 to pH 8 up to 1.26 ± 0.16 AU/mL. At pH 5, the slope was ≈ 30% lower compared to those at neutral pH. At pH 9, the slowest binding kinetics of 0.53 ± 0.04 AU/mL was observed. For pH 10, no fitting to a logistic function was possible, as the kinetics was too slow to reach a final plateau within the defined experimental setup.

For the single domain antibody, the differences in the binding kinetics were negligible between pH 5 and pH 9. In this pH region the minimal slope of 0.61 ± 0.05 AU/mL was obtained for pH 9 and the maximal slope of 0.79 ± 0.06 AU/mL was calculated for pH 8. The only significant variation of the binding kinetics was observed for the pH 10 setup, yielding an overall minimum of 0.43 ± 0.06 AU/mL.

The highest slope for lysozyme of 3.12 ± 0.32 AU/mL was calculated for pH 5 with a continuous decrease towards alkaline conditions. The slowest kinetics was observed for pH 10 with 1.59 ± 0.21 AU/mL.

pH [-]	Kinetics$_{Ch-GST}$ [AU/mL]	Kinetics$_{V_HH}$ [AU/mL]	Kinetics$_{Lys}$ [AU/mL]
5	0.85 ± 0.06	0.76 ± 0.12	3.12 ± 0.32
6	1.24 ± 0.06	0.74 ± 0.08	2.79 ± 0.35
7	1.17 ± 0.24	0.66 ± 0.09	2.46 ± 0.26
8	1.26 ± 0.16	0.79 ± 0.06	2.53 ± 0.19
9	0.53 ± 0.04	0.61 ± 0.05	2.29 ± 0.19
10	n/a	0.43 ± 0.06	1.59 ± 0.21

Table 1: Maximal slopes of the fitted breakthrough curves as a measure of binding kinetics depending on the pH value for the three investigated proteins - Cherry-GST, single domain antibody (V_HH), Lysozyme.

3.4 Investigation of Lysozyme Integrity & Recovery

To investigate samples of increased protein binding for structural integrity after elution, a principal component analysis of protein spectra was conducted. The analysis was performed with lysozyme, as it was the protein of the highest purity (98%) of all investigated biomolecules. Spectra of TCA and, alternatively, urea denatured lysozyme were compared to samples before and after binding to the HIC column. The number of principal components (PCs) describing 99.3% of the system was determined to be 2 (87.3% variance described by PC 1 and 12.0% variance described by PC 2). Creating models of more PCs resulted in no further improvements and measurement noise was found to be included into the model. Fig. 6A illustrates the scatter plot for the score values. The maximal deviance in the score plot of PC 1 was determined for the TCA denatured samples, both located in one isolated cluster. Fig. 6B shows line plots for the loading values of PC 1 and PC 2. Looking at the loading plot for PC 1, those differences were mainly detected in the region from 240 to 248 nm. For PC 2, the score scatter plot revealed a maximal deviation for the urea denatured lysozyme sample. Again, an isolated cluster was observed. The loading plot for PC 2 revealed the wavelength range of 244 to 260 nm to be the most influential one, with a second important region beginning from 284 nm. All remaining samples from the BTC binding experiments merged in one final cluster close to the coordinate origin of the score scatter plot.
In addition to protein integrity studies, lysozyme recoveries were determined in terms of total mass balances for the above-mentioned conditions (pH 5, pH 7, and pH 10). The mass of lysozyme in the elution fraction was divided by the total mass of bound lysozyme until breakthrough. At pH 5 the recovery rate of lysozyme was determined to be 90.7%. For pH 7 94.3% and for pH 10 100.2% of bound lysozyme were recovered.

4 Discussion

4.1 Protein Solubility Screenings

The protein solubility screenings were carried out to identify pH and solubility boundaries suitable to correlate dynamic binding capacities obtained on HIC with systems expressing different protein solubility (Fig. 2). At pH 3 and pH 4, an instant product loss occurred for Cherry-GST, indicating an instability towards acidic conditions induced by protona-

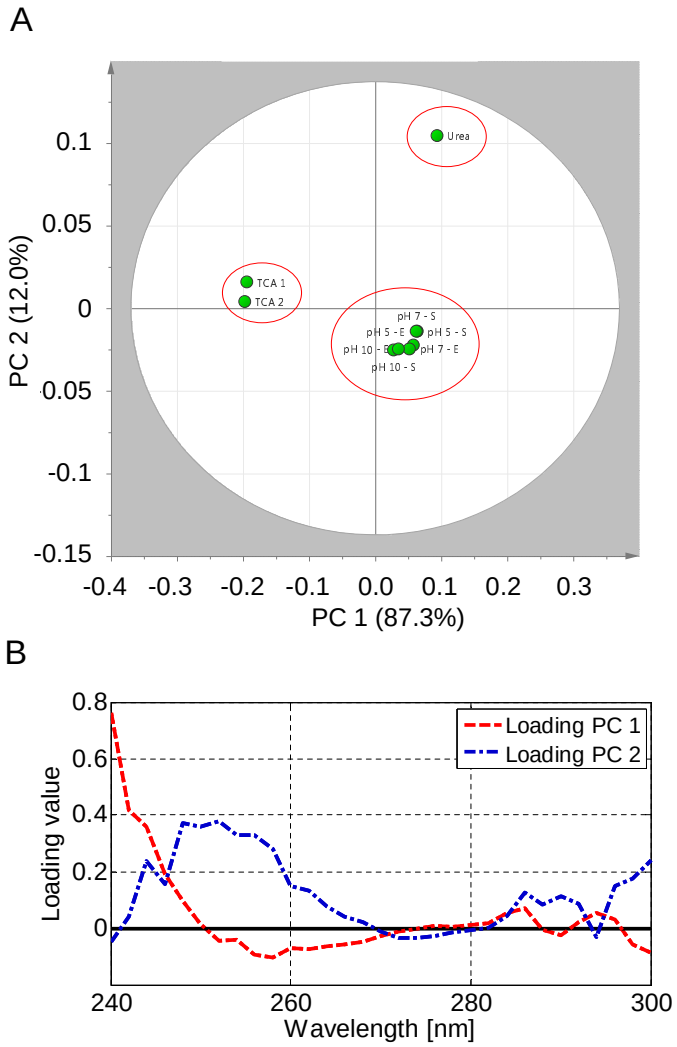

Figure 6: Principal component analysis of lysozyme spectra. Calibration experiments included urea and TCA denatured spectra as well as spectra of samples and elution fractions of the chromatography experiments. A: Scatter plot of the resulting score values for a system of two principal components. B: Line plots of the loading values of the two principal components as a function of the wavelength.

tion of amino acid residues. For all other pH values investigated between pH 5 and pH 10, the protein was stable even at concentrations of up to 60 mg/mL. These findings agree with the reported stabilizing effect of the fused Cherry-Tag^{TM} resulting in an increased protein solubility [27, 28].
The single domain antibody (V_HH) showed a much lower solubility over the whole investigated pH range, with a maximum solubility of 5 mg/mL in presence of 1.25 M NaS. Acidic conditions again resulted in instant product loss, as was discussed for Cherry-GST. The reduced protein solubility at pH 7 compared to pH 6 and pH 8 correlates with the isoelectric point of the V_HH of 7.4.
The most alkaline protein investigated, namely lysozyme, again revealed an instant product loss at pH 3 and pH 4. The protonation of amino acid residues showed a strong negative impact on the protein solubility for all investigated protein species. As expected, lysozyme showed a strong decrease in solubility towards alkaline pH conditions

close to its isoelectric point of pH 10.9. The solubility maximum was found in the neutral pH region. Here, lysozyme is stabilized towards amino acid residue protonation, as well as towards aggregation close to the isoelectric point.
When comparing the solubility screenings of all investigated proteins, it can be summarized that strongly acidic conditions (pH 3) result in instant product losses even at protein concentrations below 1 mg/mL. Finally, for all investigated proteins a negative impact of conditions close to the isoelectric point on the protein's solubility was observed.

4.2 Influence of Binding pH Close to the Protein's pI on DBC

In Fig. 4B the DBCs of the different proteins are normalized to the values determined at the respective pI. The acidic protein Cherry-GST (pI = 5.2) revealed an increase in HIC binding towards acidic buffer conditions compared to pH 7 (Fig. 4B - red). However, the maximal DBC was determined for alkaline conditions at pH 9. The single domain antibody (pI = 7.4) as a protein of neutral pI showed the maximal HIC protein binding capacity close to the pI (Fig. 4B - blue). The same results were obtained for lysozyme (pI = 10.9) as the most alkaline protein with a maximal DBC at pH 10 (Fig. 4B - green). In summary, all investigated proteins showed an increase in protein binding towards their pI as illustrated by predominantly negative relative DBCs in Fig. 4B. These findings are in agreement with the pI's definition: As proteins carry a net surface charge of zero at their specified pI, electrostatic repulsions are minimized leading to a domination of hydrophobic forces. This leads to an increased interaction of the protein with hydrophobic ligands of HIC media. As proteins are destabilized close to their respective isoelectric point and structural changes are thus favored, increases in protein binding are most likely based on facilitated partial unfolding in accordance to Jungbauer et al. describing the HIC ligands as a catalyst for partial protein unfolding [10].

4.3 Influence of Protein Solubility on DBC

For Cherry-GST, an increase in DBC was observed under acidic as well as under alkaline conditions. The solubility screenings revealed that Cherry-GST is not stable below pH 5 and above pH 10, indicating an increase in HIC binding towards the solubility boundaries. Those findings match the new insights into the HIC binding mechanism being based on partial protein unfolding upon adsorption. Destabilization of the protein in unfavorable buffers facilitates partial unfolding during the HIC binding process.
Those findings were substantiated by the results obtained for the V_HH, which was most stable under alkaline conditions and revealed the lowest DBCs in this pH region. The HIC binding again increased towards conditions of decreased solubility, namely, acidic pH values and the isoelectric point as illustrated in Fig. 5A.
For lysozyme, as a protein of alkaline pI, the maximal DBCs were determined close to the isoelectric point and at the system point of lowest solubility (Fig. 5B) under the investigated conditions in the miniaturized column chromatography experiments. The lowest protein binding was obtained again at the system point of maximal solubility (pH 6). Starting from pH 6 towards more acidic pH values, protein binding was observed to increase again corresponding to the decline in solubility as illustrated in Fig. 5B.
The maximal DBC was not always found at the respective pI for all investigated proteins.

Although the pI is not generally the optimal system point for HIC protein binding, it may be a good starting point for increasing protein purification productivity. However, there is a correlation between protein solubility and binding behavior in HIC. System points of low protein solubility increase HIC protein binding, whereas conditions of high solubility have the opposite effect (Fig. 5). Those findings again indicate favored protein binding in HIC under destabilized conditions, as was discussed above.

4.4 Correlation of Binding Kinetics and Dynamic Binding Capacities

When comparing the DBCs (Fig. 4A) to the respective binding kinetics (Table 1), a clear inverse trend can be seen for lysozyme and Cherry-GST. Conditions of increased binding in HIC showed a decrease in the binding kinetics. The minimal binding kinetics were observed for the setups resulting in highest capacities and vice versa. For the single domain antibody, those kinetic effects were not that pronounced, as the pH was not a strongly influencing factor in all setups investigated. It can be concluded that the inverse correlation of DBCs and binding kinetics is due to a change of protein orientation during the binding process induced by higher adsorber loadings. This reorientation process slows down protein binding and, thus, decreases the binding kinetics.

4.5 Investigation of Protein Integrity & Recovery

As the determined system points of increased HIC protein binding might be accompanied by structural changes after elution, a spectral protein analysis was conducted. The PCA of the lysozyme spectra resulted in three different score clusters (Fig. 6A). The differently denatured samples formed two distinct score clusters, namely, the TCA cluster (mainly described by PC 1) and the urea cluster (mainly described by PC 2). The two fundamentally different denaturation procedures thus expanded a large area of scoring instabilities of lysozyme. All applied samples and elution pools from the lysozyme DBC experiments merged in one final cluster close to the origin of the score plot, indicating no changes in protein integrity after elution. If increased protein binding as an effect of altered pH was due to partial unfolding of the protein, this would be a reversible process after elution and can be neglected.
As HIC processes are reported to suffer from incomplete product elution [29] the recovery rates of the above-mentioned lysozyme samples were determined. It was shown that all investigated setups yielded in recoveries of 90 - 100% and product losses for conditions of increased DBCs were negligible.

5 Conclusions

The pH and protein solubility are highly influential parameters in HIC and should be considered for process optimization. Choosing an operational pH in the neutral region might be a good condition to choose for some proteins but can also be the reason why HIC can not be employed for some proteins at all until now as shown by [17] for cytochrome c. The screening results show a correlation of the dynamic binding capacity in HIC with

the operational pH value applied. Binding at a pH value close to the protein's isoelectric point as well as conditions near the solubility limit resulted in increased protein binding. These findings indicated a structural change upon binding in HIC, which are favored under destabilizing conditions. However, when comparing lysozyme spectra of the applied samples to the elution fractions in a principal component analysis, native conformation was verified. It can thus be assumed that the induced partial unfolding of lysozyme, if it occurs during binding, is a reversible process under the investigated conditions. To increase the DBCs of HIC adsorbers, choosing a pH close to the protein's pI may be a good starting point for process development. The most influencing factor, however, was shown to be the solubility limit. pH conditions resulting in decreased protein solubility have a positive effect on the binding in HIC.
As an additional factor, the protein binding kinetics were investigated and compared to the protein binding behavior. The kinetics followed an inverse trend compared to the DBCs. The highest DBCs were obtained for the setups of slowest kinetics. Thus, it was concluded that a protein reorientation process took place for high adsorber loadings. This slowed down the binding process.
In summary, different pH-dependent mechanisms like structural changes and protein reorientation upon binding help increase the DBC under varied buffer conditions. As no irreversible structural changes of the protein were investigated without significant product loss during elution for selected setups such an optimization strategy should be exploited for HIC process development.

Acknowledgments

The authors would like to thank Nina Brestrich for the kind introduction into multivariate data analysis and principal component analysis. In addition, the authors would like to acknowledge the financial support by the German Federal Ministry of Education and Research (BMBF) - funding codes 0316071B & 0315342B - and the general support by the industrial partners DelphiGenetics (Belgium) and BAC (The Netherlands). The authors bear the complete responsibility for the content of this publication. The authors declare no conflict of interest.

References

[1] F. Kröner, D. Elsässer, J. Hubbuch, A high-throughput 2D-analytical technique to obtain single protein parameters from complex cell lysates for in silico process development of ion exchange chromatography, J Chrom A 1318 (2013) 84–91.

[2] F. Kröner, A. T. Hanke, B. K. Nfor, M. W. H. Pinkse, P. D. E. M. Verhaert, M. Ottens, J. Hubbuch, Analytical characterization of complex, biotechnological feedstocks by pH gradient ion exchange chromatography for purification process development, J Chrom A 1311 (2013) 55–64.

[3] T. Ahamed, B. K. Nfor, P. D. E. M. Verhaert, G. W. K. V. Dedem, L. A. M. V. D. Wielen, M. H. M. Eppink, E. J. A. X. V. D. Sandt, M. Ottens, pH-gradient ion-

exchange chromatography: An analytical tool for design and optimization of protein separations, J Chrom A 1164 (2007) 181–188.

[4] T. Ahamed, S. Chilamkurthi, B. K. Nfor, P. D. E. M. Verhaert, G. W. K. V. Dedem, L. A. M. V. D. Wielen, M. H. M. Eppink, E. J. A. X. V. D. Sandt, M. Ottens, Selection of pH-related parameters in ion-exchange chromatography using pH-gradient operations, J Chrom A 1194 (2008) 22–29.

[5] J. A. Queiroz, C. T. Tomaz, J. M. S. Cabral, Hydrophobic interaction chromatography of proteins, J Biotech 87 (2001) 143–159.

[6] X. Geng, L. Guo, J. Chang, Study of the retention mechanism of proteins in hydrophobic interaction chromatography, J Chrom 507 (1990) 1–23.

[7] H. P. Jennissen, Hydrophobic interaction chromatography, Int J Bio Chromatogr 5 (2000) 131–138.

[8] H.-M. Huang, F.-Y. Lin, W.-Y. Chen, R.-C. Ruaany, Isothermal Titration Microcalorimetric Studies of the Effect of Temperature on Hydrophobic Interaction between Proteins and Hydrophobic Adsorbents, J Colloid Interf Sci 229 (2000) 600–606.

[9] F.-Y. Lin, W.-Y. Chen, R.-C. Ruaany, H.-M. Huang, Microcalorimetric studies of interactions between proteins and hydrophobic ligands in hydrophobic interaction chromatography: effects of ligand chain length, density and the amount of bound protein, J Chrom A 872 (2000) 37–47.

[10] A. Jungbauer, M. Christine, H. Rainer, Hydrophobic interaction chromatography of proteins III. Unfolding of proteins upon adsorption, J Chrom A 1079 (2005) 221–228.

[11] R. W. Deitcher, J. P. O'Connell, E. J. Fernandez, Changes in solvent exposure reveal the kinetics and equilibria of adsorbed protein unfolding in hydrophobic interaction chromatography, J Chrom A 1217 (2010) 5571–5583.

[12] R. Rosenfeld, K. Benedek, Conformational changes of brain-derived neurotrophic factor during reversed-phase high-performance liquid chromatography, J Chrom 632 (1993) 29–36.

[13] B. L. Karger, B. Rigoberto, The effect of on-column structural changes of proteins on their HPLC behavior, Talanta 36 (1989) 243–248.

[14] J. L. Fogle, J. P. O'Connell, E. J. Fernandez, Loading, stationary phase, and salt effects during hydrophobic interaction chromatography: alpha-Lactalbumin is stabilized at high loadings, J Chrom A 1121 (2006) 209–218.

[15] T. T. Jones, E. J. Fernandez, Hydrophobic Interaction Chromatography Selectivity Changes Among Three Stable Proteins: Conformation Does Not Play a Major Role, Biotechnol Bioeng 87 (2003) 388–399.

[16] B. C. S. To, A. M. Lenhoff, Hydrophobic interaction chromatography of proteins I. The effects of protein and adsorbent properties on retention and recovery, J Chrom A 1141 (2007) 191–205.

[17] S. Hjerten, K. Yao, K.-O. Eriksson, B. Johansson, Gradient and isocratic high-performance hydrophobic interaction chromatography of proteins on agarose columns, J Chrom 359 (1986) 99–109.

[18] J. Chen, J. Tetrault, A. Ley, Comparison of standard and new generation hydrophobic interaction chromatography resins in the monoclonal antibody purification process, J Chrom A 1177 (2008) 272–281.

[19] E. M. Lienqueo, A. Mahn, C. J. Salgado, J. A. Asenjo, Current insights on protein behaviour in hydrophobic interaction chromatography, J Chrom B 849 (2007) 53–68.

[20] M. M. Diogo, J. A. Queiroz, M. G. A., G. N. M. Martins, S. A. M. Ferreira, P. D. M. F., Purification of a Cystic Fibrosis Plasmid Vector for Gene Therapy Using Hydrophobic Interaction Chromatography, Biotechnol Bioeng 68 (1999) 576–583.

[21] M. Fountoulakis, M.-F. Takacs, B. Takacs, Enrichment of low-copy-number gene products by hydrophobic interaction chromatography, J Chrom A 833 (1999) 157–168.

[22] M. M. Diogo, J. A. Queiroz, D. M. F. Prazeres, Studies on the retention of plasmid DNA and Escherichia coli nucleic acids by hydrophobic interaction chromatography, Bioseparation 10 (2001) 211–220.

[23] J. F. Kramarczyk, B. D. Kelley, C. J. L., High-Throughput Screening of Chromatographic Separations: II. Hydrophobic Interaction, Biotechnol Bioeng 100 (2008) 707–720.

[24] P. Baumann, N. Bluthardt, S. Renner, A. Osberhaus, J. Hubbuch, Integrated Development of Up- and Downstream Processes Supported by the Cherry-Tag for Realtime Tracking of Stability and Solubility of Proteins, J Biotech 200 (2015) 27–37.

[25] A. Werner, E. Hackemann, H. Hasse, Temperature dependence of adsorption of PEGylated lysozyme and pure polyethylene glycol on a hydrophobic resin: Comparison of isothermal titration calorimetry and van't Hoff data, J Chrom A 1356 (2014) 188–196.

[26] E. L. McGown, H. D. G., Multichannel pipettor performance verified by measuring pathlength of reagent dispensed into a microplate, Anal Biochem 258.1 (1998) 155–157.

[27] Delphi Genetics SA, Cherry Codon Kit., 2009.

[28] Delphi Genetics SA, Cherry Express Kit., 2009.

[29] R. Hahn, K. Deinhofer, C. Machold, A. Jungbauer, Hydrophobic interaction chromatography of proteins: II. Binding capacity, recovery and mass transfer properties, J Chrom B 790 (2003) 99–114.

Prediction of Salt Effects on Protein Phase Behavior by HIC Retention and Thermal Stability

Kai Baumgartner[1,*], Steffen Großhans[1,*], Juliane Schütz[1,*] and Jürgen Hubbuch[1,**]

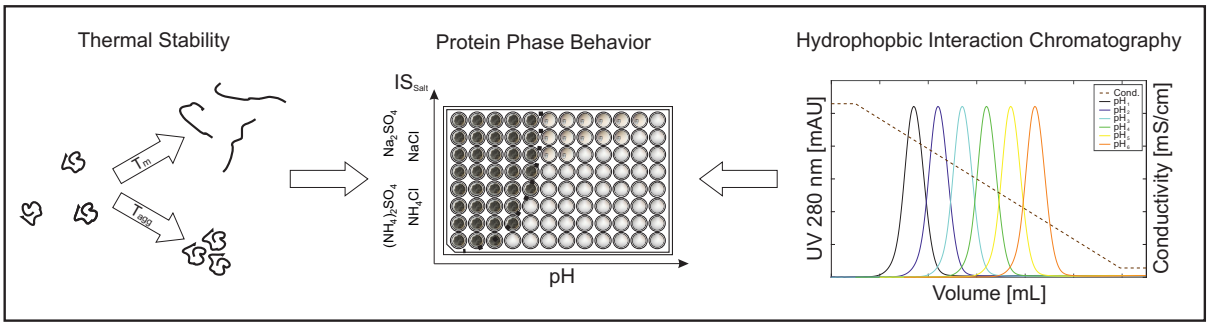

[1] : *Institute of Engineering in Life Sciences, Section IV: Biomolecular Separation Engineering, Karlsruhe Institute of Technology, Engler-Bunte-Ring 3, 76131 Karlsruhe, Germany*

[*] *: Contributed equally to this work*

[**] *: Corresponding author; mail: juergen.hubbuch@kit.edu*

Journal of Pharmaceutical and Biomedical Analysis

Submitted: 24. September 2015

Abstract

In the biopharmaceutical industry it is mandatory to know and ensure the correct protein phase state as a critical quality attribute in every process step. Unwanted protein precipitation or crystallization can lead to column, pipe or filter blocking. In formulation, the formation of aggregates can even be lethal when injected into the patient. The typical methodology to illustrate protein phase states is the generation of protein phase diagrams. Commonly, protein phase behavior is shown in dependence of protein and precipitant concentration. Despite using high-throughput methods for the generation of phase diagrams, the time necessary to reach equilibrium is the bottleneck. Faster methods to predict protein phase behavior are desirable.
In this study, hydrophobic interaction chromatography retention times were correlated to crystal size and form. High-throughput thermal stability measurements (melting and aggregation temperatures), using an Optim®2 system, were successfully correlated to glucose isomerase stability. By using hydrophobic interaction chromatography and thermal stability determinations, glucose isomerase conformational and colloidal stability were successfully predicted for different salts in a specific pH range.

Keywords: Protein Phase Diagram, High-Throughput Screening, Hydrophobic Interaction Chromatography, Thermal Stability

1 Introduction

In biopharmaceutical processes knowledge and control of protein phase behavior is of high importance. Controlling protein phase states - being in most processes a critical quality attribute - is on the one hand essential to avoid protein loss during upstream, downstream, and formulation of biopharmaceutical drugs, on the other hand the application of phase transitions such as precipitation or crystallization can be used as downstream unit operation. The influence of changing protein-solvent and protein-protein interactions due to a change in process parameters - defining these parameters as critical process parameters - on macroscopic protein phase behavior can be displayed in protein phase diagrams as a function of protein concentration and precipitant concentration [1, 2].
On a molecular level, the acting forces include long-range and short-range interactions. In this context, electrostatic interactions are generally defined as long-range forces whereas hydrogen bridges, van-der-Waals forces or hydrophobic interactions are examples for short-range forces [3]. Changing these interactions can influence protein phase behavior and therefore lead to phase transitions. Intermolecular electrostatic repulsive interactions between equally charged protein molecules have a stabilizing effect on protein solutions. Short-range attractive forces are superimposed by these long-range interactions. By increasing the ionic strength of a solution, these electrostatic repulsive effects are shielded and short-range attractive forces are predominant [4, 5].
During purification, biomolecules are often exposed to high-salt conditions. In high-salt conditions additional salt ion effects are induced and are not entirely understood. The preferential interaction theory, first postulated by Arakawa et al. [6, 7], is the most promising approach for explaining these effects. They distinguish between preferential binding of co-solutes to protein and preferential exclusion from protein surface. The for-

mer type is provoked by chaotropic agents which are found to enhance protein solubility (salting-in) but destabilize the native protein conformation. These agents are nonpolar and therefore weakly hydrated. The latter is induced by polar kosmotropic agents that increase protein stability or lead to salting-out effects due to their strongly hydrated character. Arakawa et al. [8] postulated that the hydration of a protein in a concentrated solution of co-solute is at a constant level independently whether this solute shows a preferential interaction or not.

Protein stability comprises conformational and colloidal stability. Conformational stability is important to assess as an indicator for protein unfolding. Exposed hydrophobic surface patches can enhance aggregate formation. Colloidal instability describes the aggregate formation due to clustering of protein molecules. Increased conformational and colloidal stability are believed to enhance overall protein stability [9]. Long-term stability tests under stressed conditions [10, 11, 12] are generally used to assess protein stability in pharmaceutical industry. In recent years, high-throughput techniques to evaluate protein stability were established to determine melting temperatures and aggregation temperatures. Differential scanning fluorescence measures protein conformational stability by using extrinsic dyes, such as SYPRO Orange, that bind to hydrophobic protein patches [13]. Differential static light scattering monitors light scattering of protein solutions due to aggregate formation [10, 14]. The combination of both parameters, melting temperature and aggregation temperature, is important to evaluate protein stability [10]. These two parameters have not been investigated in literature in dependence of the kosmotropic and chaotropic character of the salts, their ionic strengths, and pH values in respect to the protein's isoelectric point so far.

In this study, the impact of pH value and ionic strength of different salts on protein phase behavior was investigated using glucose isomerase as model protein. Sodium sulfate, ammonium sulfate, sodium chloride, and ammonium chloride were used as precipitants to investigate the influence of the two cations - sodium and ammonium - and of the anions - chloride and sodium - on the protein phase behavior. The high-throughput method to obtain protein phase diagrams was established earlier by Baumgartner et al. [15]. In the present work, this method was adapted to obtain information about protein phase behavior at varying pH values and different salt ionic strengths at a constant protein concentration. A multi-component buffer system [16] was used to ensure a constant buffer capacity over a defined pH range. By using the same buffer for the whole investigated pH range, buffer effects were excluded. The protein phase states are examined after 40 days of incubation. Hydrophobic interaction chromatography (HIC) was used to investigate changes in hydrophobicity of glucose isomerase caused by changing salt type and pH values. Applying HIC bind-elute experiments, the diversity of short-range forces is reduced to hydrophobic interactions. Furthermore, correlation of thermal stability measurements to protein phase behavior was investigated measuring the melting and aggregation temperature in the respective solutions.

The present work demonstrates the use of HIC bind-elute experiments and thermal stability measurements to predict protein conformational and colloidal stability in fast time and at low sample consumption. A schematic drawing of the used methodologies is shown in Figure 1.

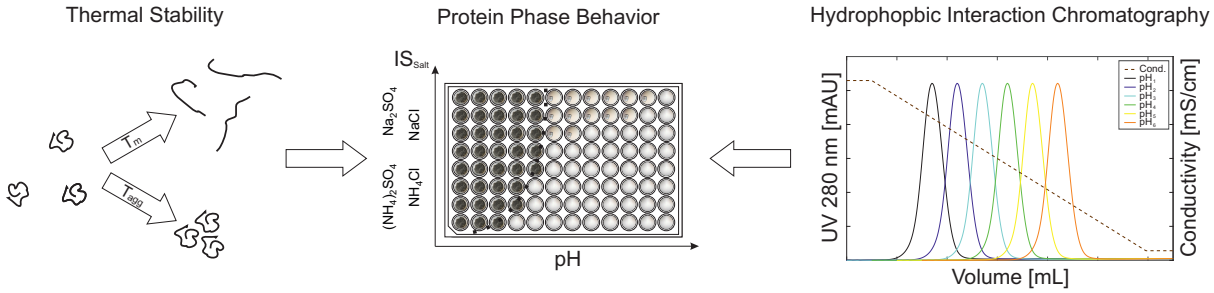

Figure 1: Schematic illustration of the experimental setup: Melting temperatures (T_m) and aggregation temperatures (T_{agg}) and retention volumes in hydrophobic interaction chromatography were used to estimate protein phase behavior.

2 Materials & Methods

2.1 Materials

The multicomponent buffer with a linear buffering range from pH 3.5 to pH 11.5 consisted of the organic acids CABS (4-(cyclohexylamino)butane-1-sulfonic acid) (Santa Cruz Biotechnology, USA), AMPSO (2-hydroxy-3-[(1-hydroxy-2-methylpropan-2-yl)amino]propane-1-sulfonic acid) (Sigma-Aldrich, USA), TAPSO (3-[[1,3-dihydroxy-2-(hydroxymethyl)propan-2-yl]amino]-2-hydroxypropane-1-sulfonic acid) (Sigma-Aldrich, USA), MES (2-morpholin-4-ylethanesulfonic acid) (AppliChem, Germany), acetic acid (Merck Millipore, Germany), and formic acid (Merck Millipore, Germany). The investigated salts sodium chloride, sodium sulfate and ammonium chloride were obtained from Merck Millipore (Germany). Ammonium sulfate was purchased from AppliChem (Germany). Sodium hydroxide for pH adjustment was obtained from Merck Millipore (Germany). pH adjustment was performed using a five-point calibrated pH meter (HI-3220, Hanna Instruments, USA) equipped with a SenTix®62 pH electrode (Xylem Inc., USA) or an InLab® Semi-Micro pH electrode (Mettler Toledo, Switzerland) dependent on the application. All buffers were filtered through 0.2 μm, and precipitant solutions through 0.45 μm cellulose acetate filters (Sartorius, Germany). Glucose isomerase (HR7-100) produced in *streptomyces rubiginosus* (PDB: 3KBS, pI: 4.78 [15]) was supplied by Hampton Research (USA). Protein solutions were filtered through 0.2 μm syringe filters with PTFE membranes (VWR, USA). Size exclusion chromatography was conducted using HiTrap Desalting Columns (GE Healthcare, Sweden) on an AEKTA™prime plus system (GE Healthcare, Sweden). A subsequent protein concentration step was performed using Vivaspin centrifugal concentrators (Sartorius, Germany) with PES membranes and molecular weight cutoff of 30 kDa.

Protein phase diagrams were prepared on MRC Under Oil 96-Well Crystallization Plates (Swissci, Switzerland) in microbatch experiments using a Freedom EVO®100 (Tecan, Switzerland) automated liquid handling station controlled by Evoware 2.5 (Tecan, Switzerland). Calibration of pipetting for liquid handling of buffers, precipitant solutions, and protein solutions were generated using a WXTS205DU analytical balance (Mettler-Toledo, Switzerland). The microbatch plates were covered with HDclear™ sealing tape (ShurTech Brands, USA) to prevent evaporation. A Rock Imager 182/54 (Formulatrix, USA) was used as an automated imaging system for determining protein phase states.

Protein concentration measurements were conducted using a NanoDrop2000c UV-Vis spectrophotometer (Thermo Fisher Scientific, USA).
For hydrophobic interaction chromatography runs a 0.5 mL Toyopearl Butyl-650M column (Atoll, Germany) on an AEKTA^{TM}purifier (GE Healthcare, Sweden) was applied. The AEKTA^{TM}purifier is equipped with an autosampler, UV detector, and a conductivity cell. The operating software package for system control and data analysis was Unicorn 5.1 (GE Healthcare, USA).
For determining protein melting temperatures and aggregation temperatures using Optim®2 (Avacta Analytical, UK), operated with the Optim Client, protein samples were analyzed in multi-cuvette arrays (MCAs) (Avacta Analytical, UK). Static light scattering and intrinsic fluorescence data analysis was performed with the integrated Optim Analysis software to evaluate protein thermal stability.
Data processing and creation of figures was performed in Matlab®R2014b (MathWorks, USA) and CorelDRAW® Graphics Suite X5 (Corel Corporation, Canada).

2.2 Methods

2.2.1 Preparation of Stock Solutions

Buffers were prepared by weighing and dissolving all buffer components in ultrapure water to 90% of the final buffer volume. This volume was splitted into three identical batches and pH value was adjusted using 4 M sodium hydroxide solution as titrant. The pH value was adjusted to both ends of the desired pH gradient and an intermediate pH value. After filling up to the final buffer volume all buffers were filtered through 0.2 μm cellulose acetate filters. Precipitant stock solutions were filtered through 0.45 μm cellulose acetate filters. Buffers and precipitant stock solutions were used at the earliest one day after preparation and after repeated pH verification. The pH value was again adjusted at the day of use with an accuracy of $\pm$ 0.05 pH units. The global buffer capacity of 20 mM was chosen over the buffering range of pH 3.5 to pH 11.5 . The buffer composition (Table 1) was calculated using a Matlab tool developed by Kröner et al. [16].
Sodium sulfate, ammonium sulfate, sodium chloride, and ammonium chloride were used as precipitants. Precipitant stock solutions contained an additional ionic strength of 2.5 M and 5.0 M, respectively. The intermediate salt concentration ensured pH stability while mixing (data not shown). Otherwise, by mixing low-salt buffer (buffer without additional salt) with 5.0 M buffer at the same pH value, the pH value would shift [15, 16]. To set up the protein stock solutions the crystal suspension of glucose isomerase was diluted

Table 1: Multi-component buffer composition with 20 mM buffer capacitiy in a pH range of pH 3.5 to pH 11.5 based on Kröner et al. [16].

Substance	Concentration [mM]	pK_a
CABS	32.96	10.70
AMPSO	30.58	9.14
TAPSO	27.93	7.64
MES	29.52	6.10
Acetic acid	25.18	4.76
Formic acid	24.06	3.75

with low-salt buffer at pH 7.0 to redissolve the protein. Centrifugal concentrators were used to reduce the volume. The protein solution then was filtered through 0.2 μm syringe filters to remove particulates and desalted using size exclusion chromatography. Protein concentration was adjusted via centrifugal concentrators to 50 $\frac{mg}{ml}$.

2.2.2 Generation of Protein Phase Diagrams

Protein phase diagrams were prepared in high-throughput mode using the method described by Baumgartner et al. [15]. The protein phase diagrams were established on 96-well crystallization plates in microbatch experiments using an automated liquid handling station. For buffer and precipitant solutions a maximum pipetting deviation of below 2% could be realized [15]. For protein solutions the maximal deviation was below 3 %. The protein phase behavior at constant glucose isomerase concentration of 10 $\frac{mg}{ml}$ was investigated with varying precipitant concentration and pH value (Figure 1 center). The pH value of the precipitant stock solutions of identical ionic strength (0.0 M, 2.5 M, and 5.0 M) was varied in twelve steps from pH 3.5 to pH 7.0 on one sample plate. To ensure a linear pH performance while mixing, an intermediate pH step at pH 5.5 was included. This has shown to smoothen pH deviations occurring due to high salt contents to an experimentally satisfying extend (data not shown). Further, for each pH step 0.0 M, 2.5 M, and 5.0 M ionic strength were mixed to create eight uniform salt dilution steps on a second sample plate.
The protein phase diagrams were then generated by adding 6 μL of 50 $\frac{mg}{ml}$ protein solution (low-salt buffer at pH 7.0) to 24 μL of the previously mentioned diluted precipitant solution on the crystallization plate. The precipitant concentration was varied per row and pH value was varied per column.
The final phase diagram was investigated at a resulting glucose isomerase concentration of 10 $\frac{mg}{ml}$ in the pH range from pH 4.2 to pH 7.0 and an ionic strength between 0.0 M and 4.0 M for sodium sulfate, ammonium sulfate, sodium chloride, and ammonium chloride. Crystallization plates were then centrifuged for 1 min at 1000 rpm to remove air bubbles and afterwards covered using optically clear and UV compatible sealing film. The sealed plates were stored in the Rock Imager for automated imaging for 40 days at 20°C. The automated imaging was performed as described earlier by Baumgartner et al. [15] to visually identify phase states such as clear solution, crystallization, precipitation, and skin formation. With polarized light at 90° crystals can be identified. Exposure to UV light was used to distinguish between protein and salt crystals due to fluorescence of aromatic amino acids.

2.2.3 Hydrophobic Interaction Chromatography Bind-Elute Experiments

Bind-elute experiments in hydrophobic interaction mode were conducted on a 0.5 mL Toyopearl Butyl-650M column. Protein retention was evaluated at different pH values (pH 5.47 - pH 7.00) and salt ionic strengths of 2.86 M, 3.43 M, and 4.00 M. The high salt conditions at protein injection were chosen to match the conditions at the protein phase diagrams. Equilibration was performed with 10 column volumes (CV) desalted water and subsequently 4 CV of low-salt buffer at a flowrate of 1 $\frac{mL}{min}$. This was followed by high-salt equilibration for 6 CV at 1 $\frac{mL}{min}$ and 4 CV at 0.2 $\frac{mL}{min}$. After equilibration, 100 μL protein solution with 10 $\frac{mg}{ml}$, in the respective high-salt buffer, were injected using an

autosampler. Elution was conducted in a linear salt gradient of 20 CV at 0.2 $\frac{mL}{min}$ from high-salt to low-salt. Subsequently, a column wash with low-salt buffer was performed for 10 CV. A constant pH value for the entire experiment was ensured. The 280 nm UV signal was used to determine the protein retention time. By using predetermined calibration curves, the conductivity signal was converted into the ionic strength value of the applied salt. These 3^{rd} degree calibration curves were obtained due to reduction of high-salt (5.0 M) to low-salt (0.0 M) condition in 5% steps.

2.2.4 Determination of Melting and Aggregation Temperature

Melting and aggregation temperatures were determined using an Optim®2 system, which combines intrinsic fluorescence and static light scattering measurements. This device allows simultaneous analysis of the same low-volume sample in high-throughput mode. Intrinsic tryptophan fluorescence is exploited to obtain information about protein folding. The fluorescence spectra shift to red wavelengths due to a change in the vicinity of the tryptophan residues from hydrophobic to hydrophilic environment while protein unfolding. This label-free technique eliminates the possible influence of extrinsic dyes on protein-protein interactions. The simultaneously measured static light scattering evaluates the aggregation formation within the applied thermal shift. Thermal stability was investigated using a temperature gradient from 20°C to 90°C with a linear slope of 0.25 $\frac{K}{min}$ in the Optim®2 system. Measurements of 9 μL protein samples, pipetted into multi-cuvette arrays (MCAs), were investigated in triplicates using static light scattering at 473 nm to determine aggregation temperatures. Further, melting temperatures were determined by simultaneous measuring of intrinsic fluorescence.

3 Results

3.1 Protein Phase Diagrams

Protein phase diagrams were established in microbatch format to obtain information about protein phase behavior in dependence of pH value and precipitant ionic strength at a constant protein concentration. This high-throughput approach provided a versatile tool to screen protein phase behavior at low protein consumption.
Glucose isomerase phase behavior was investigated in a pH range of pH 4.20 to pH 7.00 with the precipitants sodium sulfate, ammonium sulfate, sodium chloride, and ammonium chloride in microbatch format.
10 $\frac{mg}{ml}$ glucose isomerase was soluble at low-salt (buffer without additional salt) conditions with a pH value higher than pH 4.45. At pH 4.45 and below precipitation occurred. For the investigated precipitants, phase transitions like precipitation, crystallization, and skin formation were observed. The determined phase diagrams are illustrated in Figure 2.

3.1.1 Sodium Sulfate as Precipitant

For glucose isomerase with sodium sulfate as precipitant, phase transitions to precipitation and crystallization occurred over the entire investigate pH range (Figure 2 A).

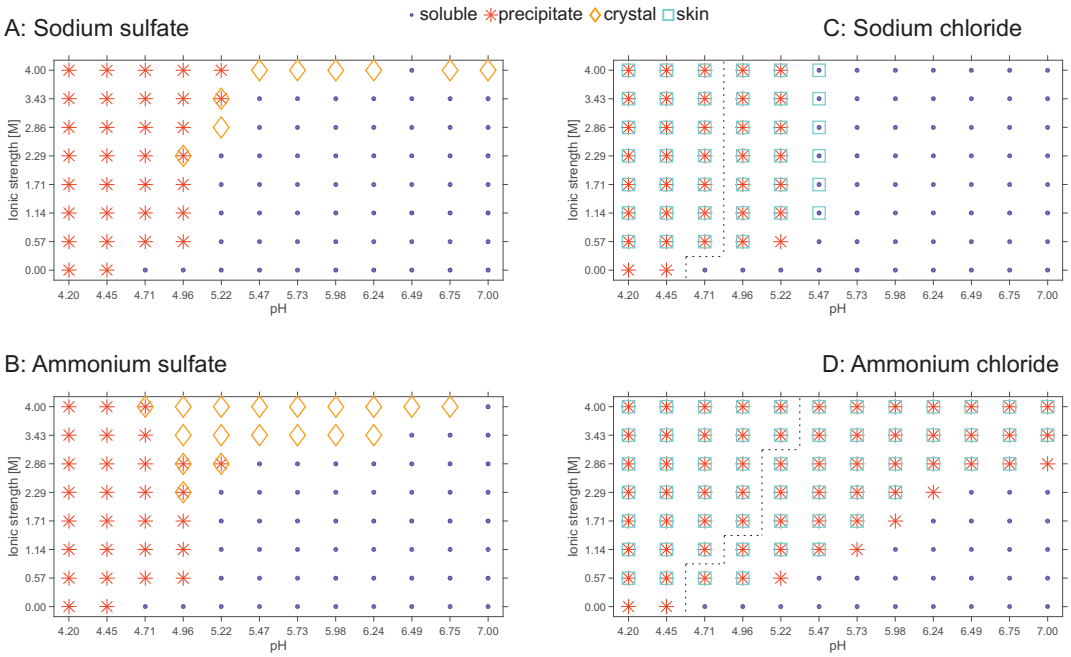

Figure 2: Phase diagrams of 10 $\frac{mg}{mL}$ glucose isomerase for an ionic strength range of 0.00 M to 4.00 M of sodium sulfate (A), ammonium sulfate (B), sodium chloride (C), and ammonium chloride (D) in the pH range of pH 4.20 to pH 7.00. Four phase states for glucose isomerase were observed: soluble, precipitate, crystal, skin. The dashed lines in the sodium and ammonium chloride phase diagrams separates immediate and evolving precipitation zones.

For and below pH 4.96 precipitation occurred independent of ionic strength and additionally for pH 5.22 at the two highest ionic strength conditions (3.43 M and 4.00 M).
Crystallization occurred at 4.00 M ionic strength for conditions above pH 5.22 with an exception at pH 6.49. Crystallization was additionally observed for three conditions (pH 4.96 with 2.29 M; pH 5.22 with 2.86 M or 3.43 M) in the transition phase to precipitation. These crystals partially co-existed with precipitation.
All ionic strength conditions below the mentioned crystallizing conditions, from and above pH 5.22, were soluble.
Regarding the crystal structure at 4.00 M ionic strength it has to be noted that at higher pH values three-dimensional tetragonal crystal formes were observed. Towards lower pH values (for example pH 5.47) the crystals were more elongated needles (Figure 3).

3.1.2 Ammonium Sulfate as Precipitant

For glucose isomerase with ammonium sulfate as precipitant phase transitions to precipitation and crystallization occurred (Figure 2 B).
Precipitation occurred at all conditions at and below pH 4.96 independent of ionic strength with two exceptions at 3.43 M and 4.00 M ionic strength for pH 4.96. For pH 5.22 and 2.86 M ionic strength an additional precipitated condition was observed.
Crystallization was observed for 4.00 M ionic strength in the pH range from pH 4.96 to pH 6.75 and for 3.43 M ionic strength up to pH 6.24.
In the transition phase from precipitation to crystallization, co-existent precipitate and crystals were observed (pH 4.71 at 4.00 M ionic strength; pH 4.96 at 2.29 M - 2.86 M ionic

strength; pH 5.22 at 2.86 M ionic strength). All observed crystals were needle shaped. At lower pH value and higher ionic strengths the extent of crystallization increased (Figure 3).

3.1.3 Sodium Chloride as Precipitant

For glucose isomerase with sodium chloride as precipitant phase transitions to precipitation and skin formation occurred at conditions with a pH value lower than pH 5.73 (Figure 2 C). At higher pH values all conditions were soluble.
Precipitation occurred for all conditions below pH 5.47. The precipitation can be divided into two zones of different kinetics. At precipitated conditions below pH 4.96, precipitation occurred immediately whereas the precipitation at higher pH values evolved over time. Additional skin formation, which evolved over time, was observed for all precipitated conditions with exception of the condition at pH 5.22 and 0.57 M ionic strength. Additionally, skin formation was observed for conditions at pH 5.47 and ionic strength higher than 0.57 M although no precipitation was detected.

3.1.4 Ammonium Chloride as Precipitant

For glucose isomerase with ammonium chloride precipitation and skin formation occurred over the entire investigated pH range (Figure 2 D). A soluble region occurred at low precipitant concentrations and high pH values. This region starts at 0.57 M ionic strength for pH values above pH 5.22 up to conditions below 2.86 M ionic strength for pH 6.49 to pH 7.00.
The precipitation region at higher precipitant concentrations and lower pH values can be divided in two zones of different kinetics. At conditions below pH 5.47 and 4.00 M ionic strength immediate precipitation occurred. At lower pH values lower ionic strength sufficed for immediate precipitate formation. Between the immediately precipitated and soluble region, slowly evolving precipitation occurred during the 40 days of incubation. At higher pH values and lower ionic strengths precipitation kinetics decelerated.
Skin formation evolved over time at and above 0.57 M ionic strength for precipitation conditions excluding the conditions for each ionic strength at the respective highest pH value for 0.57 M to 2.86 M ionic strength.

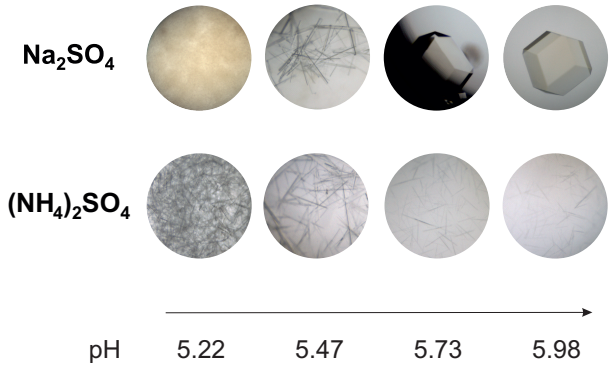

Figure 3: Determined crystal size and form of 10 $\frac{mg}{mL}$ glucose isomerase at an ionic strength of 4.00 M sodium sulfate and ammonium sulfate in the pH range from pH 5.22 to pH 5.98.

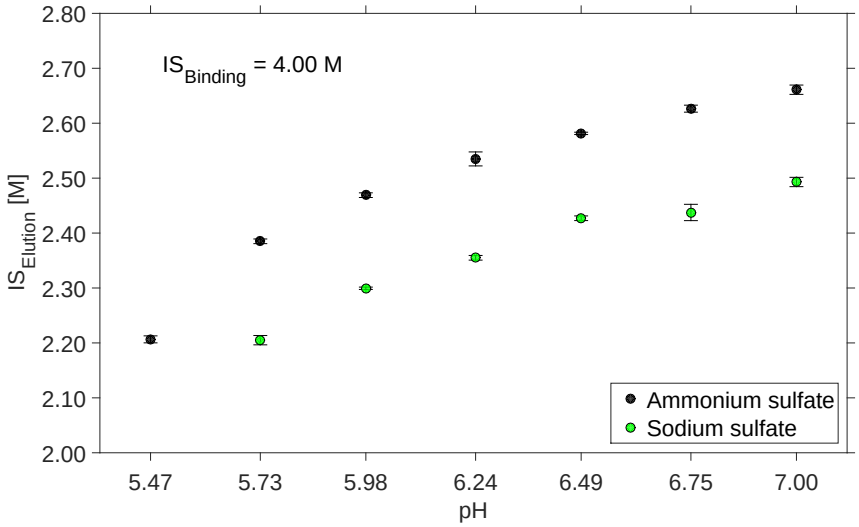

Figure 4: Hydrophobic interaction chromatography elution ionic strength ($IS_{Elution}$) of glucose isomerase at 4.00 M binding ionic strength ($IS_{Binding}$) of sodium sulfate (green) and ammonium sulfate (black) in dependence of the pH value.

3.2 Hydrophobic Interaction Chromatography Bind-Elute Experiments

Hydrophobic interaction chromatography (HIC) bind-elute experiments of glucose isomerase on a Toyopearl Butyl-650M adsorber were performed on an AEKTA^{TM}purifier system. The retention behavior was used as a degree of protein hydrophobicity. In Figure 4, the corresponding ionic strengths to the retention volumes of the bind-elute experiments are exemplarily shown at a binding ionic strength of 4.00 M for ammonium sulfate (black) and sodium sulfate (green) in dependence of the respective pH value. For both salts, the retention volumes in dependence of pH value show the same logarithmic progression, seeming to slowly converge to a threshold at higher pH values. With increasing pH value the ionic strength of the retention volumes increased, implying an earlier elution from the HIC column. For ammonium sulfate, the elution ionic strengths were between 2.21 M at pH 5.47 and 2.66 M at pH 7.00. The elution ionic strengths for experiments with sodium sulfate were generally lower with the minimum of 2.20 M at pH 5.73 and the maximum of 2.49 M at pH 7.00. Using sodium sulfate at pH 5.47, glucose isomerase precipitated immediately in this scale and thus no HIC experiment was possible. The bind-elute experiments at varied binding ionic strengths (2.86 M and 3.43 M) showed the same progressions. For sodium chloride and ammonium chloride no binding of glucose isomerase to the HIC column was feasible at the same ionic strengths.

3.3 Thermal Stability

For determining thermal stability of glucose isomerase, melting temperatures and aggregation temperatures were measured using the Optim®2 system.

3.3.1 Melting Temperature

Melting temperatures of glucose isomerase in dependence of salt type, salt ionic strength and pH value are shown in Figure 5. The melting temperatures of 10 $\frac{mg}{ml}$ glucose isomerase at low-salt conditions increased from 71.4°C at pH 5.47 to 84.9°C at pH 7.00. The melting temperatures with precipitant were generally lower regarding the same pH value.
For sodium sulfate as precipitant, melting temperatures varied between 67.0°C at pH 5.47 and 78.9°C at pH 7.00 with an ionic strength of 2.29 M (Figure 5 A). With an increasing amount of sodium sulfate the melting temperatures are in a similar range.
Using ammonium sulfate as precipitant (Figure 5 B), melting temperatures were generally lower compared to results determined with precipitant sodium sulfate. At an ammonium sulfate ionic strength of 2.29 M the temperatures varied between 63.4°C at pH 5.47 and 74.6°C at pH 7.00. For 2.86 M to 4.00 M ionic strength of ammonium sulfate, the temperatures stayed constant between ≈ 64.0°C at pH 5.47 and ≈ 70.0°C at pH 7.00.
For sodium chloride as precipitant (Figure 5 C), melting temperatures decrease with increasing ionic strength. At pH 7.00 the melting temperature decreased from 73.7°C at an ionic strength of 2.29 M to 65.5°C at an ionic strength of 4.00 M. The same trend was observed at the other investigated pH values.
Using ammonium chloride as precipitant (Figure 5 D), the determined melting tempera-

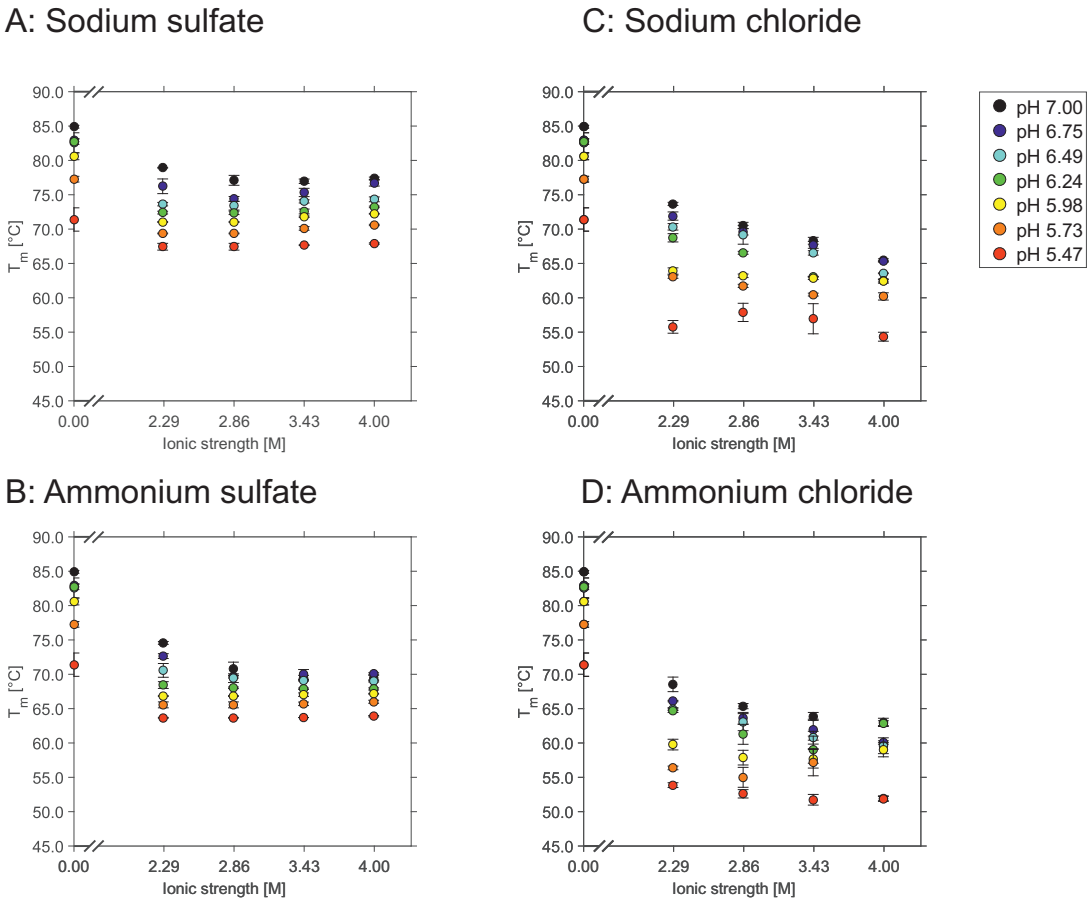

Figure 5: Melting temperatures of 10 $\frac{mg}{mL}$ glucose isomerase in dependence of pH value and ionic strength of sodium sulfate (A), ammonium sulfate (B), sodium chloride (C), and ammonium chloride (D).

tures were lowest in comparison to the other applied precipitants with the overall minimum of 51.7°C at pH 5.47 and 3.43 M ionic strength. As already noticed for sodium chloride, the melting temperatures of glucose isomerase decreased with an increasing ionic strength of ammonium chloride. At pH 7.00 the melting temperature decreased from 68.5°C at an ionic strength of 2.29 M to 63.0°C at 4.00 M. The same trend was observed at the other investigated pH values.
When comparing the melting temperatures at a constant ionic strength and different pH values, the temperatures generally decreased with decreasing pH value. For sodium sulfate and ammonium sulfate the differences in melting temperatures at constant ionic strengths and varying pH values were much lower ($\approx \Delta\, 10$ K) compared to sodium chloride and ammonium chloride ($\approx \Delta\, 20$ K).

3.3.2 Aggregation Temperature

In Figure 6 the aggregation temperatures of 10 $\frac{mg}{ml}$ glucose isomerase are shown in dependence of ionic strength of the applied precipitants at varying pH values. At low-salt conditions the aggregation temperatures were between 60.0°C at pH 7.00 and 39.2°C at pH 5.47. Adding salt to the protein solution generally decreased the determined aggre-

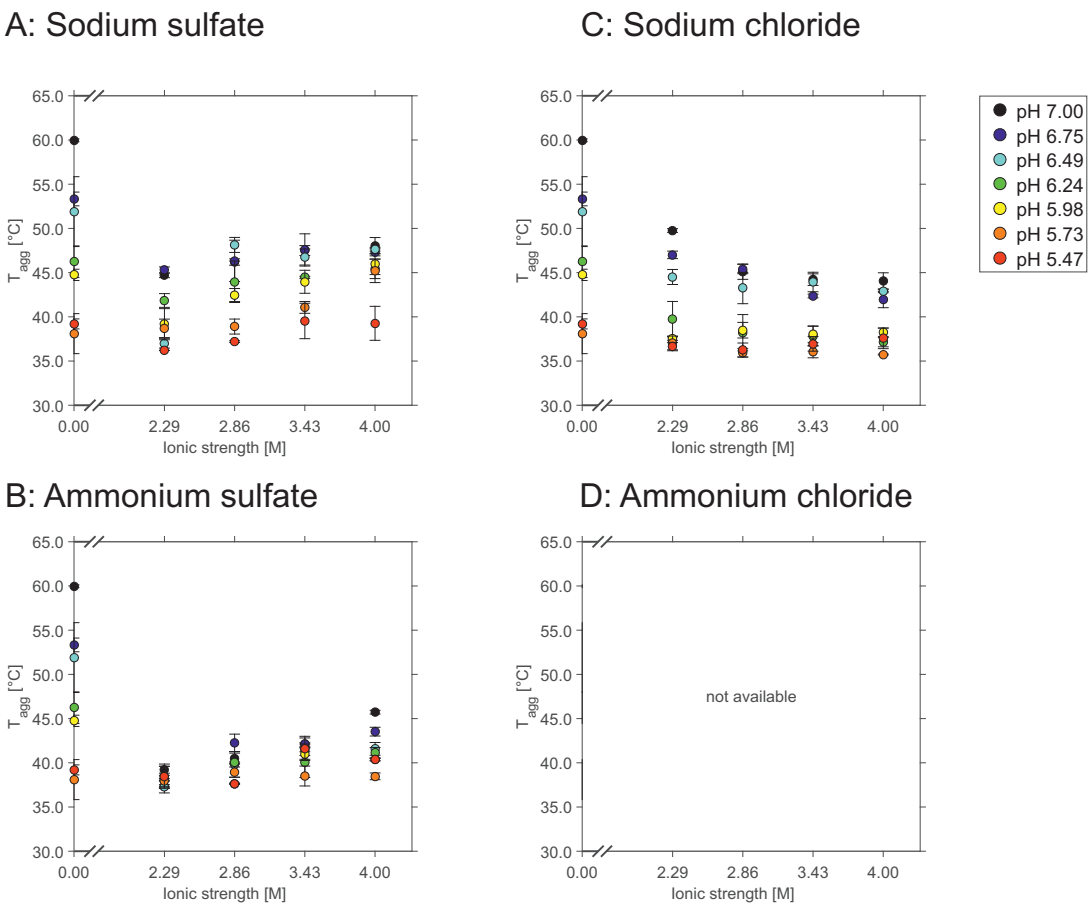

Figure 6: Aggregation temperatures of 10 $\frac{mg}{mL}$ glucose isomerase in dependence of pH value and ionic strength of sodium sulfate (A), ammonium sulfate (B), sodium chloride (C), and ammonium chloride (D).

gation temperatures.
At an ionic strength of 2.29 M sodium sulfate aggregation temperatures were between 45.3°C at the highest pH values and 36.2°C at pH 5.47 (Figure 6 A). With an increasing ionic strength aggregation temperatures increased approximately +3°C.
Using ammonium sulfate as precipitant (Figure 6 B), aggregation temperatures were lower compared to sodium sulfate as precipitant. At an ionic strength of 2.29 M ammonium sulfate the determined aggregation temperatures were around 38.0°C at all investigated pH values. With increasing ionic strength aggregation temperatures increased up to 45.8°C at pH 7.00 at an ionic strength of 4.00 M.
Aggregation temperatures of glucose isomerase with sodium chloride as precipitant (Figure 6 C) were in a similar region as determined for the precipitants sodium and ammonium sulfate. However, the progression of aggregation temperatures is different. Starting at aggregation temperatures of 50.0°C at an ionic strength of 2.29 M at pH 7.00 the aggregation temperatures decreased to 44.1°C at an ionic strength of 4.00 M sodium chloride. The aggregation temperatures at lower pH values decreased towards 35.7°C at an ionic strength of 4.00 M.
For ammonium chloride as precipitant large errorbars were observed (data not shown).
When comparing aggregation temperatures at different pH values and constant ionic strengths, aggregation temperatures decreased with decreasing pH value. The observed difference was largest at low-salt conditions. By adding precipitant this distinction reduced.

4 Discussion

4.1 Protein Phase Diagrams

In this paper a method to create protein phase diagrams with variation in pH value and ionic strength at a constant protein concentration is presented. These microbatch experiments were realized in high-throughput as described earlier by Baumgartner et al. [15]. The utilization of a multi-component buffer system, developed by Kröner et al. [16], provides the possibility to manipulate pH linearly due to a constant buffer capacity over the whole pH range. The desired pH value was maintained by mixing different starting pH values in microbatch format.
One protein phase diagram consists of 96 different conditions with eight equidistant steps of ionic strength and twelve equidistant pH steps at a constant protein concentration.

4.1.1 Phase Behavior of Glucose Isomerase

Glucose isomerase phase behavior at a concentration of 10 $\frac{mg}{mL}$ was investigated in dependence of pH value and ionic strength. The pH value was varied between pH 4.20 and pH 7.00. Precipitant ionic strengths of sodium sulfate, ammonium sulfate, sodium chloride, and ammonium chloride were altered in an range of 0.00 M to 4.00 M.
An influence of ionic strength on protein phase transitions was found for all investigated precipitants. For sodium sulfate and ammonium sulfate, precipitation and crystallization zones were observed. Precipitation was observed at lower pH values close to the isoelectric point (pI) and crystallization at higher pH values and high ionic strengths. The

crystallization zones were found for sodium sulfate and ammonium sulfate at pH values from and above pH 4.96 and pH 4.71, respectively. In the transition zone from precipitation to crystallization both phase states co-existed. Although the crystallization zone for ammonium sulfate was larger compared to sodium sulfate, the crystal yield was higher for sodium sulfate. Here, at 4.00 M ionic strength three-dimensionally shaped crystals developed whereas for ammonium sulfate needle-shaped crystals were found. The formation of three-dimensional crystals requires a larger number of specific binding sites on the protein surface compared to two-dimensional needle-shaped crystals [17]. Due to shielding of long-range electrostatic forces at high-salt conditions it is assumed that short-range forces on protein surface provoke protein-protein attractive interactions, possibly resulting in crystallization. These short-range interactions like van-der-Waals or hydrophobic interactions contribute to protein crystal stability and formation [17, 18, 19]. These short-range interactions have to be higher for sodium sulfate compared to ammonium sulfate. Additionally, the nucleation onset of glucose isomerase was observed much earlier for conditions with sodium sulfate compared to ammonium sulfate.
Further, the pH value had an additional influence on crystal form and size. For sodium sulfate, needle-shaped crystals were found close to the precipitation zone at pH 5.47, whereas three-dimensional crystals were observed at higher pH values. Altering the pH value, salt bridges and hydrogen bonds as well as hydration of protein are influenced [20]. At lower pH values, close to the pI, glucose isomerase has a lower number of surface charges. This was verified using PDB structure 3kbs using the molecular dynamics simulation tool Yasara (YASARA Biosciences) (data not shown). Resulting, glucose isomerase is less hydrated and attractive hydrophobic forces are higher. Due to this fact faster crystal nucleation and growth leads to many small needle-shaped crystals. In the precipitation zone attractive forces are too high for protein molecules to form structured crystal lattices [21]. For ammonium sulfate as precipitant the extent of crystallization is higher, whereas crystal size is smaller at lower pH values. This can be attributed to higher attractive forces close to the pI. In summary, sodium sulfate had a stronger tendency to induce short-range protein-protein interactions for glucose isomerase, enhancing crystallization, at the investigated pH range from pH 4.20 to pH 7.00, when compared to ammonium sulfate. This is consistent with findings for lysozyme from Lin et al. [22].
The phase behavior of glucose isomerase with sodium chloride or ammonium chloride as precipitant, phase transition to precipitation and skin formation occurred. For sodium chloride, no significant influence of ionic strength on precipitation and skin formation was noted. For ammonium chloride, higher ionic strengths led to a broader precipitated area at higher pH values. It can be concluded that ammonium chloride had a more destabilizing effect on glucose isomerase phase behavior compared to sodium chloride.
The impact of pH on phase behavior was clearly distinguishable for sodium chloride and ammonium chloride as precipitants. At low pH values close to the isoelectric point of glucose isomerase precipitation and skin formation was observed for both precipitants. Skin formation is believed to be attributed to protein denaturation [2, 23] and therefore lower conformational stability. For glucose isomerase, higher pH values, implying more charges on the protein surface, resulted in more stable solutions. Ammonium chloride destabilized glucose isomerase more strongly compared to sodium chloride.
The impact on glucose isomerase phase behavior was found to be mainly dependent on the anion [24, 25]. Larger precipitation zones were found for salts containing chloride

than for sulfate. Additionally, skin formation and thereby protein denaturation can be attributed to chloride. Sulfate led to crystallization for both investigated salts. The impact of the cations sodium and ammonium was not as distinctively as of the anions. The ammonium cation was found to obtain a more chaotropic character compared to sodium.

4.2 Hydrophobic Interaction Chromatography

In this study, retention volumes in hydrophobic interaction chromatography (HIC) were examined to describe protein hydrophobic properties [6] as a component of the short-range interactions mentioned in 4.1.1. Due to high ionic strengths used at binding to the adsorber, it can be assumed that electrostatic interactions are shielded and predominantly hydrophobic interactions are decisive. Generally, in HIC lower ionic strengths at elution imply stronger binding to the HIC adsorber. Therefore, lower elution ionic strengths, as determined for sodium sulfate compared to ammonium sulfate, imply stronger hydrophobic interactions of glucose isomerase with the adsorber using sodium sulfate. This observation is compliant with findings made by Lin et al. [22], who found sodium sulfate to enhance hydrophobic interactions of lysozyme stronger compared to ammonium sulfate. For sodium chloride and ammonium chloride, no HIC retention experiments were possible under the given conditions. The applied ionic strengths at binding were too low to achieve binding of glucose isomerase to the adsorber. Hence, it was observed that sulfate ions increased hydrophobicity of glucose isomerase more strongly in comparison to chloride ions. This is in accordance with literature [24], where it has been recorded that anions have the main influence on binding in HIC.
The elution ionic strengths of glucose isomerase were lower at lower pH values. This observation can be explained by the proximity to the isoelectric point of glucose isomerase (pI: 4.78). At the isoelectric point protein surface net charge is zero. But also the total amount of surface charges is smaller compared to conditions at higher pH values for glucose isomerase (4.1.1). This weakens the hydration shell and thus, hydrophobic interactions are strengthened. Therefore, elution ionic strengths decrease rapidly with the proximity to the pI. At pH values towards pH 7.00 retention volumes only change slightly. This behavior can be explained by the titration curve. Above the pI, total amount of surface charges decreases rapidly close to the pI, whereas further away the total amount of surface charges approaches a threshold.
Concluding, the pH value has a big influence on protein hydrophobicity. The degree of hydrophobic interactions increase with decreasing distance to the isoelectric point. This observation also correlates with the observations made by Baumann et al. [26]. Baumann et al. found that binding at pH values close to the proteins' pI increased the binding behavior in HIC.
The progression of elution ionic strengths of sodium sulfate and ammonium sulfate are similar in dependence of pH value. The small vertical shift of the two curves can be attributed to the different cations sodium and ammonium.
Retention times in HIC were used to describe protein hydrophobic properties. These relative hydrophobicities directly correlate with crystal size and form, determined by the phase diagrams. The yield of protein crystallization was higher for sodium sulfate compared to ammonium sulfate. Additionally, three-dimensional crystals were found for sodium sulfate implying more specific binding sites. When comparing these two salts at

the same pH value, enhanced hydrophobic interactions led to three-dimensionally shaped crystals whereas reduced hydrophobic interactions resulted in two-dimensional crystals. Regarding the pH value, crystal size decreased with decreasing distance to the pI. Here, hydrophobicity is significantly higher, leading to faster crystallization kinetics. The fast kinetics hinders the formation of complex large crystals [17]. The HIC results indicate that hydrophobic interactions can directly be correlated to crystal complexity.

4.3 Melting Temperature

In this study, melting temperatures were examined to correlate protein thermal stability to protein phase behavior and bind-elute experiments on hydrophobic interaction chromatography. Glucose isomerase was investigated at low-salt (buffer without additional salt) and high-salt (2.29 - 4.00 M ionic strength) conditions of sodium sulfate, ammonium sulfate, sodium chloride and ammonium chloride. The higher melting temperatures at low-salt conditions for all tested pH values compared to high-salt conditions indicate a higher stability of glucose isomerase. Salt ions influence the protein hydration, which was earlier described as preferential interaction theory [7, 27]. Preferential interaction of ions with the protein weakens protein hydration whereas preferential exclusion sustains hydration and is believed to stabilize the protein in solution [8]. The observed decrease in melting temperature for glucose isomerase indicates a weakening of the protein hydration in the investigated ionic strength range for the analyzed salt types. This observation is in accordance to the preferential interaction theory that all investigated salts should exhibit preferential interaction with the protein, thus destabilizing the native protein conformation and decreasing protein thermal stability [28, 29, 30, 31]. The above-mentioned observations are in concert with the observed phase behavior of glucose isomerase. The solubility of glucose isomerase decreased with increasing salt ionic strength. This behavior was mainly noticeable at pH values close to the isoelectric point where the precipitation zone enlarged with addition of salt. Different salt type specific influences on melting temperatures were observed. When comparing the melting temperatures an order of ammonium chloride < sodium chloride < ammonium sulfate < sodium sulfate was found, where ammonium chloride shows the most destabilizing properties and sodium sulfate the most stabilizing. Dupeux et al. [32] correlated thermal stability to higher crystallization success rates. This is in agreement with the generated data presented in this manuscript. Higher glucose isomerase melting temperatures were observed for experiments using sodium sulfate and ammonium sulfate whilst leading to crystallization as determined with the phase diagrams. The order of melting temperatures corresponds to protein solubility and stability behavior observed with the phase diagrams.

When comparing the cations sodium and ammonium, higher melting temperatures were found for sodium. Thus, sodium stabilizes glucose isomerase more strongly compared to ammonium. This can be correlated to glucose isomerase solubility and stability phase behavior. For salts with sulfate as anion, sodium leads to bigger crystals compared to ammonium. Hence, the solubility of glucose isomerase is higher in the crystallization zone for ammonium sulfate compared to sodium sulfate. This is in concert with ammonium being a weakly hydrated chaotropic agent [25] known to increase solubility.

For salts with chloride as anion, sodium shows a smaller precipitation area with skin formation compared to ammonium. Ammonium interacts more strongly with the protein

inducing destabilization of the native conformation which can be observed by reduced thermal stability and macroscopically as skin formation [33].
The determined results imply higher stabilizing effects for sodium when compared to ammonium which is in agreement with findings from Collins [25]. Sodium is a strongly hydrated ion with kosmotropic properties, whereas ammonium is a weakly hydrated ion with chaotropic properties.
When comparing the anions sulfate and chloride, higher melting temperatures were observed for sulfate compared to chloride. Thus, sulfate stabilizes glucose isomerase more strongly compared to chloride. This is in concert with findings from Arakawa and Timasheff [34] that for sulfate preferential exclusion is higher compared to chloride.
Melting temperatures were successfully correlated to glucose isomerase stability. Sulfate is more stabilizing, leading to crystallization in combination with both investigated cations sodium and ammonium. In contrast, chloride is more destabilizing, inducing larger precipitation zones and skin formation. Regarding the preferential interaction theory, chloride preferentially interacts with the protein and leads to protein destabilization and consequently to lower thermal stability.
Regarding the pH value, with decreasing distance to the proteins' isoelectric point the melting temperatures decreased for all investigated salt ionic strengths. The number of protein surface charges of glucose isomerase decreases with decreasing distance to its pI (4.1.1). Therefore, stabilizing electrostatic interactions between proteins and water molecules are reduced. Hence, the hydration shell around the protein is weakend and the native protein conformation is perturbed leading to lower thermal stability as was found for all ionic strengths. This is also in agreement with the determined macroscopic phase behavior of glucose isomerase. It can be concluded that the anions and cations have a distinct impact on protein solubility and stability as investigated using melting temperature. Those findings could successfully be correlated to protein phase behavior. Anions were found to have a stronger effect on protein solubility and stability compared to cations which is in agreement with literature [24, 25, 34]. Concluding from that, this is a comparatively fast method to evaluate protein solubility and stability. Distinctions between native (crystal, soluble, precipitate) and non-native (skin formation) phase behavior can be made. Thus, melting temperatures can help to assess estimations for protein phase behavior.

4.4 Aggregation Temperature

The thermal aggregation temperatures were examined to study glucose isomerase stability. Low-salt and high-salt (2.29 M - 4.00 M ionic strength) conditions of sodium sulfate, ammonium sulfate, sodium chloride, and ammonium chloride were investigated for glucose isomerase using the Optim®2. The resolution limit of this method was found to be around 36°C resulting in problems to discriminate conditions close to the isoelectric point of glucose isomerase.
The higher aggregation temperatures at low-salt conditions for all tested pH values compared to high-salt conditions indicate a higher colloidal stability of glucose isomerase. This is in concert with the results for the melting temperatures. Glucose isomerase thermal stability is reduced by the addition of the investigated salts in the given ionic strength and pH range.

The comparison of the cations sodium and ammonium, only possible for sulfate as anion, shows higher aggregation temperatures for sodium compared to ammonium. Thus, sodium cations stabilize glucose isomerase more strongly compared to ammonium cations. This is in accordance to findings for melting temperature and glucose isomerase phase behavior. Sodium, having a kosmotropic character, stabilizes glucose isomerase more and leads to bigger crystals, whereas ammonium is chaotropic and reduces crystal size.
The comparison of the anions sulfate and chloride, only possible for sodium as cation, shows higher aggregation temperatures for sulfate. Thus, sulfate stabilized glucose isomerase more strongly compared to chloride. This in concert with findings for melting temperatures and glucose isomerase phase behavior.
The results for ammonium chloride showed large standard deviations for repeated measurements indicating the existence of light scattering aggregates at the starting conditions (data not shown). The results for ammonium chloride are in accordance with the observation concerning glucose isomerase phase behavior where ammonium chloride led to evolving precipitation and skin formation in the investigated ionic strength and pH range. Here, thermal aggregation temperatures support the statements made by the evaluation of the melting temperatures.

5 Conclusions and Outlook

The present work shows that protein hydrophobicity and thermal stability measurements can be used as tools for estimating protein stability. Protein phase behavior was determined using a high-throughput methodology for generation of protein phase diagrams. Protein phase behavior was investigated at a constant protein concentration in dependence of precipitant ionic strength and pH value. Using for different salt types, the influence of two anions and two cations on glucose isomerase phase behavior was investigated. The results confirmed findings from literature [24, 25, 34], that anions influence protein phase behavior more strongly compared to cations. Using hydrophobic interaction chromatography (HIC) and thermal stability measurements, initially and completely soluble conditions were investigated.
Using retention behavior in HIC a deeper understanding of hydrophobic forces in protein-protein interaction was generated. The differences in crystal form and size, using sodium sulfate and ammonium sulfate, can be described by protein surface hydrophobicity and thus estimated by HIC.
Melting temperatures and aggregation temperatures were measured to characterize glucose isomerase thermal stability. Sulfate was found to have a less destabilizing effect on glucose isomerase compared to chloride regarding conformational and colloidal stability. Thermal stability measurements can be used to distinguish between native (crystal, soluble, precipitate) and non-native (skin formation) phase behavior.
Using HIC experiments and thermal stability measurements, glucose isomerase stability can be estimated in relation to variations of parameter settings. The observed correlations should be verified for other biomolecules and variations of parameters.

6 Acknowledgments

The authors are grateful for the financial support by the German Federal Ministry of Education and Research (BMBF) - funding code 0315342B - and by Novo Nordisk. The authors bear the complete responsibility for the content of the publication. The authors have declared no conflict of interest.

References

[1] W. Wang, S. Nema, D. Teagarden, Protein aggregationpathways and influencing factors, International journal of pharmaceutics 390 (2) (2010) 89–99.

[2] T. Ahamed, B. N. A. Esteban, M. Ottens, G. W. K. van Dedem, L. A. M. van der Wielen, M. A. T. Bisschops, A. Lee, C. Pham, J. Thömmes, Phase behavior of an intact monoclonal antibody, Biophys. J. 93 (2) (2007) 610–619.

[3] B. L. Neal, D. Asthagiri, O. D. Velev, A. M. Lenhoff, E. W. Kaler, Why is the osmotic second virial coefficient related to protein crystallization, Journal of Crystal Growth 196 (2-4) (1999) 377–387.

[4] R. Piazza, Interactions and phase transitions in protein solutions, Current Opinion in Colloid & Interface Science 5 (2000) 38–43.

[5] S. Beretta, G. Chirico, G. Baldin, Short-Range Interactions of Globular Proteins at High Ionic Strengths, Macromolecules 33 (2000) 8663–8670.

[6] T. Arakawa, S. N. Timasheff, Protein stabilization and destabilization by guanidinium salts, Biochemistry 23 (1984) 5924–5929.

[7] T. Arakawa, R. Bhat, S. N. Timasheff, Preferential interactions determine protein solubility in 3-component solutions the MgCl2 system, Biochemistry 29 (1990) 1914–1923.

[8] T. Arakawa, Hydration as a Major Factor in Preferential Solvent–Protein Interactions, Crystal Growth & Design 2 (6) (2002) 549–551.

[9] G. Senisterra, I. Chau, M. Vedadi, Thermal denaturation assays in chemical biology, Assay and drug development technologies 10 (2) (2012) 128–136.

[10] D. S. Goldberg, S. M. Bishop, A. U. Shah, H. A. Sathish, Formulation development of therapeutic monoclonal antibodies using high-throughput fluorescence and static light scattering techniques: Role of conformational and colloidal stability, Journal of pharmaceutical sciences 100 (4) (2011) 1306–1315.

[11] H.-C. Mahler, R. Müller, W. Friess, A. Delille, S. Matheus, Induction and analysis of aggregates in a liquid IgG1-antibody formulation, European Journal of Pharmaceutics and Biopharmaceutics 5G9 (2005) 407–417.

[12] H.-C. Mahler, W. Friess, U. Grauschopf, S. Kiese, Protein aggregation: Pathways, induction factors and analysis, Journal of Pharmaceutical Science 98 (2009) 2909–2934.

[13] U. B. Ericsson, B. M. Hallberg, G. T. Detitta, N. Dekke, P. Nordlund, Thermofluor-based high-throughput stability optimization of proteins for structural studies, Anal Biochem. 357 (2006) 289–298.

[14] G. A. Senisterra, P. J. J. Finerty, High throughput methods of assessing protein stability and aggregation, Mol Biosyst. 5 (2009) 217–223.

[15] K. Baumgartner, L. Galm, J. Nötzold, H. Sigloch, J. Morgenstern, K. Schleining, S. Suhm, S. A. Oelmeier, J. Hubbuch, Determination of protein phase diagrams by microbatch experiments: Exploring the influence of precipitants and ph, International Journal of Pharmaceutics 479 (1) (2015) 28–40.

[16] F. Kröner, J. Hubbuch, Systematic generation of buffer systems for ph gradient ion exchange chromatography and their application, Journal of Chromatography A 1285 (2013) 78–87.

[17] S. D. Durbin, G. Feher, Protein Crystallization, Annu. Rev. Phys. Chem. 47 (1996) 171–204.

[18] S. A. Islam, D. L. Weaver, Molecular Interactions in Protein Crystals: Solvent Accessible Surface and Stability, PROTEINS: Structure, Function, and Genetics 8 (1990) 1–5.

[19] P. W. Goodenough, A review of protein engineering for the food industry, International Journal of Food Science and Technology 30 (1995) 119–139.

[20] A. C. Dumetz, A. M. Chockla, E. W. Kaler, A. M. Lenhoff, Effects of pH on proteinprotein interactions and implications for protein phase behavior, Biochimica et Biophysica Acta (BBA) - Proteins and Proteomics 1784 (2008) 600–610.

[21] R. A. Curtis, J. Ulrich, A. Montaser, J. M. Prausnitz, H. W. Blanch, Protein-Protein Interactions in Concentrated Electrolyte Solutions, Biotechnology and Bioengineering 79 (2002) 367–380.

[22] F.-Y. Lin, W.-Y. Chen, M. T. W. Hearn, Microcalorimetric Studies on the Interaction Mechanism between Proteins and Hydrophobic Solid Surfaces in Hydrophobic Interaction Chromatography: Effects of Salts, Hydrophobicity of the Sorbent, and Structure of the Protein, Analytical Chemistry 73 (2001) 3875–3883.

[23] N. Asherie, Protein crystallization and phase diagrams, Methods 34 (3) (2004) 266–272.

[24] Y. Zhang, P. S. Cremer, Interactions between macromolecules and ions: The Hofmeister series, Current opinion in chemical biology 10 (2006) 658–663.

[25] K. D. Collins, Ions from the Hofmeister series and osmloytes: effects on proteins in solution and in the crystallization process, Methods 34 (2004) 300–311.

[26] P. Baumann, K. Baumgartner, J. Hubbuch, Influence of Binding pH and Protein Solubility on the Dynamic Binding Capacity in Hydrophobic Interaction Chromatography, Journal of Chromatography A 1396 (2015) 77–85.

[27] T. Arakawa, S. N. Timasheff, Preferential interactions of proteins with salts in concentrated solutions, Biochemistry 21 (1982) 6545–6552.

[28] M. C. Manning, D. K. Chou, B. M. Murphy, R. W. Payne, D. S. Katayama, Stability of Protein Pharmaceuticals: An Update, Pharmaceutical Research 27 (2010) 544–575.

[29] P. H. von Hippel, K.-Y. Wong, Neutral Salts: The Generality of Their Effects on the Stability of Macromolecular Conformations, Science 145 (1964) 577–580.

[30] P. H. von Hippel, K.-Y. Wong, On the Conformational Stability of Globular Proteins: THE EFFECTS OF VARIOUS ELECTROLYTES AND NONELECTROLYTES ON THE THERMAL RIBONUCLEASE TRANSITION, Journal of Biological Chemistry 240 (1965) 3909–3923.

[31] E. Y. Chi, S. Krishnan, B. S. Kendrick, B. S. Chang, J. F. Carpenter, T. W. Randolph, Roles of conformational stability and colloidal stability in the aggregation of recombinant human granulocyte colony-stimulating factor, Protein Science 12 (2003) 903–913.

[32] F. Dupeux, M. Röwer, G. Seroul, D. Blot, J. A. Marquez, A thermal stability assay can help to estimate the crystallization likelihood of biological samples, Acta Crystallographica Section D 67 (2011) 915–919.

[33] J. P. Zeelen, Interpretation of the Crystallization Drop Results, in: T. M. Bergfors (Ed.), Protein Cryst., 2nd Edition, Internat'l University Line, 2009, Ch. 10, pp. 175–194.

[34] T. Arakawa, S. N. Timasheff, Mechanism of protein salting in and salting out by divalent cation salts: Balance between hydration and salt binding, Biochemistry 23 (1984) 5912–5923.

4 Conclusion & Outlook

This doctoral thesis contributes to the critical demands of the 'Time to Market' principles in process development of biopharmaceuticals and tackles the drawback of low binding capacities of hydrophobic interaction chromatography (HIC) adsorbers. The traditional heuristic approaches were questioned and better operational conditions for HIC binding were determined. Additionally, new tools for predicting the binding behavior were developed. In this context the following fields were approached:

- Automated generation of phase diagrams in high-throughput
- Enhancing binding behavior in HIC and development of predictive tools
- Discovering the main influencing factors of HIC binding
- Developing fast tools for estimating protein phase behavior

The first part of this thesis described the development of a general methodology for generating phase diagrams in an automated way and in high-throughput on a robot-based pipetting platform. Within two hours and with a protein consumption of less than 150 mg per plate the protein phase behavior was determined at 96 different conditions (varying salt and protein concentration) at a fixed pH value. With this method, broad knowledge of the influence of the pH value and the precipitant on the phase behavior can be generated without the use of surface covering oils, falsifying the results. By storing the microbatch plates in an automated and temperature controlled device, that takes pictures of the wells at configured time points, also long-term stability studies were feasible. This general method can be used to create a broad databank describing the phase behavior of for example monoclonal antibodies and other therapeutic proteins in dependence of different pH values and additives.
The second and third section of this doctoral thesis focused on the purification using hydrophobic interaction chromatography. The major bottleneck of HIC is the low binding capacities of the adsorbers compared to for example ion-exchange chromatography. Therefore, a new strategy was developed for increasing the binding capacities by using salt mixtures of kosmotropic and chaotropic salts. A higher ratio of chaotropic salt increased the binding behavior significantly. Additionally, straightforward tools for predicting the binding behavior in HIC were established. Measuring the surface tension by using an in-house-developed stalagmometric method showed that the 'Cavity Theory', saying that higher surface tensions lead to higher binding capacities, was not valid for salt mixtures. By multiplying the critical salt concentration from the solubility screenings with its corresponding ionic strength, the binding behavior followed the same progression, making it an easy and fast tool for estimating the binding behavior in HIC. This aspect has to be investigated and generalized for other scenarios. What is the reason for this observation or is this behavior only valid for the investigated mixtures? Another straightforward tool is determining the aggregation temperature. The aggregation temperature can be used as a degree of hydrophobic forces. Lower aggregation temperatures indicated stronger hydrophobic forces and higher binding capacities. The correlation of the surface tensions and aggregation temperatures to the binding behavior in HIC should be confirmed for a broader range of proteins and salts.

The third section of this dissertation questioned the standard environmental conditions using HIC as a purification method. As mentioned above, HIC is commonly operated at neutral pH independent of the protein's nature. A robot-based high-throughput method was developed using miniaturized robotic chromatography columns (RoboColumns) for determining the main influencing factors on the binding behavior in HIC. It was shown that binding close to the protein's isoelectric point yielded in higher binding capacities. The overall strongest influencing factor was identified to be the proximity to the solubility limit. Conditions of decreased solubility yielded in increased binding capacities. Additionally, an inverse correlation of the binding kinetics to the binding behavior was observed suggesting a reorientation during binding at slow binding kinetics. Although the binding capacity was increased significantly, the protein integrity was ensured. This methodology gives the opportunity to determine the optimal binding environment in HIC in a fast and fully automated way. This screening method should be applied to a broader basis of proteins and industrially relevant biomolecules like monoclonal antibodies. Also the proposed reorientation process during binding should be investigated in more detail. The multi-variate data analysis method for investigating protein unfolding should be implemented on the robotic station and in high-throughput format.
The last part of this thesis combined the previously described experiments. Reaching equilibrium in protein-precipitant solutions is time-consuming. Therefore, fast tools for estimating protein phase behavior are desirable. The phase behavior of glucose isomerase was determined for four different salts by using the high-throughput technique, developed in the first section. This method was adapted to generate phase diagrams at varying precipitant concentrations and varying pH values at a constant protein concentration. HIC retention times in dependence of the salts sodium sulfate, ammonium sulfate, sodium chloride, and ammonium chloride were used to determine the protein's hydrophobicity. The retention times were successfully correlated to crystal size and form, determined in phase diagrams. By measuring thermal stability - melting and aggregation temperatures - stabilizing and destabilizing behavior of the salt ions were found. Concluding from this, by determining HIC retention volumes and melting and aggregation temperatures, the stability of glucose isomerase can be predicted in relation to variations of parameter settings in a fast and easy way. These observed correlations should be verified for other biomolecules and parameter variations.

5 Abbreviations

Abbreviation	Definition
AC	Affinity chromatography
AEX	Anion-exchange
BMBF	German Federal Ministry of Education and Research
BTC	Breakthrough curve
CAPSO	3-(Cyclohexylamino)-2-hydroxy-1-propanesulfonic acid
CEX	Cation-exchange
CHES	2-(Cyclohexylamino)ethanesulfonic acid
CV	Column volume
DBC	Dynamic binding capacity
DLVO	Deryagin-Landau-Verwey-Overbeek
DoE	Design of experiments
DSP	Downstream process
FDA	Food and Drug Administration
GST	Glutathione-S-Transferase
HCl	Hydrochloric acid
HIC	Hydrophobic interaction chromatography
HT	High-throughput
HTE	High-throughput experiment
HTS	High-throughput screening
IEC/IEX	Ion-exchange chromatography
IS	Ionic strength
LLPS	Liquid-liquid phase separation
MCA	Multi-cuvette array
MES	2-(N-morpholino)ethanesulfonic acid
MOPSO	3-Morpholino-2-hydroxypropanesulfonic acid
MVDA	Multi-variate data analysis
NaCl	Sodium chloride
NaOH	Sodium hydroxide
NaS	Sodium sulfate
PC	Principal component
PCA	Principal component analysis
PEG	Polyethylene glycol
PES	Polyether sulfone
pI	Isoelectric point
PTFE	Polytetrafluoroethylene
QbD	Quality by Design
SEC	Size exclusion chromatography
T_{agg}	Aggregation temperature
T_m	Melting temperature
TAPS	N-Tris(hydroxymethyl)methyl-3-aminopropanesulfonic acid
TCA	Trichloro acetic acid
UV	Ultraviolet
V_HH	Single domain antibody

References

Ahamed, T., Chilamkurthi, S., Nfor, B. K., Verhaert, P. D. E. M., Dedem, G. W. K. V., Wielen, L. A. M. V. D., Eppink, M. H. M., Sandt, E. J. A. X. V. D. and Ottens, M. (2008). *Selection of pH-related parameters in ion-exchange chromatography using pH-gradient operations.* Journal of Chromatography A, 1194:22.

Ahamed, T., Esteban, B. N. A., Ottens, M., van Dedem, G. W. K., van der Wielen, L. A. M., Bisschops, M. A. T., Lee, A., Pham, C. and Thömmes, J. (2007a). *Phase behavior of an intact monoclonal antibody.* Biophys. J., 93(2):610.

Ahamed, T., Nfor, B. K., Verhaert, P. D. E. M., Dedem, G. W. K. V., Wielen, L. A. M. V. D., Eppink, M. H. M., Sandt, E. J. A. X. V. D. and Ottens, M. (2007b). *pH-gradient ion-exchange chromatography: An analytical tool for design and optimization of protein separations.* Journal of Chromatography A, 1164:181.

Amrhein, S., Bauer, K., Galm, L. and Hubbuch, J. (2015). *Non-Invasive High Throughput Approach for Protein Hydrophobicity Determination Based on Surface Tension.* Biotechnology and Bioengineering, pages –.

Anandakrishnan, R., Aguilar, B. and Onufriev, A. V. (2012). *H++ 3.0: automating pK prediction and the preparation of biomolecular structures for atomistic molecular modeling and simulations.* Nucleic Acids Res., 40(Web Server issue):W537.

Annunziata, O., Asherie, N., Lomakin, A., Pande, J., Ogun, O. and Benedek, G. B. (2002). *Effect of polyethylene glycol on the liquid-liquid phase transition in aqueous protein solutions.* Proc. Natl. Acad. Sci. U. S. A., 99(22):14165.

Arakawa, T. (2002). *Hydration as a Major Factor in Preferential Solvent–Protein Interactions.* Crystal Growth & Design, 2(6):549.

Arakawa, T., Bhat, R. and Timasheff, S. N. (1990). *Preferential interactions determine protein solubility in 3-component solutions – the MgCl2 system.* Biochemistry, 29:1914.

Arakawa, T. and Timasheff, S. N. (1982). *Preferential interactions of proteins with salts in concentrated solutions.* Biochemistry, 21:6545.

Arakawa, T. and Timasheff, S. N. (1984a). *Mechanism of protein salting in and salting out by divalent cation salts: Balance between hydration and salt binding.* Biochemistry, 23:5912.

Arakawa, T. and Timasheff, S. N. (1984b). *Protein stabilization and destabilization by guanidinium salts.* Biochemistry, 23:5924.

Asakura, S. and Oosawa, F. (1958). *Interaction between Particles Suspended in Solutions of Macromolecules.* J. Polym. Sci., 33(126):183.

Asherie, N. (2004). *Protein crystallization and phase diagrams.* Methods, 34(3):266.

Atha, D. H. and Inghamg, K. C. (1981). *Mechanism of Precipitation of Proteins by Polyethylene Glycols.* J. Biol. Chem., 256(23):12108.

Baumann, P., Baumgartner, K. and Hubbuch, J. (2015a). *Influence of Binding pH and Protein Solubility on the Dynamic Binding Capacity in Hydrophobic Interaction Chromatography.* Journal of Chromatography A, 1396:77.

Baumann, P., Bluthardt, N., Renner, S., Osberhaus, A. and Hubbuch, J. (2015b). *Integrated Development of Up- and Downstream Processes Supported by the Cherry-Tag for Real-time Tracking of Stability and Solubility of Proteins.* Journal of Biotechnology, 200:27.

Baumgartner, K., Galm, L., Noetzold, J., Sigloch, H., Morgenstern, J., Schleining, K., Suhm, S., Oelmeier, S. and Hubbuch, J. (2015). *Determination of protein phase diagrams by microbatch experiments: Exploring the influence of precipitants and pH.* Int J Pharm, 479:28.

Baynes, B. M. and Trout, B. L. (2004). *Rational design of solution additives for the prevention of protein aggregation.* Biophys. J., 87(3):1631.

Beretta, S., Chirico, G. and Baldini, G. (2000). *Short-Range Interactions of Globular Proteins at High Ionic Strengths.* Macromolecules, 33(23):8663.

Berg, A., Oelmeier, S. A., Kittelmann, J., Dismer, F. and Hubbuch, J. (2012). *Development and characterization of an automated high throughput screening method for optimization of protein refolding processes.* Journal of Separation Science, 35:3149.

Boistelle, R. and Astier, J. P. (1988). *Crystallization mechanisms in solution.* J. Cryst. Growth, 90:14.

Carta, G. and Jungbauer, A. (2010). *Chromatography Media*, chapter 3, pages 85–124. Wiley-VCH Verlag GmbH & Co. KGaA.

Chayen, N., Akins, J., Campbell-Smith, S. and Blow, D. M. (1988). *Solubility of glucose isomerase in ammonium sulphate solutions.* J. Cryst. Growth, 90:112.

Chayen, N. E. and Saridakis, E. (2008). *Protein crystallization: from purified protein to diffraction-quality crystal.* Nat. Methods, 5(2):147.

Chen, J., Tetrault, J. and Ley, A. (2008). *Comparison of standard and new generation hydrophobic interaction chromatography resins in the monoclonal antibody purification process.* Journal of Chromatography A, 1177:272.

Chi, E. Y., Krishnan, S., Randolph, T. W. and Carpenter, J. F. (2003). *Physical stability of proteins in aqueous solution: mechanism and driving forces in nonnative protein aggregation.* Pharmaceutical Research, 20:1325.

Collins, K. D. (2004). *Ions from the Hofmeister series and osmolytes: effects on proteins in solution and in the crystallization process.* Methods, (3):300.

Curtis, R. A., Prausnitz, J. M. and Blanch, H. W. (1998). *Protein-protein and protein-salt interactions in aqueous protein solutions containing concentrated electrolytes.* Biotechnol. Bioeng., 57(1):11.

Curtis, R. A., Ulrich, J., Montaser, A., Prausnitz, J. M. and Blanch, H. W. (2002). *Protein-protein interactions in concentrated electrolyte solutions.* Biotechnol. Bioeng., 79(4):367.

Czitrom, V. (1999). *One-factor-at-a-time versus designed experiments.* The American Statistician, 53:126.

D'Arcy, A., Mac Sweeney, A., Stihle, M. and Haber, A. (2003). *The advantages of using a modified microbatch method for rapid screening of protein crystallization conditions.* Acta Crystallogr. Sect. D Biol. Crystallogr., 59(2):396.

De Young, L. R., Fink, A. L. and Dills, K. A. (1993). *Aggregation of globular proteins.* Accounts of Chemical Research, 26:614.

Debye, P. and Hückel, E. (1923). *Zur Theorie der Elektrolyte.* Phys. Zeitschrift, 24(11):185.

Deitcher, R. W., O'Connell, J. P. and Fernandez, E. J. (2010). *Changes in solvent exposure reveal the kinetics and equilibria of adsorbed protein unfolding in hydrophobic interaction chromatography.* Journal of Chromatography A, 1217:5571.

Delphi Genetics SA (2009a). *Cherry^{TM}Codon kit Manual (v3.0).* Accessed: 2014-09-10.

Delphi Genetics SA (2009b). *Cherry^{TM}Express kit Manual (v3.0).* Accessed: 2014-09-10.

Diogo, M. M., Prazeres, D. M. F., Pinto, N. and a Queiroz, J. (2003). *Hydrophobic interaction chromatography of homo-oligonucleotides on derivatized sepharose CL-6B. Using and relating two different models for describing the effect of salt and temperature on retention.* Journal of Chromatography A, 1006:137.

Diogo, M. M., Queiroz, J. A., A., M. G., Martins, G. N. M., S. A. M. Ferreira and F., P. D. M. (1999). *Purification of a Cystic Fibrosis Plasmid Vector for Gene Therapy Using Hydrophobic Interaction Chromatography.* Biotechnology and Bioengineering, 68:576.

Diogo, M. M., Queiroz, J. A. and Prazeres, D. M. F. (2001). *Studies on the retention of plasmid DNA and Escherichia coli nucleic acids by hydrophobic interaction chromatography.* Bioseparation, 10:211.

Dumetz, A. C., Chockla, A. M., Kaler, E. W. and Lenhoff, A. M. (2008a). *Effects of pH on protein–protein interactions and implications for protein phase behavior.* Biochimica et Biophysica Acta (BBA) - Proteins and Proteomics, 1784:600.

Dumetz, A. C., Chockla, A. M., Kaler, E. W. and Lenhoff, A. M. (2008b). *Protein phase behavior in aqueous solutions: crystallization, liquid-liquid phase separation, gels, and aggregates.* Biophys. J., 94(2):570.

Dupeux, F., Röwer, M., Seroul, G., Blot, D. and Marquez, J. A. (2011). *A thermal stability assay can help to estimate the crystallization likelihood of biological samples.* Acta Crystallographica Section D, 67:915.

Durbin, S. D. and Feher, G. (1996). *Protein Crystallization.* Annu. Rev. Phys. Chem., 47:171.

Faber, C. and Hobley, T. J. (2006). *Measurement and Prediction of Protein Phase Behaviour and Protein-Protein-Interactions.* Ph.D. thesis.

Fogle, J. L., O'Connell, J. P. and Fernandez, E. J. (2006). *Loading, stationary phase, and salt effects during hydrophobic interaction chromatography: alpha-Lactalbumin is stabilized at high loadings.* Journal of Chromatography A, 1121:209.

Fountoulakis, M., Takacs, M.-F. and Takacs, B. (1999). *Enrichment of low-copy-number gene products by hydrophobic interaction chromatography.* Journal of Chromatography A, 833:157.

Furuike, S., Levadny, V. G., Li, S. J. and Yamazaki, M. (1999). *Low pH Induces an Interdigitated Gel to Bilayer Gel Phase Transition in Dihexadecylphosphatidylcholine Membrane.* Biophysical Journal, 77:2015.

Geng, X., Guo, L. and Chang, J. (1990). *Study of the retention mechanism of proteins in hydrophobic interaction chromatography.* Journal of Chromatography, 507:1.

George, A. and Wilson, W. W. (1994). *Predicting protein crystallization from a dilute solution property.* Acta Crystallogr. D. Biol. Crystallogr., 50(Pt 4):361.

Goldberg, D. S., Bishop, S. M., Shah, A. U. and Sathish, H. A. (2011). *Formulation development of therapeutic monoclonal antibodies using high-throughput fluorescence and static light scattering techniques: Role of conformational and colloidal stability.* Journal of Pharmaceutical Sciences, 100:1306.

Goodenough, P. W. (1995). *A review of protein engineering for the food industry.* International Journal of Food Science and Technology, 30:119.

Hagen, M. H. J. and Frenkel, D. (1994). *Determination of phase diagrams for the hard-core attractive Yukawa system.* J. Chem. Phys., 101(5):4093.

Hahn, R., Deinhofer, K., Machold, C. and Jungbauer, A. (2003). *Hydrophobic interaction chromatography of proteins II. Binding capacity, recovery and mass transfer properties.* Journal of Chromatography B, 790:99.

Hansen, S. K., Jamali, B. and Hubbuch, J. (2013). *Selective high throughput protein quantification based on uv absorption spectra.* Biotechnology and Bioengineering, 110:448.

Hjerten, S., Yao, K., Eriksson, K.-O. and Johansson, B. (1986). *Gradient and isocratic high-performance hydrophobic interaction chromatography of proteins on agarose columns.* Journal of Chromatography, 359:99.

Hofmeister, F. (1888). *Zur Lehre von der Wirkung der Salze.* Arch. für Exp. Pathol. und Pharmakologie, 25(1):1.

Horváth, C., Melander, W. and Molnár, I. (1976). *Solvophobic Interactions in Liquid Chromatography with Nonpolar Stationary Phases.* Journal of Chromatography, 125:129.

Huang, H.-M., Lin, F.-Y., Chen, W.-Y. and Ruaany, R.-C. (2000). *Isothermal Titration Microcalorimetric Studies of the Effect of Temperature on Hydrophobic Interaction between Proteins and Hydrophobic Adsorbents.* Journal of Colloid and Interface Science, 229:600.

Islam, S. A. and Weaver, D. L. (1990). *Molecular Interactions in Protein Crystals: Solvent Accessible Surface and Stability.* PROTEINS: Structure, Function, and Genetics, 8:1.

Jennissen, H. P. (2000). *Hydrophobic interaction chromatography.* Int J Bio-Chromatogr, 5:131.

Jones, T. T. and Fernandez, E. J. (2003). *Hydrophobic Interaction Chromatography Selectivity Changes Among Three Stable Proteins: Conformation Does Not Play a Major Role.* Biotechnology and Bioengineering, 87:388.

Jungbauer, A. (2005). *Chromatographic media for bioseparation.* Journal of Chromatography A, 1065:3.

Jungbauer, A., Machold, C. and Hahn, R. (2005). *Hydrophobic interaction chromatography of proteins III. Unfolding of proteins upon adsorption.* Journal of Chromatography A, 1079:221.

Kalisz, H. M., Hecht, H.-J., Schomburg, D. and Schmis, R. D. (1990). *Crystallization and preliminary X-ray diffraction studies of a deglycosylated glucose oxidase from Aspergillus niger.* J. Mol. Biol., 213:207.

Karger, B. L. and Rigoberto, B. (1989). *The effect of on-column structural changes of proteins on their HPLC behavior.* Talanta, 36:243.

Klempnauer, K.-H., Fischer, L. and Otto, M. K. (2011). *pH-Abhängigkeit der Proteinfunktion.* In Chmiel, H. (editor), *Bioprozesstechnik*, chapter 2, pages 31–32. Spektrum Akademischer Verlag, Springer, 3nd edition.

Kramarczyk, J. F., Kelley, B. D. and L., C. J. (2008). *High-Throughput Screening of Chromatographic Separations: II. Hydrophobic Interaction.* Biotechnology and Bioengineering, 100:707.

Kröner, F., Elsässer, D. and Hubbuch, J. (2013a). *A high-throughput 2D-analytical technique to obtain single protein parameters from complex cell lysates for in silico process development of ion exchange chromatography.* Journal of chromatography A, 1318:84.

Kröner, F., Hanke, A. T., Nfor, B. K., Pinkse, M. W. H., Verhaert, P. D. E. M., Ottens, M. and Hubbuch, J. (2013b). *Analytical characterization of complex, biotechnological feedstocks by pH gradient ion exchange chromatography for purification process development.* Journal of chromatography A, 1311:55.

Kröner, F. and Hubbuch, J. (2013). *Systematic generation of buffer systems for pH gradient ion exchange chromatography and their application.* J. Chromatogr. A, 1285:78.

Kyte, J. and Doolittle, R. F. (1982). *A Simple Method for Displaying the Hydropathic Character of a Protein.* Journal of Molecular Biology, 157:105.

Leckband, D. and Israelachvili, J. (2001). *Intermolecular forces in biology.* Q. Rev. Biophys., 34(2):105.

Lee, J. C. and Lee, L. L. Y. (1981). *Preferential solvent interactions between proteins and polyethylene glycols.* J. Biol. Chem., 256(2):625.

Lienqueo, M. E., Mahn, A., Salgado, J. C. and Asenjo, J. A. (2007). *Current insights on protein behaviour in hydrophobic interaction chromatography.* Journal of Chromatography B, 849:53.

Lin, F.-Y., Chen, W.-Y. and Hearn, M. T. W. (2001). *Microcalorimetric Studies on the Interaction Mechanism between Proteins and Hydrophobic Solid Surfaces in Hydrophobic Interaction Chromatography: Effects of Salts, Hydrophobicity of the Sorbent, and Structure of the Protein.* Analytical Chemistry, 73:3875.

Lin, F.-Y., Chen, W.-Y., Ruaany, R.-C. and Huang, H.-M. (2000). *Microcalorimetric studies of interactions between proteins and hydrophobic ligands in hydrophobic interaction chromatography: effects of ligand chain length, density and the amount of bound protein.* Journal of Chromatography A, 872:37.

Lin, Y.-B., Zhu, D.-W., Wang, T., Song, J., Zou, Y.-S., Zhang, Y.-L. and Lin, S.-X. (2008). *An Extensive Study of Protein Phase Diagram Modification: Increasing Macromolecular Crystallizability by Temperature Screening.* Cryst. Growth Des., 8(12):4277.

Lu, J., Wang, X.-J. and Ching, C.-B. (2003). *Effect of Additives on the Crystallization of Lysozyme and Chymotrypsinogen A.* Cryst. Growth Des., 3(1):83.

Luft, J. R. and DeTitta, G. T. (2009). *Rational Selection of Crystallization Techniques.* In Bergfors, T. M. (editor), *Protein Cryst.*, chapter 2, pages 11–46. Internat'l University Line, 2nd edition.

Mahler, H.-C., Friess, W., Grauschopf, U. and Kiese, S. (2009). *Protein aggregation: Pathways, induction factors and analysis.* Journal of Pharmaceutical Sciences, 98:2909.

McGown, E. L. and G., H. D. (1998). *Multichannel pipettor performance verified by measuring pathlength of reagent dispensed into a microplate.* Analytical Biochemistry, 258.1:155.

McMurry, J. E. (2010). *Isoelectric Points.* In McMurry, J. E. (editor), *Fundamentals of Organic Chemistry*, chapter 15.2, pages 509–511. Brooks Cole, 7th edition.

McPherson, A. (1976). *Crystallization of Proteins from Polyethylene Glycol.* J. Biol. Chem., 251(20):6300.

McPherson, A. (2001). *A comparison of salts for the crystallization of macromolecules.* Protein Sci., 10:418.

McPherson, A. and Cudney, B. (2006). *Searching for silver bullets: an alternative strategy for crystallizing macromolecules.* J. Struct. Biol., 156(3):387.

Melander, W. and Horváth, C. (1977). *Salt Effects on Hydrophobic Interactions in Precipitation and Chromatography of Proteins: An Interpretation of the Lyotropic Series.* Archives of Biochemistry and Biophysics, 183:200.

Müller, E., Vajda, J., Josic, D., Schröder, T., Dabre, R. and Frey, T. (2013). *Mixed electrolytes in hydrophobic interaction chromatography.* Journal of separation science, 36:1327.

Neal, B. L., Asthagiri, D., Velev, O. D., Lenhoff, A. M. and Kaler, E. W. (1999). *Why is the osmotic second virial coefficient related to protein crystallization.* Journal of Crystal Growth, 196(2-4):377.

Oelmeier, S. A., Dismer, F. and Hubbuch, J. (2011). *Application of an aqueous two-phase systems high-throughput screening method to evaluate mAb HCP separation.* Biotechnol. Bioeng., 108(1):69.

Pace, C. N., Shirley, B. A., McNutt, M. and Gajiwala, K. (1996). *Forces contributing to the conformational stability of proteins.* FASEB Journal, 10:75.

Pawar, S. A. and Deshpande, V. V. (2000). *Characterization of acid-induced unfolding intermediates of glucose/xylose isomerase.* Eur. J. Biochem., 267(21):6331.

Queiroz, J., Tomaz, C. and Cabral, J. (2001). *Hydrophobic interaction chromatography of proteins.* Journal of Biotechnology, 87:143.

Rathore, A. S. and Winkle, H. (2009). *Quality by design for biopharmaceuticals.* Nature Biotechnology, 27:26.

Ries-Kautt, M. M. and Ducruix, A. F. (1989). *Relative effectiveness of various ions on the solubility and crystal growth of lysozyme.* J. Biol. Chem., 264(2):745.

Rose, G. D., Geselowitz, A. R., Lesser, G. J., Lee, R. H. and Zehfus, M. H. (1985). *Hydrophobicity of Amino Acid Residues in Globular Proteins.* Science, 229:834.

Rosenfeld, R. and Benedek, K. (1993). *Conformational changes of brain-derived neurotrophic factor during reversed-phase high-performance liquid chromatography.* Journal of Chromatography, 632:29.

Schwierz, N., Horinek, D. and Netz, R. R. (2010). *Reversed anionic Hofmeister series: the interplay of surface charge and surface polarity.* Langmuir, 26(10):7370.

Scopes, R. K. (1994). *Separation by Precipitation.* In *Protein Purif. Princ. Pract.*, chapter 4, pages 71–101. Springer-Verlag New York, Inc., 3rd edition.

Senczuk, A., Klinke, R., Arakawa, G., T. Vedantham and Yigzaw, Y. (2009). *Hydrophobic interaction chromatography in dual salt system increases protein binding capacity.* Biotechnology and bioengineering, 103:930.

Senisterra, G., Chau, I. and Vedadi, M. (2012). *Thermal denaturation assays in chemical biology.* Assay and drug development technologies, 10(2):128.

Sinanoglu, O. (1980). *The Solvophobic Theory for the Prediction of Molecular Conformations and Biopolymer Binding in Solutions with Recent Direct Experimental Tests.* International Journal of Quantum Chemistry, 18:381.

Sleutel, M., Willaert, R., Gillespie, C., Evrard, C., Wyns, L. and Maes, D. (2009). *Kinetics and Thermodynamics of Glucose Isomerase Crystallization.* Cryst. Growth Des., 9(1):497.

Stradner, A., Sedgwick, H., Cardinaux, F., Poon, W. C. K., Egelhaaf, S. U. and Schurtenberger, P. (2004). *Equilibrium cluster formation in concentrated protein solutions and colloids.* Nature, 432(7016):492.

Tardieu, A., Bonneté, F., Finet, S. and Vivarès, D. (2002). *Understanding salt or PEG induced attractive interactions to crystallize biological macromolecules.* Acta Crystallogr. Sect. D Biol. Crystallogr., 58(10):1549.

To, B. and Lenhoff, A. (2007a). *Hydrophobic interaction chromatography of proteins. II. Solution thermodynamic properties as a determinant of retention.* Journal of Chromatography A, 1141:235.

To, B. C. S. and Lenhoff, A. M. (2007b). *Hydrophobic interaction chromatography of proteins I. The effects of protein and adsorbent properties on retention and recovery.* Journal of Chromatography A, 1141:191.

Velev, O. D., Kaler, E. W. and Lenhoff, A. M. (1998). *Protein interactions in solution characterized by light and neutron scattering: comparison of lysozyme and chymotrypsinogen.* Biophys. J., 75(6):2682.

Vivarès, D., Belloni, L., Tardieu, a. and Bonneté, F. (2002). *Catching the PEG-induced attractive interaction between proteins.* Eur. Phys. J. E. Soft Matter, 9(1):15.

Vlachy, V., Blanch, H. W. and Prausnitz, J. M. (1993). *Liquid-liquid phase separations in aqueous solutions of globular proteins.* AIChE J., 39(2):215.

Vlachy, V. and Prausnitz, J. M. (1992). *Donnan Equilibrium. Hypernetted-Chain Study of One-Component and Multicomponent Models for Aqueous Polyelectrolyte Solutions.* J. Phys. Chem., 96(15):6465.

Wang, W., Li, N. and Speaker, S. (2010a). *External Factors Affecting Protein Aggregation.* In Wang, W. and Roberts, C. J. (editors), *Aggreg. Ther. Proteins*, chapter 4, pages 119–204. John Wiley & Sons, 1st edition.

Wang, W., Nema, S. and Teagarden, D. (2010b). *Protein aggregation - Pathways and influencing factors.* International Journal of Pharmaceutics, 390:89.

Werner, A., Hackemann, E. and Hasse, H. (2014). *Temperature dependence of adsorption of PEGylated lysozyme and pure polyethylene glycol on a hydrophobic resin: Comparison of isothermal titration calorimetry and van't Hoff data.* Journal of Chromatography A, 1356:188.

Werner, A. and Hasse, H. (2013). *Experimental study and modeling of the influence of mixed electrolytes on adsorption of macromolecules on a hydrophobic resin.* Journal of chromatography A, 1315:135.

Xia, F., Nagrath, D., Garde, S. and Cramer, S. M. (2004). *Evaluation of Selectivity Changes in HIC Systems Using a Preferential Interaction Based Analysis.* Biotechnology and Bioengineering, 87:354.

Zeelen, J. P. (2009). *Interpretation of the Crystallization Drop Results.* In Bergfors, T. M. (editor), *Protein Cryst.*, chapter 10, pages 175–194. Internat'l University Line, 2nd edition.

Zhang, Y. and Cremer, P. S. (2006). *Interactions between macromolecules and ions: The Hofmeister series.* Current opinion in chemical biology, 10:658.

Zhang, Y. and Cremer, P. S. (2009). *The inverse and direct Hofmeister series for lysozyme.* Proc. Natl. Acad. Sci. U. S. A., 106(36):15249.

Ziegler, G. R. and Foegeding, E. A. (1990). *The Gelation of Proteins.* In Kinsella, J. E. (editor), *Adv. Food Nutr. Res.*, pages 203–298. Academic Press.